INVESTIGATION OF NEAR EARTH SPACE ENVIRONMENT

THESIS SUBMITTED TO

MANONMANIAM SUNDARANAR UNIVERSITY

IN PARTIAL FULFILMENT OF THE REQUIREMENTS
FOR THE AWARD OF THE DEGREE OF

DOCTOR OF PHILOSOPHY

IN

PHYSICS

BY

MANU S.

REG. NO. 8431

EQUATORIAL GEOPHYSICAL RESEARCH LABORATORY
INDIAN INSTITUTE OF GEOMAGNETISM
KRISHNAPURAM, TIRUNELVELI

MANONMANIAM SUNDARANAR UNIVERSITY
TIRUNELVELI
JUNE 2015

Prof. S. Gurubaran,

Professor 'F',

Equatorial Geophysical Research Laboratory,

Indian Institute of Geomagnetism,

Krishnapuram, Tirunelveli-627011,

Tamilnadu, India.

CERTIFICATE

This thesis entitled ''**INVESTIGATION OF NEAR EARTH SPACE ENVIRONMENT**'' submitted by **Manu S.**, for the award of Degree of Doctor of Philosophy in Physics of Manonmaniam Sundaranar University is a record of bonafide research work done by him and it has not been submitted for the award of any degree, diploma, associateship, fellowship of any University/Institution.

Place: Tirunelveli

Date:

(S. GURUBARAN)

Manu S.,

Research Scholar,

Equatorial Geophysical Research Laboratory,

Indian Institute of Geomagnetism,

Krishnapuram, Tirunelveli-627011,

Tamilnadu, India.

DECLARATION

I hereby declare that the thesis entitled **''INVESTIGATION OF NEAR EARTH SPACE ENVIRONMENT''** submitted by me for the award of Degree of **Doctor of Philosophy in Physics** of Manonmaniam Sundaranar University is the result of my original and independent research work carried out under the guidance of **Prof. S. Gurubaran**, Equatorial Geophysical Research Laboratory, Indian Institute of Geomagnetism, Tirunelveli, and it has not been submitted for the award of any degree, diploma, associateship, fellowship of any University or Institution.

Place: Tirunelveli

(MANU S.)

Date:

DEDICATED TO MY FAMILY

(SUJATHA, M., SHANMUGAM, P.S., VINAY, S., MADHUVANTHI, N., ARAVIND, M., NAGARAJAIAH, N., SUJATHA, H.)

ACKNOWLEDGMENT

I take this opportunity to thank my supervisor Prof. S. Gurubaran for introducing me to this field. I am very much indebted to him for his valuable guidance, encouragement, kindness and keen interest throughout the course of this work. I extend my sincere thanks to the former Director of Indian Institute of Geomagnetism Prof. A. Bhattacharya, former Director in-charge Prof. Mita Rajaram, and Prof. S. G. Gokarn for their encouragement and support to complete my research work and the present Director Dr. D. S. Ramesh for allowing me to complete my Thesis.

I acknowledge with thanks the technical support rendered by Dr. K. Jawahar, for his support in completing the balloon experiment and my thesis work. I owe my sincere thanks to Dr. C. Panneerselvam for his moral support and valuable suggestions. I thank Dr. A. K. Sinha and Mr. Rahul Rawat for providing me Schumann resonance data that is used in the thesis. I thank to Dr. S. Tulasiram, Dr. C. P. Anil Kumar, Mr. K. U. Nair, Mr. C. Selvaraj, Mr. K. Emperumal, Mr. K. Jeeva, and Mr. P. Elango for their support. I am very much pleased to thank Dr. S. SathishKumar, Head of EGRL for his enthusiastic support. Thanks to Mr. Gopalsingh Rathod, Mr. P. Sheikbareeth, Mr. Laxman and Ms. Ananthi for their support. I am thankful to the administrative staffs Mr. Senthil Kumar (former account assistant), Mr. Gaurav Kumar and Mr. S. S. Mondal for their assistance. My special thanks to Mr. L. Muthukrishnan for his help and support throughout my stay at EGRL. My special thanks to Mr. Somasundaram (Late), Mrs. Velammal, Mrs. Chellama Patti and Mr. Pandurangan

for providing delicious food. I thank all the research scholars Jeni Victor, Sukanta Sau, and Muhammed Kutty, for their constant support and sweet memories. I offer my sincere thanks to our former librarian Ms. Divya Mehta and present Librarian Ms. Smitha Chandra, for their support in library matters. I am thankful to Mrs. Selvarajeswari and Mrs. Punithavathi, for sending the scientific reprints and other reference materials in time.

I am greatly thankful to Prof. A .Robson Benjamin, Head, Department of Physics, The American College, Madurai for his constant support and motivation. Several people have played a decisive role in my life to come to this stage. Among those the most important and unforgettable is Prof. R. Srinivasan, Shri. G. Srinivasalu, Shri. Sundararajan, Prof. P. R. Vishwanath, Prof. T P Prabhu, Dr. R. Ramesh, Dr. Kathirevan, of Indian Institute of Astrophysics and Prof. B S Acharya of TIFR for giving me a taste of research.

My heartfelt thanks to Mr. Sreenivasan, Mr. Vasudevan, Mr. Anand, Mr. Venkateshwara Rao, Mr. Kapardhi, Mr. Anmi Reddy, Mr. Sunil Kumar, Mr. Dharmesh, and other staff member, cooks (Mr. Muktar Ali and Mr. Srikanth) of National Balloon Facility, TIFR, Hyderabad for their hard work and co-operation. Without them BEENS experiment would not have been possible.

I wish to record my sincere thanks to my friends Leela, Meetu, Chitra, Premal, Jibu, Raghavendra, Santhosh, Achal, Madhusudhan, Gurumurthy, Shivakumar, Naveen, Devanandhan, Selvakumaran, Elizabeth, Partho Pal, Jayashree, Sarvesh Chandra, Prasanna Mahavarkar, Ramanathan for their understanding and moral support.

Words fail to thank my friends, Dr. R. Dhanya and Mr. Indrajit V Barve, who believed in me when I had no hope in myself, for giving me a push whenever I stopped. I thank Mr. S. Ramani, Mrs. R. Vijayalakshmi, Ms. R. Divya and Mr. K. R. Rajesh for supporting me throughout my Ph.D. The love, patience, support, sacrifice, understanding and constant encouragement from my parents and my beloved wife made this work possible. I thank also my parent in laws for their advice, support and inspiration that made this work possible. I thank others who helped me at various times and are not mentioned here. Finally, I thank God for blessing me with this great opportunity.

PREFACE

The thesis deals with the study of the near Earth space environment using balloon borne and ground-based measurement techniques. The near Earth space environment is the region of space where in-situ measurements can be carried out without artificial and natural noise source perturbations which would affect the measurements. The Earth‘s middle atmosphere, which is known to be near space, cannot be probed easily either by ground based remote sensing techniques like radar and satellites orbiting the Earth. One can probe this region of space by in-situ measurements from a balloon platform.

The middle atmosphere is weakly conducting region and behaves as an electrically passive region between the cloud tops and the ionosphere. By measuring certain known parameters, one can understand the dynamics and electrodynamics of the Near Earth space environment. In this thesis, two experiments were made use of to probe the near Earth space environment. Firstly, in-situ measurements of electric field and magnetic field were designed to be carried out over a balloon platform to study the thunderstorm generated and ionospheric origin electric field at stratospheric heights with in-house development and fabrication of electrometer. Secondly, high quality data obtained from an experiment that used induction coil magnetometers are used to analyze the diurnal and seasonal variations of the resonance formed due to the Earth-ionosphere cavity called Schumann resonance. The contents of thesis chapters in brief are given below.

The first chapter provides a brief introduction to historical overview of using balloon as a platform to conduct different experiments. Introduction to the Earth‘s atmosphere is given in brief. An overview of the atmospheric electrical conductivity, global electric circuit and the outline of thesis are provided in chapter 1. The second chapter is devoted to the instrumentation of electronics designed and developed for measuring vector electric fields at stratospheric heights. The various errors involved due to the input resistance loading, input bias current loading, shunt resistance loading and guarding in fabricating the electrometer are discussed in this chapter. A brief introduction is provided on dealing with very high input impedance operational amplifiers and the type of insulation material to be used for making error free measurements. Establishment of anti-static laboratory at Equatorial Geophysical Research Laboratory, Tirunelveli helped in handling the high input impedance electrometer. The BEENS experiment was conceived for dc and ac measurements of vector electric fields and ac magnetic field measurement using search coil magnetometer. A brief description on the double Langmuir probe technique used for the measurements of electric fields is given in this chapter. The description of the search coil magnetometer used for the measurement of ELF and VLF waves is also described. The third chapter deals with the experimental procedures of the BEENS experiment. The chapter discusses on the design of the gondola for placing the scientific payload and boom deployment mechanism for electric field sensors. Various subsystems like telemetry and telecommand, orientation platform, fluxgate magnetometer for finding the orientation of gondola and power budget to the scientific payload are described. Brief discussion on testing and qualification of scientific

payload for balloon flight is given. Pre-flight testing and integration of all the subsystems and payload readiness for the balloon flight and procedures undertaken for launching the BEENS experiment are presented in chapter 3. The fourth chapter discusses on the electric field measurement results obtained from the BEENS experiment. The BEENS experiment was carried out from the National Balloon facility, Hyderabad (17.5° N, 78.6° E, geographic; 8.7° N, geomagnetic), India, during the dawn hours on 14 December 2013 to probe and understand the processes that drive the various electric field sources at low latitude. The availability of stratospheric electric field measurements at low latitudes is rare to find. The objective of this experiment is to measure the electric fields at stratospheric altitudes which are of ionospheric origin (horizontal electric field) and fields generated by thunderstorm sources from the lower atmosphere (vertical electric field). It was also designed to measure the ac component of global electric circuit which arises due to the ELF and VLF sources of thunderstorm origin. The fifth chapter reports the measurements of the ac component of global electric circuit. The chapter deals with the results of Schumann resonances measured at Maitri, Antarctica during 2011. The diurnal and seasonal variation of Schumann resonances parameters from Maitri, Antarctica (70° 45′ 52′′ S, 11° 44′ 03′′ E, 117 m AMSL) are studied. Chapter 6 discusses on the summary of the entire work carried out and scope for future work is also presented in this chapter.

Place: Tirunelveli

Date: **(MANU S.)**

Contents

1 Introduction: Overview and Fundamentals **1**

1.1 Historical Overview 1

1.2 The Earth‘s Atmosphere 4

1.3 Atmospheric Conductivity 6

1.4 Global Electric Circuit 9

1.4.1 DC Circuit 10

1.4.2 AC Circuit 11

1.5 Outline of the Thesis 12

2 Instrumentation **14**

2.1 Introduction 14

2.1.1 Need for a High Input Impedance Electrometer 14

2.2 Designing of an Electrometer 16

2.2.1 Input Resistance Loading 16

2.2.2 Input Bias Current Loading 17

2.2.3 Shunt Resistance Loading and Guarding 19

2.3 Insulation Resistance 21

2.4 Working with High Impedance Op-Amps at EGRL, Tirunelveli 23

2.5 Double Langmuir Probe Technique 29

2.6 BEENS Electric Field Measurement 30

2.7 Circuit for Atmospheric Electric Field Measurement in BEENS Experiment . 31

2.8 Search Coil Magnetometer 33

3 Experimental Procedure for BEENS **35**

3.1 Introduction . . . 35

3.2 BEENS Balloon Configuration - An Outline . . . 36

3.3 Gondola Design . . . 38

3.4 Boom Design and Deployment Mechanism . . . 39

3.5 Cleaning of Booms . . . 44

3.6 Reaction Wheel . . . 45

3.7 Subsystems in the BEENS Payload . . . 46

3.7.1 Telemetry system . . . 46

3.7.2 Data Transmission . . . 47

3.7.3 PCM Encoder . . . 47

3.7.4 Telemetry Transmitter . . . 50

3.7.5 Telecommand System . . . 50

3.7.6 GPS Receiver . . . 51

3.7.7 Ballast . . . 52

3.7.8 Apex Value . . . 52

3.7.9 Timer . . . 53

3.7.10 Beacon . . . 53

3.7.11 ATC Radar Transponder . . . 53

3.8 Packing of Electronics . . . 54

3.9 Power Supply Unit . . . 55

3.10 Battery Packs . . . 56

3.11 Fluxgate Magnetometer . . . 56

3.12 Environmental Testing . . . 57

3.13 Mechanical and Electrical integration . . . 59

3.14 Long Duration Test . . . 60

3.15 Launch Procedure for BEENS Experiment . . . 60

3.15.1 Scheduling of Flight . . . 61

3.15.2 Launch sequence 63
3.15.3 Tracking and Recovery 65

4 Results of BEENS Experiment **70**

4.1 Introduction 70
4.2 Electric Field Results of BEENS Experiment 71
4.2.1 Imapct of Using Five Boom Configuration 79
4.2.2 Distortion over the Sinusoidal Variation of the Electric Field in the Rotating Platform 82
4.2.3 Vertical Electric Field 87
4.2.4 Horizontal Electric Field 88
4.3 Discussion on Horizontal Electric Field from BEENS Experiment 94

5 Schumann Resonances Observed at Maitri, Antarctica **101**

5.1 Introduction 101
5.2 Precautions to be Taken for the Installation of the Search Coil Magnetometer for Measuring Schumann Resonance 106
5.3 Experimental Setup 107
5.4 Results and Discussion of Schumann Resonance Measurement at Matiri, Antarctica 108
5.4.1 Diurnal Variation of the Mode 1 Amplitude and Frequency 111
5.4.2 Seasonal Dependence of the Diurnal Variation of Mode 1 Amplitude 114
5.4.3 Seasonal Dependence of the Diurnal Variation of Mode 1 Frequency 119

6 Summary and Scope for Future Work **125**

6.1 Electric Field Measurements from BEENS Experiment 125
6.2 Schumann Resonances Measurement from Maitri, Anatarctica 127
6.3 Scope for Future Work 128
6.4 Conclusion 132

List of Figures

1.1 Nomenclature of Earth‘s Atmosphere 5
1.2 Electrical conductivity as a function of altitude 8
1.3 Schematic illustrating various electrical processes in the global electric circuit 9

2.1 Effects of input resistance loading on voltage measurement accuracy . . 16
2.2 Effects of input bias current on voltage measurement accuracy 18
2.3 Effects of input bias current on voltage measurement accuracy 19
2.4 Effect of cable leakage resistance on voltage measurement accuracy . . 20
2.5 Guarded configuration to minimize error in measuring voltage 21
2.6 Pin configuration for AD549 23
2.7 Pin configuration for OPA128 25
2.8 Block diagram of electric field measurement using balloon platform and its electronics 27
2.9 Internal circuit and pin configuration of INA116 28
2.10 Circuit Board Guard Layout used for INA 116 28
2.11 Block diagram of electric field experiment in BEENS experiment . . . 32
2.12 Search Coil Magnetometer attached to BEENS payload 33

3.1 BEENS - A Schematic 37
3.2 Gondola design used for BEENS experiment 38
3.3 Electric field Booms of BEENS experiment in stowed condition 42
3.4 Boom in Deployed Condition (top view) 43
3.5 Boom in Deployed condition (Side view) 43

3.6 Balloon Gondola fixed with reaction wheel and universal Coupler . . . 46
3.7 Bi-phase-L encoding - A schematic . . . 49
3.8 Chapman 12 channel GPS receiver . . . 51
3.9 Power supply unit used for BEENS experiment . . . 55
3.10 Environmental Testing on BEENS payload . . . 58
3.11 Wind profile obtained from sounding balloon and UKMO data . . . 62
3.12 Panoramic View of BEENS experiment Launch . . . 64
3.13 Filling of Hydrogen Gas to the main Balloon . . . 64
3.14 BEENS payload research group . . . 65
3.15 On screen monitoring of temperature and pressure at Ground station of National Balloon Facility . . . 65
3.16 Real Time monitoring of BEENS payload data at the ground station of National Balloon Facility . . . 66
3.17 Balloon Flight operational corridor . . . 67
3.18 Crew members working on recovery of BEENS payload . . . 69

4.1 Schematic of BEENS gondola . . . 72
4.2 Performance of probe—electrometer system prior to launch . . . 73
4.3 Altitude profile of BEENS gondola . . . 74
4.4 Spatio-temporal variation of ambient wind speed and wind direction . . . 75
4.5 Electrometer gain - set and reset . . . 76
4.6 Output of Fluxfate magnetometer . . . 77
4.7 Thermal IR image from EUMETSAT . . . 78
4.8 BEENS: payload rotation . . . 79
4.9 Raw signal ouput form x- and y- channels . . . 81
4.10 Simulation depicting the effect of capacitance . . . 84
4.11 Simulation depicting the effect of sampling rate . . . 84
4.12 Effect of high frequency noise . . . 86
4.13 Temporal variation of raw output from vertical probe . . . 87

4.14 Raw output and running mean from x- and y- channels 89
4.15 Double proube output from BEENS expeiment 90
4.16 Horizontal electric field vectors derived from 1-2 and 3-4 probes 92
4.17 Electric field components derived from y- probe output 94

5.1 Schematic representation of Schumann resonance 103
5.2 Block diagram of SR experimental setup at Maitri 108
5.3 Anually averaged amplitude spectra over Maitri 110
5.4 Anually averaged diurnal amplitude variation of the SR mode-1 112
5.5 Anually averaged dirunal frequency variation of the SR mode-1 113
5.6 Mean Diurnal-Seasonal Amplitude variation of the NS component of SR mode-1 115
5.7 Mean Diurnal-Seasonal Amplitude variation of the EW component of SR mode-1 116
5.8 Mean Diurnal-Seasonal Frequency variation of the NS component of SR mode-1 121
5.9 Mean Diurnal-Seasonal Frequency variation of the EW component of SR mode-1 122

List of Tables

5.1 Schumann Resonance Amplitude and Phase 118

5.2 Schumann Resonance Frequency 119

Chapter 1

Introduction: Overview and Fundamentals

1.1 Historical Overview

The knowledge of electromagnetic environment of Earth dates back to several hundreds of years. In ancient times understanding of nature‘s electrical phenomena such as lightning and auroras is in fascination and frightening throughout time. During those times it was believed that the gods were responsible for these unexplained natural phenomena. The Earth‘s magnetic field was given recognition several centuries ago. The luminous phenomena in the arctic sky observed by Gassendi in 1623 and he named it as ‘Aurora Borealis’. Gellibrand in 1634 noticed the slow variations of the terrestrial magnetic field. These observations made the scholars to suggest all sorts of hypotheses.

In 1722, Graham, a clockmaker of London observed the first minute fluctuations in the direction of the compass needles. After 20 years Hiortier and Celsius in Uppsala made the great discovery confirming the lhypothesis of Halley‘s in 1716 that magnetic fluctuations were accompanied displays of the Aurora. Under the leadership of Humboldt the systematic study of Earth‘s magnetic fields was laid out by Gauss, Weber, and later Airy. The knowledge of the magnetic field has broadened

since the time of systematic measurements of Earth‘s magnetic field at observatories around the world.

Our understanding of the Earth‘s atmospheric electrical phenomena was studied by Ben Franklin in 1750. Ben Franklin first identified the large electric fields associated with thunderstorms and lightning. In 1952 Lemonnier discovered atmospheric electrical effects in fair weather. The detection of electric charge in a clear atmosphere was reported by John Canton in 1753. Lord Kelvins water dropper electric field sensor marked and advancement of atmospheric electrical sensors in the mid-nineteenth century. The continuous measurement of the electric field at Kew Observatory, London in 1861 was made possible by water dropper combined with the newly discovered method of photographic recording (Everett [1868]; Harrison and Aplin [2002]).

Many researchers have observed continuous and varying electric field in the atmosphere. In 1905 Gerdien found that air was weakly electrically conductive. This implied the presence of an atmospheric electric current. In 1906, Nobel Prize winner C. T. R. Wilson predicted the source of the fair weather electric field is from the flow of vertical current through the electrically resistive atmosphere. Wilson gave the concept of a global electrical circuit and the description of the sensor capable of measuring vertical current density, as well as the associated electric field. The discovery of the universal global diurnal variation in electric field during

1915 - 1928 Carnegie ship suggested a global source of diurnal variation of surface electric field. In 1929 Whipple demonstrated the global source is directly related to the intensity of global thunder storm activity. Large scale atmospheric electric currents are deduced only with long term averages from the measurements at the Earth's surface. With the advent of Balloon-borne, rocket-borne, satellite borne measurements it became possible to conduct experiments above the turbulent layer of the atmosphere. These measurements had been possible only in the last 50 years using tethered balloons, satellites, rockets and flights. Since then many Langmuir probe experiments were conducted using rockets to measure the auroral-zone electric fields by many researchers (Mozer and Bruston [1967]; Aggson and Evans [1968]; Kelley et al., [1968a,b]; Potter [1968]; Mozer and Fahleson [1968]; Főppl et al., [1968]; Wescott et al., [1968], to state a few). These experiments could not yield sufficient results of worldwide dc electric field patterns. Coroniti [1968]and Sagalyn and Fitzgerald [1965]measured the vertical electric field using balloon with fields associated with atmospheric electricity, thunderstorm and weather processes. In 1968, Kellogg and Weed proposed theoretical concept of measuring large scale horizontal ionospheric and magnetospheric convection electric fields at the stratosphere with little attenuation using Balloon. Mozer and Serlin (1969) first demonstrated the measurement of large scale horizontal electric fields of magnetospheric origin. Later experiments from Holzworth et al., [1985] and Kelley et al., [1985] showed the effects of thunderstorms extended well upto the ionosphere.

The balloon measurement over thunderstorms in the stratosphere (Holzworth et al., [1986]) during solar activity (Holzworth et al., [1987]) and from the ground (Williams and Heckman [1993]) and the results from the rocket experiments (Kelley et al., [1985, 1990]) shows the perturbations of electric fields generated by lightning penetrating up to 400 km showed significant amount of electrical energy is deposited by thunderstorm in the ionosphere.

To understand the dynamics of both neutral and charged atmosphere, the knowledge of electric field at altitudes from clouds to outer space is very important. Thus, in situ measurements of the vector electric field by balloon, rocket, and satellite platforms are required to enhance our understanding of the Earth's electric field.

This work is on electric field measurements with balloons at stratospheric heights. The chapter begins with historical overview of using balloon as a platform to conduct different experiments. Section 1.2 gives a brief introduction on the Earth's atmosphere. Section 1.3 and 1.4 provides an overview on the atmospheric electrical conductivity and global electric circuit. Section 1.5 summaries the outline of thesis.

1.2 The Earth's Atmosphere

The influence of gravity makes the atmosphere and ionosphere horizontally stratified. The Earth's atmosphere can be classified based on the variation in

altitude profile of various factors like temperature, composition, state of mixing, and ionization (refer Figure 1.1)

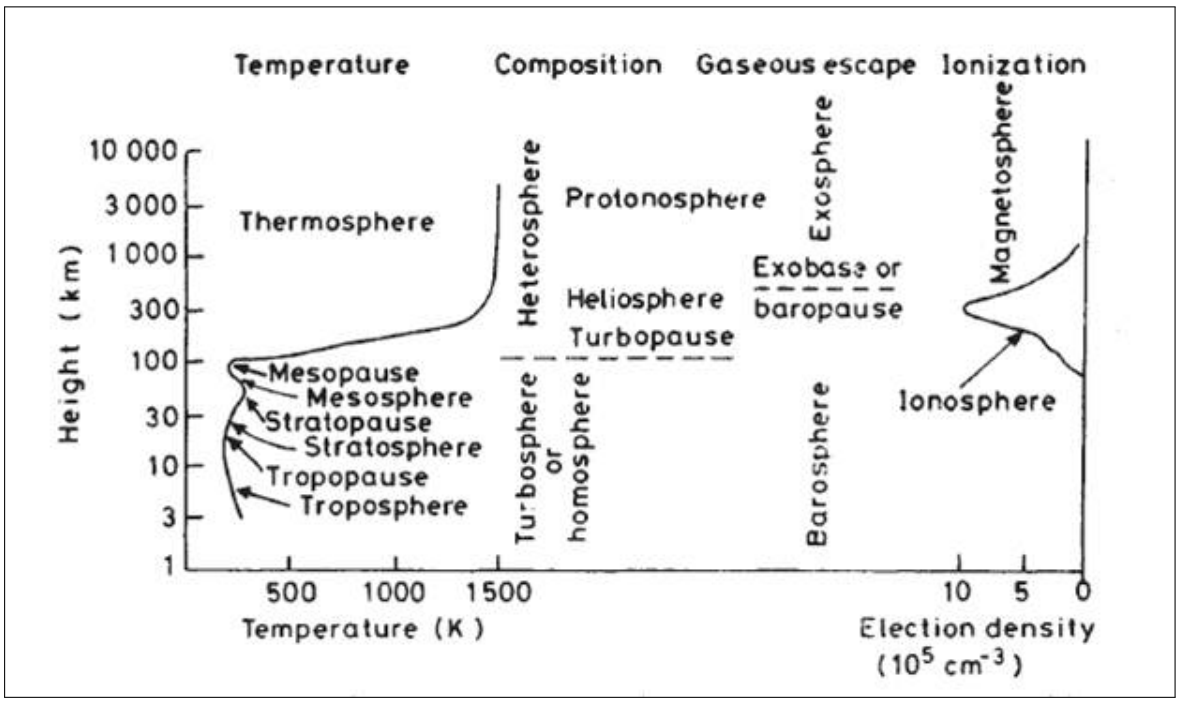

Figure 1.1: Nomenclature of atmosphere based on temperature, composition, mixing and electron density (reproduced after Hargreeves [1992])

The atmospheric temperature initially starts to decrease with a lapse rate of 6.5 K/km in the troposphere, first layer from the surface. The temperature trend reverses in tropopause and varies from about 9 km in the polar region to about 17 km in the equatorial region, from where the stratosphere begins. This increase in temperature with height is due to the absorption of solar UV radiation by ozone. The temperature reaches to maximum at 50km (stratopause), where the temperature trend again reverses at the stratopause and the mesosphere begins. Due to the radiative cooling temperature decreases sharply to a minimum of ~180 K near the mesopause at ~85 km. In thermosphere the temperature increases due to absorption

of higher energy solar UV radiation reaching an average temperature of 1500 K, which is quite variable. The region below ~100 km is realtively uniform due to turbulent mixing phenomena and is known as the homosphere or turbosphere. The region above turbosphere, molecular diffusion becomes important, known as heterosphere. Homosphere and Heterosphere are separated by turbopause. From troposphere and lower stratosphere, $<$ 15 km, is termed as lower atmosphere, upper stratosphere and mesosphere, 15- 90 km, is termed as middle atmosphere and upper atmosphere above 90 km (ionosphere).

1.3 Atmospheric Conductivity

With the advent to balloon borne and airborne measurements it was possible to understand the atmospheric electrical properties. The atmosphere below about 50 km is conducting due to the presence of both cosmic rays and the natural radioactivity of the Earth. The primary contributors to the conductivity of the lower atmosphere are the ions whose life times are of the order 100 seconds. The contribution from the electrons below 50 km can be neglected as their lifetime is of the order of microseconds (Gringel et al., [1986]; Reid [1986]). Cosmic rays are responsible for most of the ions in fair weather atmosphere. The ionization rate depends on the magnetic latitude and on the solar activity.

The current density, J, and the electric field, E, are related by Ohms law by

$$J = \sigma E$$

Where σ is the conductivity of atmosphere. In the lower atmosphere and most of the middle atmosphere, σ is scalar. Above 60 km, collision between electrons and neutral becomes infrequent enough that the bending of the electrons by the Earth's magnetic field becomes appreciable between collisions and motion perpendicular to the field becomes less easy than motion along the field. Conductivity varies from day to night due to the absence of solar ionizing radiations and changes in neutral chemistry.

The electrical conductivity of atmosphere at sea level is about 10^{-14} S/m and increases exponentially with altitude. The conductivity varies at all altitudes by more than one order of magnitude depending on conditions like the presence of aerosol, presence of clouds (Bering et al., [1980]; Holzworth et al., [1986]; Hu et al., [1989]; Pinto et al., [1988]), and latitude variation of conductivity. The latitude variation of conductivity can be explained by the variation of cosmic ray rigidity cutoffs (Norville and Holzworth [1987]). That is, cosmic ray must have higher energy to reach the equatorial atmosphere than it needs to reach the polar atmosphere because the Lorentz force will deflect the particle more efficiently if it is entering the magnetosphere perpendicular to the magnetic field. At a height of

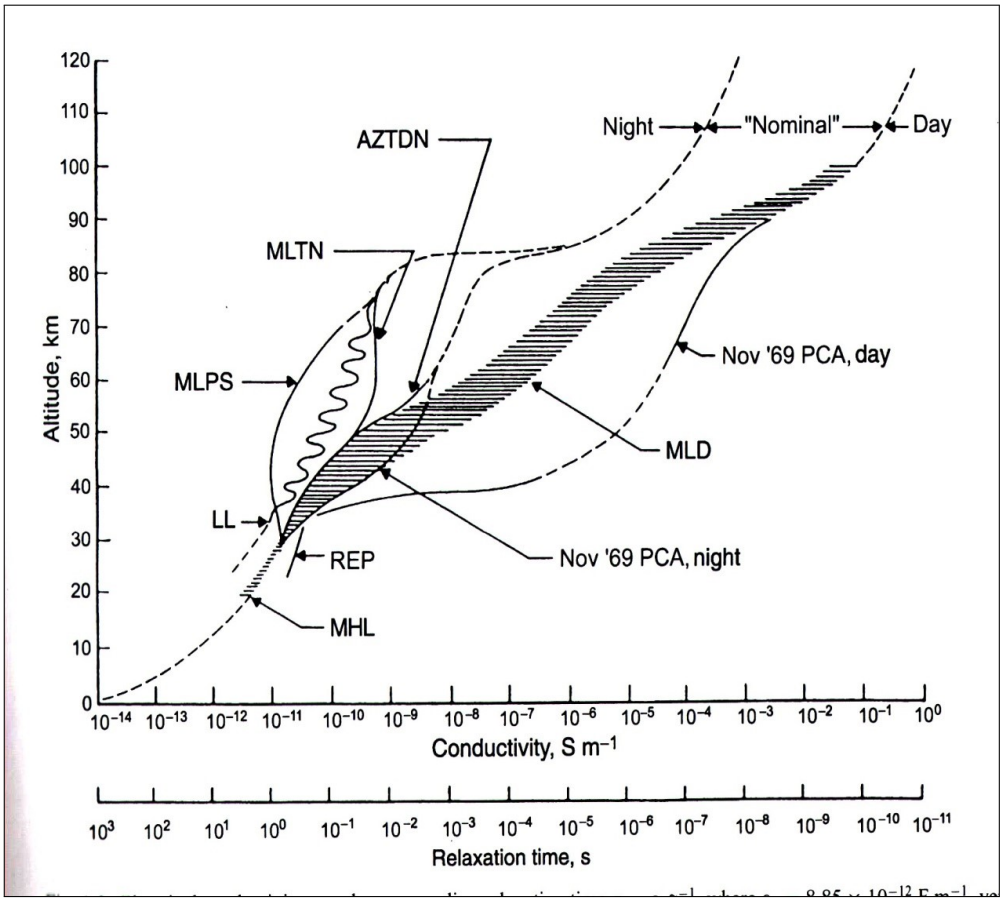

Figure 1.2: Electrical conductivity as a function of altitude (reproduced from (Hale [1984])

35 km, the air density is about one percent of that at the Earth's surface. The electrical conductivity is greater than 10^{-11} S/m, which is more than three orders of magnitude higher than at sea level. Figure 1.2 illustrates the conductivity variation up to an altitude of 120 km. Holzworth and Mozer (1979) and Holzworth et al., (1987) have shown that the solar flare can have a direct effect on the stratospheric conductivity which can result in enhanced conductivity of few orders of magnitude.

1.4 Global Electric Circuit

The highly conductive Earth‘s surface and the ionosphere form a spherical capacitor with a thin insulating air between them established global electric circuit (for example Roble and Tzur [1986]; Bering III [1995]; Rycroft et al., [2000]; Williams [2003, 2009]; Markson [2007]; Siingh et al., [2007]). This geometry of spherical capacitor is responsible for the presence of both the DC global circuit and ionospheric potential, and the electromagnetic wave guide of the AC global circuit and Schumann resonances.

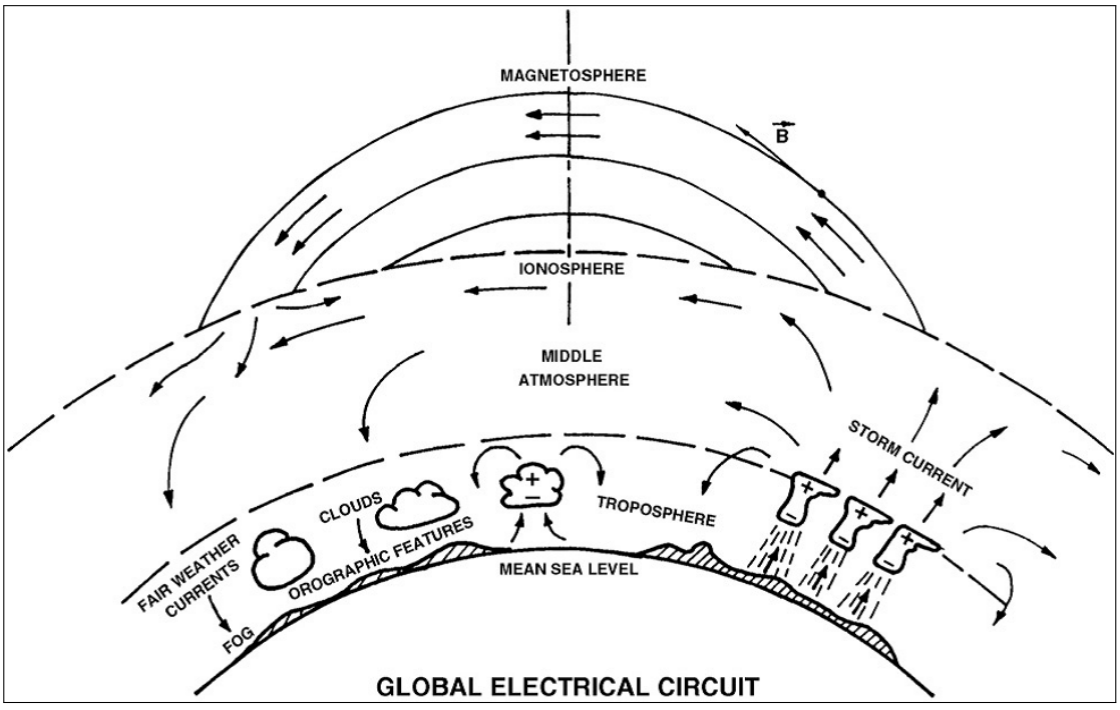

Figure 1.3: Schematic diagram of various electrical processes in the global electric circuit. The vector B shows the direction of the Earth‘s geomagnetic field, and arrows show the direction of the current flow in the regions of the tropospheric, ionospheric and magnetospheric /generators (courtesy of Roble and Tzur [1986])

Wilson (1920) first suggested that thunderstorms support global electric circuit by driving positive charge upwards to the ionosphere and negative charge downwards to the Earth's surface. This is the classical hypothesis of global electric circuit put forth by Wilson. The simple dipole model of a thunderstorm with a positive over negative charge structure would drive charge in the direction to keep the Earth - ionosphere capacitors charged as illustrated in Figure 1.3.

Typical properties of the fair-weather atmospheric electric circuit are surface potential gradient (E) is 130 V/m, vertical conduction current density (J_z) is 3 pA/m^2, air conductivity (σ) is 20 fS/m (at mean sea level), ionospheric potential (V_I) is + 250 kV, total resistance of the atmosphere (R_T) is 230Ω, total air-earth current is 1800 A and columnar resistance (R_c) is 120 PΩm^2.

1.4.1 DC Circuit

Thunderstorm clouds are both a DC battery and an AC generator in the global electric circuit. At any given time ~1000 thunderstorms active, generates an upward DC (Wilson) current of ~1 A to the ionosphere, which is an excellent conductor, at an equipotential of ~250 kV with respect to the Earth (Rycroft et al., [2000]; Singh et al., [2011], for example). The conduction current flows down in areas remote from thunderstorms, termed regions of fair weather (non-cloudy).

The atmospheric electrical conductivity increases exponentially from the ground. The increase of electrical conductivity of the neutral atmosphere from the Earth‘s surface up to the lower ionosphere is of seven orders in magnitude (Rycroft et al., [2000]; Rycroft and Odzimek [2010]). Thus it can be emphasized that conductivity profile is the most important parameter in establishing the global electric circuit (Holzworth et al., [1987]; Rycroft et al., [2008]).

The conductivity (σ) and the electrical conduction current J_z density are related by Ohm‘s law. This electric field points downwards and the potential gradient (PG) is conventionally considered positive in fair-weather (~130 V/m) at the Earth‘s surface. The atmospheric vertical electric field reduces in magnitude going up in to the atmosphere. The ionospheric potential V_I can be estimated by integrating measurement of the vertical electric field (E) made by balloon or aircraft borne instruments from the surface to the ionosphere (Markson [1986]).

1.4.2 AC Circuit

Lightning is the important source of AC electromagnetic waves within the ionosphere and magnetosphere global circuits. Lightning couples the troposphere to the Earth‘s plasma environment. The electromagnetic waves emitted by cloud-ground (CG) lighnting flashes known as atmospherics or ‘sferics′ for short, are stong in the extremely low frequency (ELF, 3 Hz - 3 kHz), Very low frequency (VLF, 3

kHz - 30 kHz) and low frequency (LF, 30 kHz - 300 kHz) bands. In the ELF band, Schumann resonances (SR) of the Earth - ionosphere cavity are excited at 8, 14, 20, 26, Hz . The Earth ionosphere waveguide exhibits a cut-off at ~1.8 kHz, and at higher harmonics, which explains the distinctive frequency - time characteristeics of nigh time sferics, termed tweeks (Kumar et al., [2009]).

The ELF radiation by lightning offers a direct method of monitoring the temporal variation of terrestrial lightning. Williams (1994), has shown that lightning flash rates are proportional to temperature and it has been suggested that the SR could offer a method of monitoring global temperature (Williams [1992]). The advantage of using SR is that measurements can be made at the surface in electromagnetically quiet regions and short - term temporal changes can be monitored (Mărcz et al., [1997]). Study of AC aspects of the global circuit is also unaffected by continental aerosol, which contributes variability in the columnar resistance of the DC global circuit.

1.5 Outline of the Thesis

Chapter 2 details the instrumentation used to measure the electric field at stratospheric height. Chapter 3 discusses on the experimental procedures carried for the launch of BEENS experiment. The results of vector electric field measurements at an altitude of 35 km are presented in Chapter 4. The diurnal and seasonal variation

of Schumann resonances measurement carried out at Maitri, Antarctica during 2011 results are given in Chapter 5. Chapter 6 deals with summary of the results of vector electric field measurements form balloon experiment and ground based measurement of Schumann resonances and introduces to the modifications to be done for the next balloon experiment.

Chapter 2

Instrumentation

2.1 Introduction

The BEENS instrumentation includes probes to measure electric fields and magnetic fields. The electric field instrument measures vector electric fields from dc to 1 kHz with a range of few mV/m to 4 V/m. The search coil magnetometer was used to measure the ac magnetic fields from dc to 16 kHz. The fluxgate magnetometer was used to provide the orientation for the measurements of the electric and magnetic fields measured relative to the geomagnetic field. The spherical spheres are electric field probes.

2.1.1 Need for a High Input Impedance Electrometer

Electric field measurements are difficult since the atmospheric resistance is so large. Mozer and Serlin (1969) computed this resistance between the atmosphere and a charge collecting probe to be

$$R_{atm} = m_i \nu_i / 4\pi n_i e^2 r_o$$

Where m_i is the ion mass, ν_i is the ion-neutral collision frequency, n_i is the ion density, e is the electronic charge of the electron, and r_o is the radius of a spherical probe. Hence, for a 30 cm diameter sphere (r_o=15 cm) at the surface of the Earth $R_{atm} \approx 10^{13}\Omega$, and at 32 km altitude $R_{atm} \approx 10^{11}\Omega$ (Mozer and Serlin [1969]).

To measure the potential difference between two points in the stratosphere accurately, the input impedance of the electronics R_{in} must be sufficiently high. If the input impedance is low compared to the atmospheric resistance R_{atm}, then the probes will short out the field that is to be measured. Thus to accurately measure the stratospheric electric fields the input impedance of measuring electronics must be greater than atmospheric resistance (Rin≫Ratm) (Mozer and Serlin [1969]).

To accomplish this impedance transform, a high input impedance to low output impedance instrumentation amplifier (INA116) is connected to the probe. The gain of the instrumentation amplifier can be adjusted to 1, 10 and 100 by sending ground command using a single external resistor. The datasheet of the INA116 confirms the input impedance of the instrumentation amplifier to be $10^{14}\Omega$, and thus $R_{in} > 10^{3}\Omega x R_{atm}$ which is more sufficient for accurate field measurements with a few percent.

2.2 Designing of an Electrometer

An electrometer is a highly sensitive voltmeter whose input impedance is of the order of $10^{15}\Omega$ and the current flowing through it can be considered to be zero. Due to very high input impedance, a special design technique has to be considered to avoid errors such as loading errors, external shunt resistance and input bias current(Keithley [2004]).The discussion of these error source and ways to minimize their affects are discussed in the following sections.

2.2.1 Input Resistance Loading

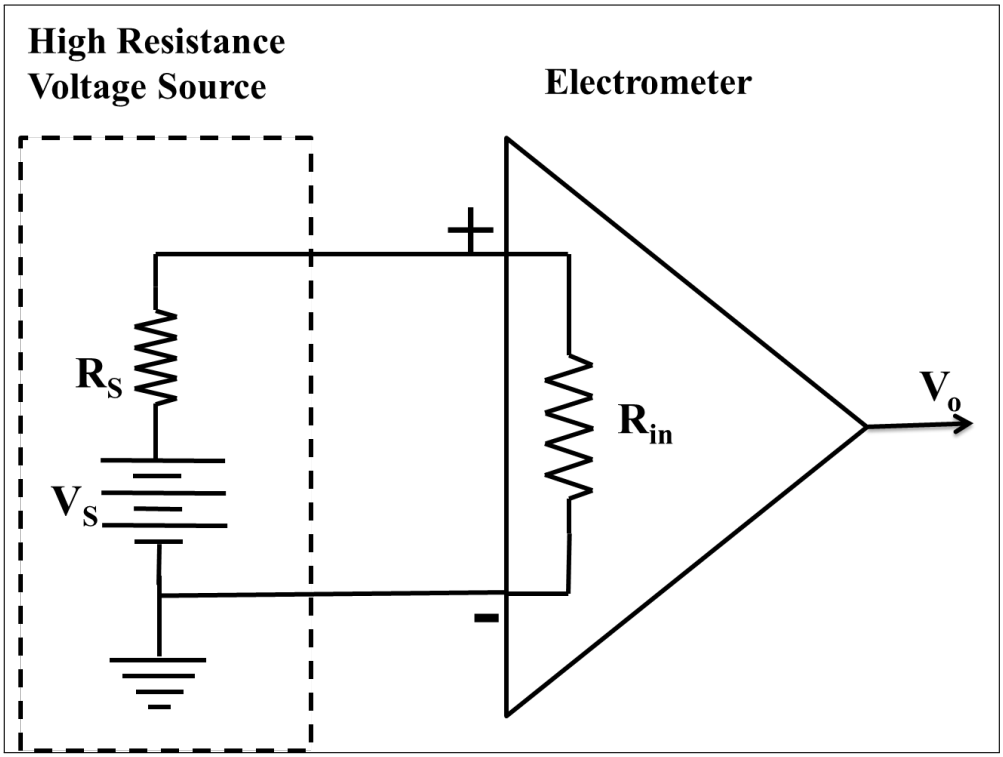

Figure 2.1: Effects of input resistance loading on voltage measurement accuracy

Consider a source with the voltage, V_s, with the source input resistance

R_s connected in series with the input of the high input impedance pins of the electrometer whose input resistance is R_{in}. This configuration is like a voltage divider circuit as shown in figure 2.1. With this configuration the measured voltage across the input terminals is given by,

$$V_m = V_s(R_{in}/(R_s + R_{in}))$$

For example, with R_s=100kΩ and R_{in} = 10MΩ. If V_s=5 V, the voltage measured by the meter is:

$$V_m = 5(10^7/(10^5 + 10^7))$$

$$V_m = 4.95V$$

Thus, input resistance loading would result in an error of 1% in this example. So for higher accuracy voltage measurements the input resistance of the electrometer used should be much higher than the source resistance.

2.2.2 Input Bias Current Loading

Another important consideration while measuring voltages from high resistance source is the input bias current of the electrometer. The bias current is generated from the internal circuit of the electrometer integrated circuit (IC). This input bias current which flows develops an error voltage across the source resistance

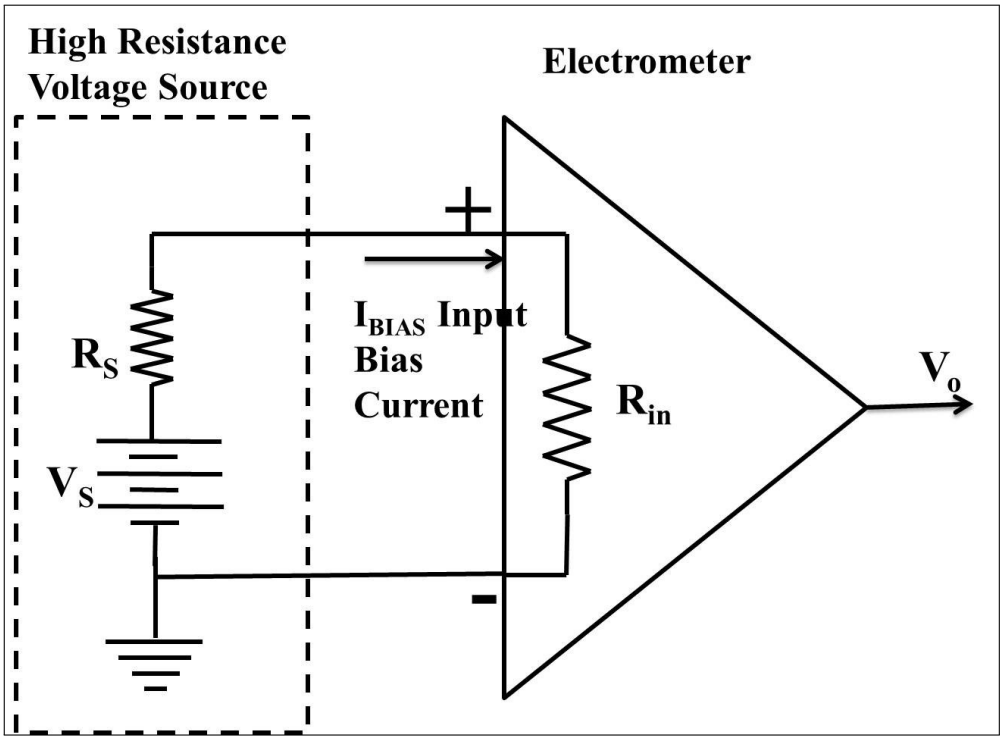

Figure 2.2: Effects of input bias current on voltage measurement accuracy

Rs. Thus the measured voltage (V_o) differs from the source voltage (V_s) as

$$V_o = V_s \pm I_{bias} * R_s$$

For example, if $I_{bias} = 1pA$, $R_s = 10\ G\Omega$, $V_s = 10\ V$, then

$$V_o = 10 \pm (10^{-12} * 10^{10})$$

$$V_o = 10 \pm 0.01 = 9.99V or 10.01V$$

An error of 0.1 % is resulted in the voltage measurement in this example.

2.2.3 Shunt Resistance Loading and Guarding

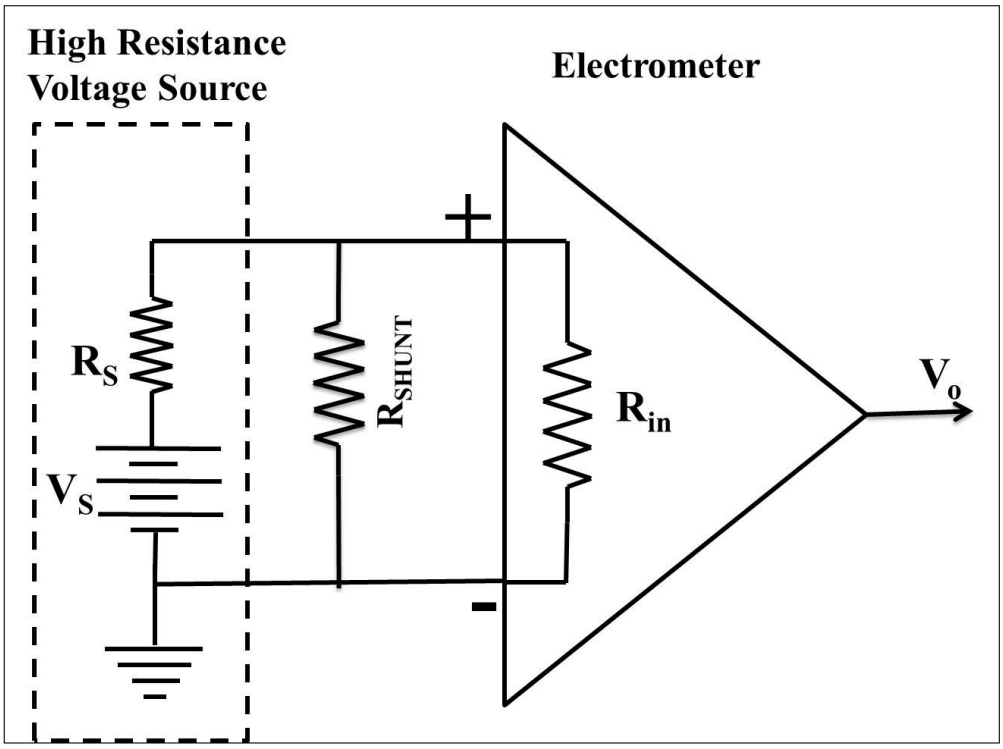

Figure 2.3: Effects of shunt resistance on voltage measurement accuracy

The external shunt resistance due to leaky cables and dirty insulators also causes loading errors in the high resistance voltage measurements. This external shunt resistance across the source voltage will attenuate the voltage measured. Figure 2.3 shows the equivalent circuit with external shunt resistance R_{shunt} and the source resistance R_s.

From Figure 2.3 shows that, it forms a voltage divider circuit as

$$V_o = V_s\left(\frac{R_{shunt}}{(R_{shunt} + R_s)}\right)$$

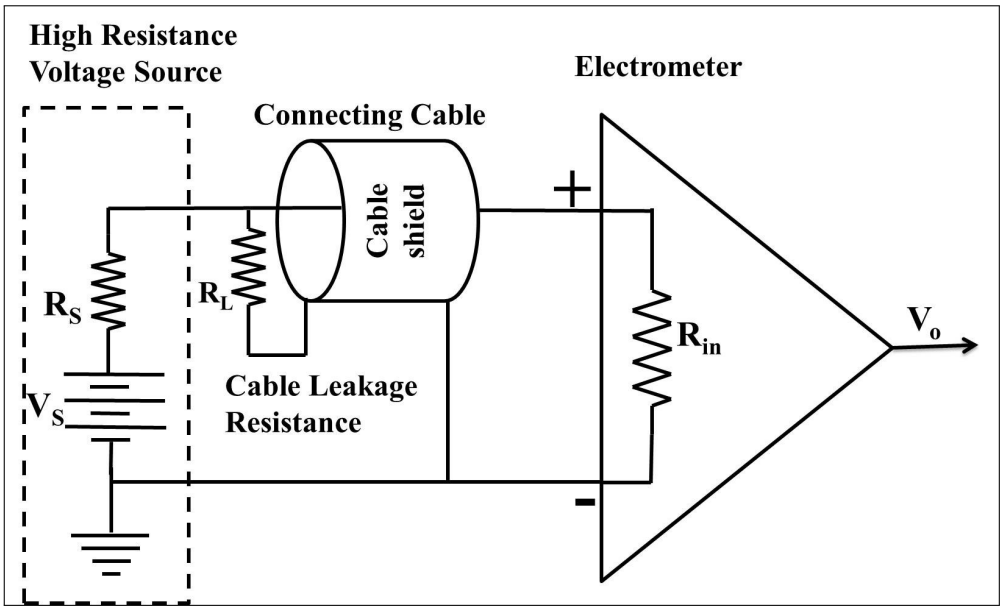

Figure 2.4: Effect of cable leakage resistance on voltage measurement accuracy

The cable leakage resistance is another common source of shunt resistance which causes loading error as shown in the figure 2.4. By using high insulation resistance for cables, connectors and test fixtures, the errors due to shunt external resistance can be minimized.

Guarding is another way of minimizing the errors due to cable leakage. Figure 2.5 shows the implementation of guard to the cable.

Guard creates low impedance point in the circuit which is at the same potential as the high impedance input terminal. In addition to this, the effective cable capacitance is also reduced making the response speed of the circuit faster. The electrometer in voltage mode is accompanied with guard amplifier. The Guard

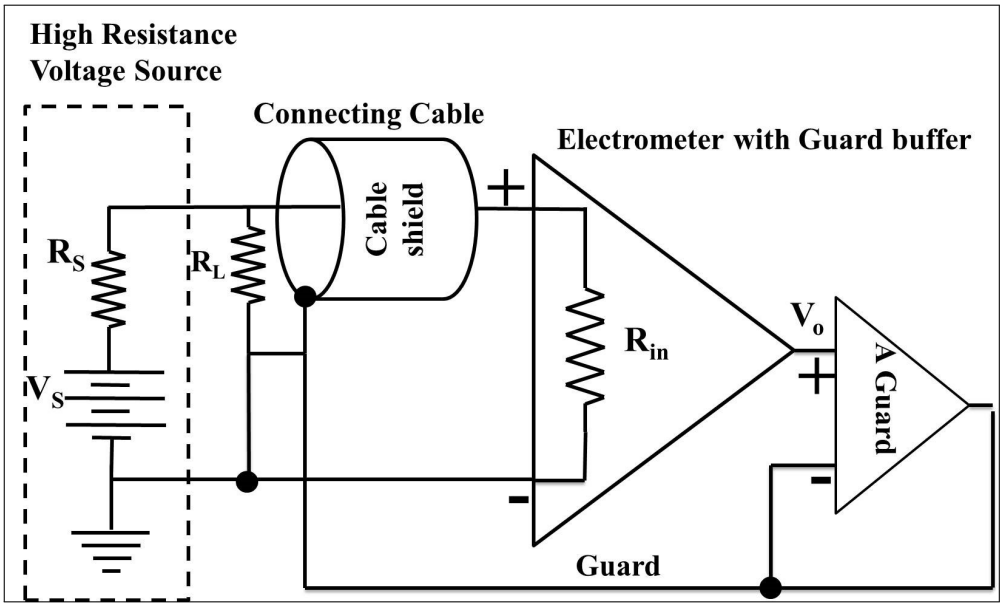

Figure 2.5: Guarded configuration to minimize error in measuring voltage

amplifier is a unity gain follower with very high open loop gain of the order of 10^4 to 10^6. The output voltage is given by

$$V_o = V_s\left(\frac{A_G * R_L}{(R_s + A_G * R_L)}\right)$$

The multiplication of gain with cable leakage resistance, the error is reduced considerably.

2.3 Insulation Resistance

High resistance voltage measurements are subjected number of error due to number of factors discussed earlier in this chapter. Another important requirement for the successful measurements from electrometer is the knowledge of the insulation

resistance. This plays an important role in designing an electrometer. There are number of insulator available in the market. Not all insulators will give better insulation resistance while measuring with high input resistance source. The insulation leakage resistance of the cable, connectors and other test fixtures must be several orders of magnitude higher than the Thevenin equivalent resistance of the circuit under test/measurement. If the insulation resistance is not higher, then the shunting effects of the insulation will reduce the source voltage being measured. The most widely used insulation in the measurement from high resistance source is Teflon. Due to its high volume resistivity and water vapor film do not form readily on its surface. Teflon insulation properties are not severely impaired by humid air. It is chemically inert, can be readily cleaned. Teflon PTFE is the type of Teflon most commonly used in electronics.

The most important factor must be kept in mind while using insulators with high input resistance measurements is to keep it clean always. Any mishandling can destroy the integrity of insulators. The oils and salts from the skin can degrade the insulator performance. Contaminants in air deposited on the insulator surface and reduce its resistance. Therefore, insulator handling should be minimized. Under no circumstances the insulator to be touched with the hand or with any material that might contaminate the surface. If the insulator becomes contaminated either through careless handling or from deposits, it should be cleaned with cotton dipped in methanol.

2.4 Working with High Impedance Op-Amps at EGRL, Tirunelveli

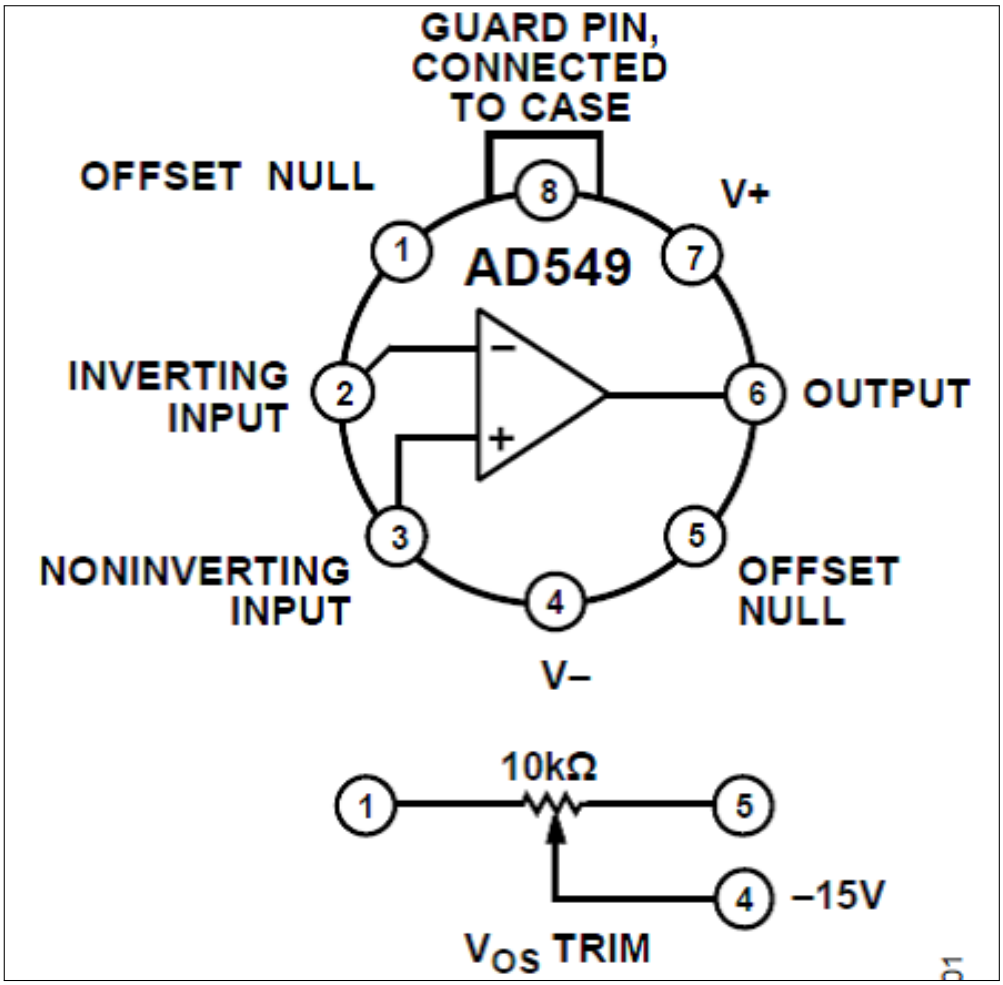

Figure 2.6: Pin out diagram of AD549

For the measurement of voltage from high resistance source would require a special type of operational amplifiers. The main requirement of an operational amplifier for these types of high resistance source voltage measurements, it should have very high input impedance in the order of 10^{15} ohms. It has already discussed in earlier section of this chapter about the errors occurring due to the very high input impedance and also steps to minimize these errors by adopting certain measurement techniques. There are few operational amplifiers available

commercially which could be used as an electrometer for the measurement of atmospheric electric field. AD549, OPA128, INA116 are the few electrometer grade operational amplifier which are used in Equatorial Geophysical Research Laboratory (EGRL), Tirunelveli to study the atmospheric electric field.

An Anti-Electrostatic laboratory was established at EGRL, Tirunelveli for handling these high static sensitive devices. The electrostatic laboratory consists of electrostatic workstation table, chair, electrostatic mat, soldering station with electrostatic compatible. The whole laboratory was grounded using a chemical earthing using a thick copper strip.

AD549 (refer to figure 2.6 for pin configuration) is a monolithic electrometer operational amplifier with very low input bias current. In this op amp both the input offset voltage and input offset voltage drift are laser trimmed for precision performance.

A new technology called Top-gate JFET technology developed by Analog Devices, Inc. gives extremely low input current JFETs compatible with a standard junction isolated bipolar process. Its common mode impedance is of the order of 10^{15} ohms achieved from the bootstrapped input stage, when the input current is independent of the common mode voltage. This op amp is used in the ground based electric field measurements in Indian Institute of Geomagnetism for several

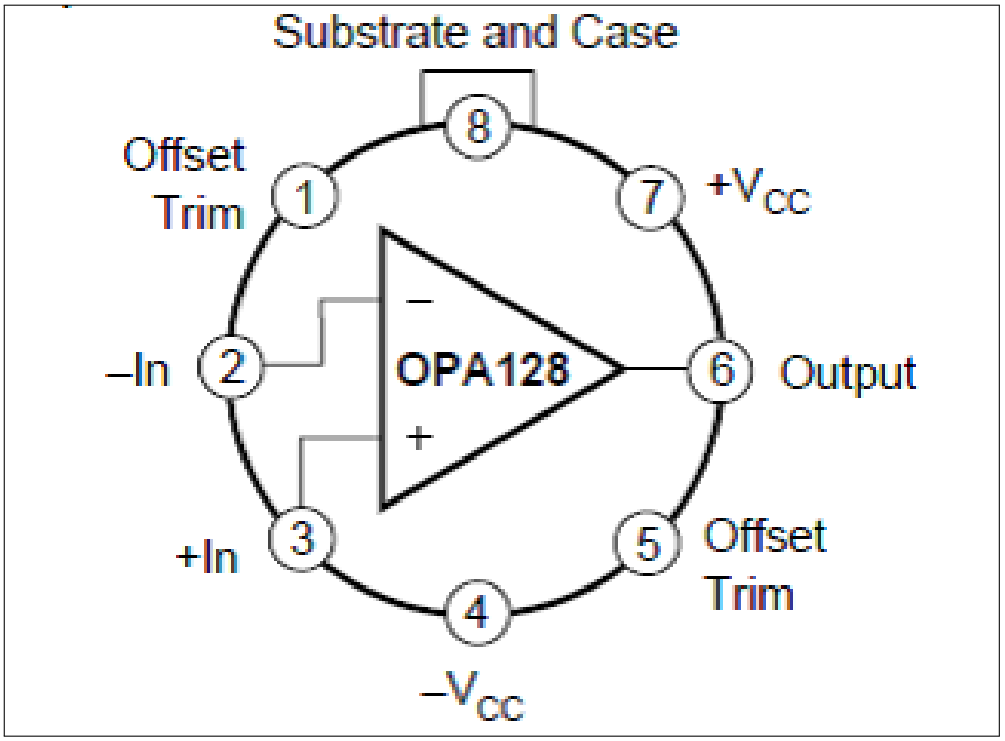

Figure 2.7: Pin out diagram of OPA128

years. Even today the same Op amp is used both at Maitri, Antarctica and Equatorial Geophysical Research Laboratory, Tirunelveli for Global electric circuit measurements. This Op amp is used in current mode at this institute for measuring air-earth current. The offset voltage keeps on changing over time and every time it has to be calibrated. AD549 is very sensitive to static charges due to its very high input impedance. Due to its high sensitivity to static charges there is all possibility that the op amp would give degraded performance if not handled properly when subjecting to tests and measurements.

OPA128 (refer to figure 2.7 for pin configuration) is another ultra-low bias current monolithic operational amplifier. This op-amp uses Dielectrically-isolated FET (Difet) inputs. This Op amp uses Difet technology which eliminates isolation-

junction leakage current which is the main contributor to input bias current using monolithic FETs. Typical monolithic FET op amps inputs must be protected against destructive currents that can flow when input FET gate-to-substrate isolation diodes are forward biased. Most BIFET amplifiers can be destroyed by the loss of -Vcc. Because of its dielectric isolation, no special protection is needed on the OPA128. However, the differential and common mode limits should be observed. Static damage can cause subtle changes in amplifier input characteristics without necessarily destroying the device. This may cause a noticeable degradation of offset voltage and drift.

The electronics used for measuring electric field at balloon altitudes are a pair pre-amplifier from two oppositely separated spherical probes and the output of the pre-amplifier is fed to the low noise differential amplifier with a guard generator. Figure 2.8 shows the block diagram of electric field measurement using balloon platform. To design a single channel electric field measurement in a single package includes a pre-amplifier AD549 or OPA128, an instrumentation amplifier AD620 and guard generator AD628. This led to circuit complication. If any mishandling of the AD549 or OPA128 op amps during the balloon experiment then entire experiment would have failed without any measurements.

An instrumentation amplifier INA116 (figure 2.9 provides information on pin configuration and internal circuit) was identified. This is a monolithic FET input

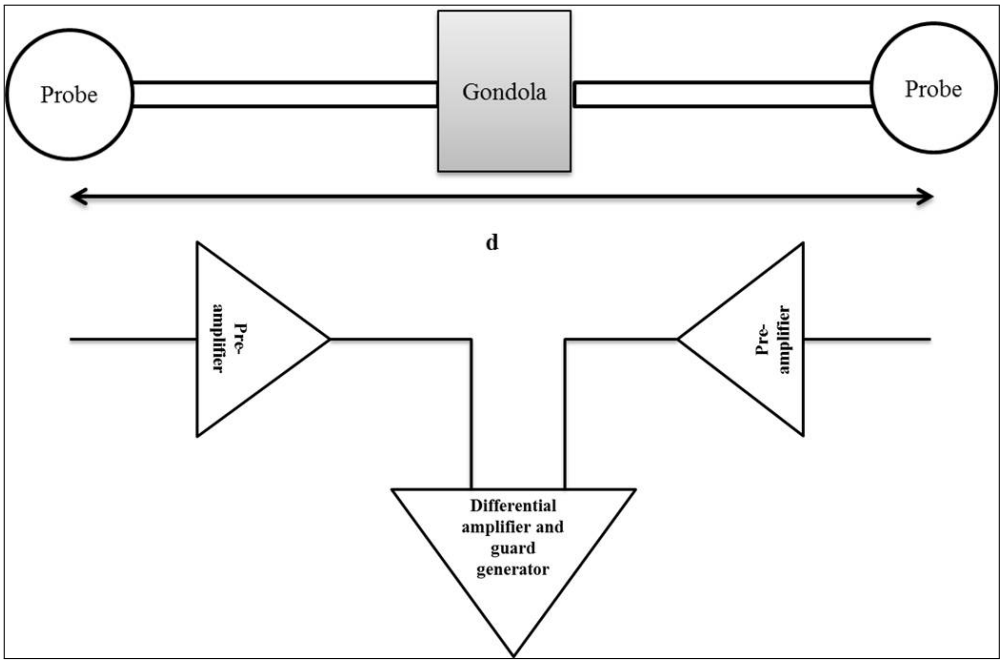

Figure 2.8: Block diagram of electric field measurement using balloon platform and its electronics

instrument ultra-low input bias current instrumentation amplifier. The same Difet technology used in OPA128 and a special guarding techniques yield input bias currents of 3 fA at 25°C and only 25 fA at 85°C. Guard pins adjacent to both input connections are used to drive circuit board and input cable guards to maintain low input bias current.

Gain of the INA116 is set by connecting a single external resistor R_G wherein the gain of the system is given by $G = 1 + \left(\frac{50}{R_G}\right) k\Omega$. INA116 is laser trimmed to achieve low offset voltage drift. Thus this instrumentation amplifier is good choice for our balloon experiment as there is no need of external offset adjustment. The Guard pins are adjacent to both input pins making it easy to guard the critical input terminal layout. Besides, it also provides an additional advantage in drawing PCB

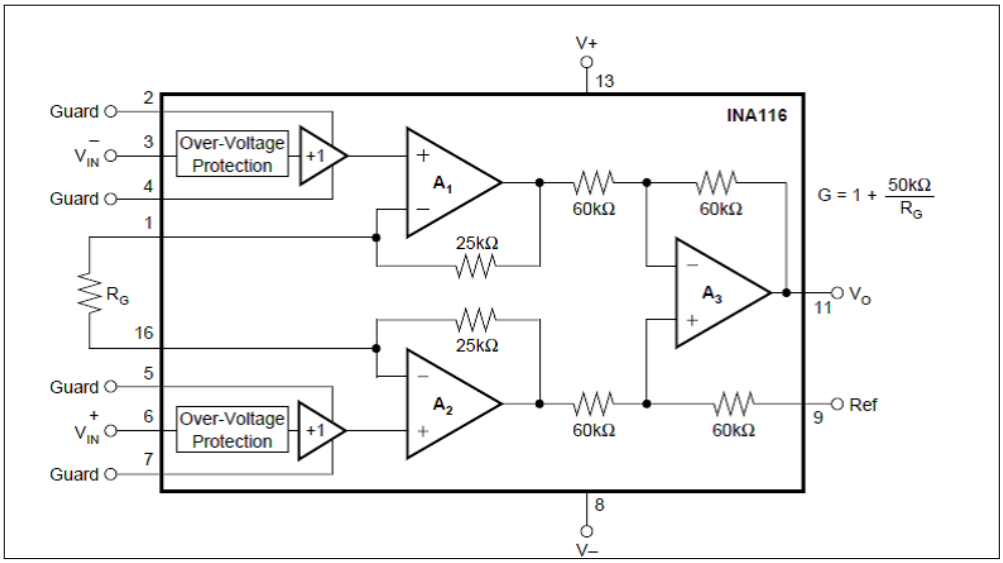

Figure 2.9: Internal circuit and pin configuration of INA116

traces around the input pins without much effort. Figure 2.10 shows the circuit board guard layout.

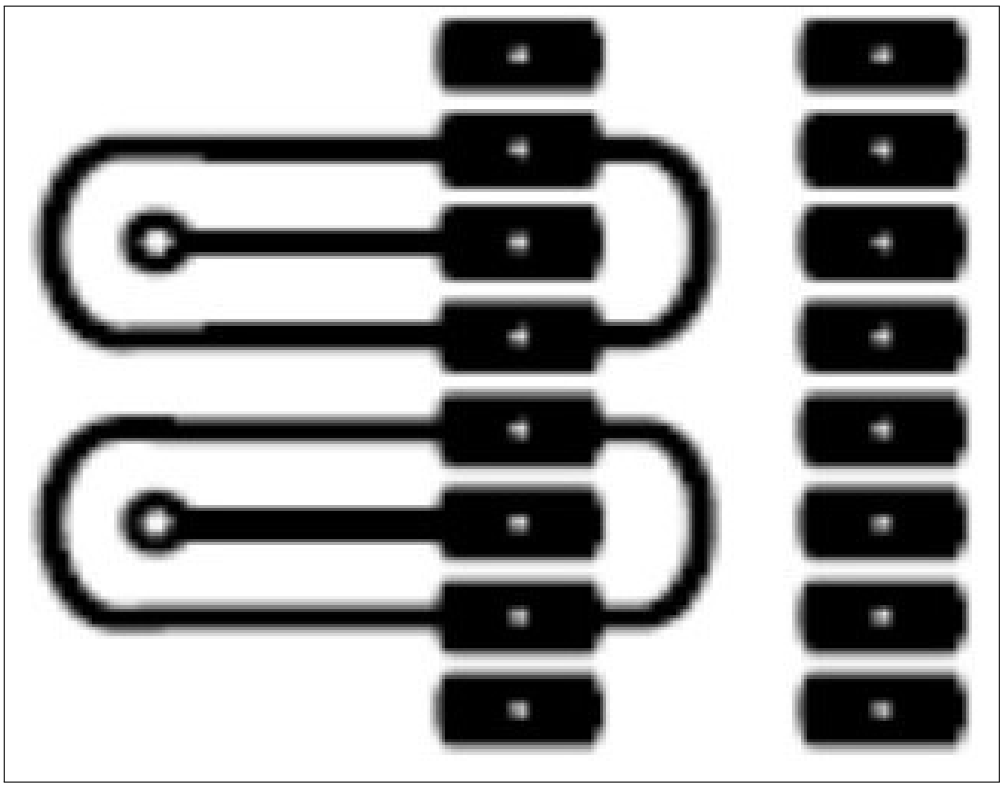

Figure 2.10: Circuit Board Guard Layout used for INA 116

2.5 Double Langmuir Probe Technique

The technique of ionospheric electric field measurements at balloon altitudes has been developed mainly by Mozer (Mozer and Serlin [1969]; Mozer and Manka [1971]; Mozer [1971a,b,c, 1972]). This technique was proposed by Kellogg and Weed (1969). The double Langmuir probe work on the principle of a voltmeter which measures the electric potential difference between two arbitrary shaped probes (Sphere, cylinder and plates) separated in space by distance, d. The probe measures the floating potential with respect to the central payload called gondola. The surface of the area of the probe should be sufficiently large to drive the electronics. Each probe will be surrounded by a plasma sheath and will acquire a potential of the surrounding plasma. The voltage drop in plasma sheath is very difficult to determine theoretically and it may not be equal for differently shaped and differently oriented probes. So the fundamental rule for probe measurements is both the probes to be equally shaped due to the weak fields to be measured. The probes must be as far away from the central payload which may disturb the symmetry of the electric fields around the measuring position.

2.6 BEENS Electric Field Measurement

For electric field measurements in BEENS experiment, spherical spheres made of aluminum of diameter 20 cm were used as electric field probes. The spherical probes were placed on the five booms to give the potential difference measurements of up to few mV to 4 V along two horizontal directions and one vertical direction. The booms made from aluminum and fiber glass. Each side of the boom is around 2.96 m($\pm$ 0.10 m) away from the gondola. The base plates of booms which are attached to the gondola are isolated using Teflon sheets with 3mm thickness. So the booms are electrically isolated from the gondola. Two orthogonal probes in horizontal directions with reference to the fluxgate magnetometers (X- probes and Y-probes) measure the potential difference along horizontal directions. The fifth probe was mounted at the end of another boom that was deployed at an angle of 45° to the horizontal plane, which along with one of the X-probe yielded a measure of the vertical electric field (Z-probe). The tip to tip distance along the two orthogonal directions for the X- probe and Y- probe was found to be 6.92 m and 7.02 m respectively. The vertical distance between Z- probe to one of the X- probes was 2.82 m. All the five sensors were connected to the high input impedance differential amplifier housed inside the gondola by Teflon coaxial cable (RG-188). The coaxial shield is driven by the instrumentation amplifier output to eliminate a voltage drop between the inner and outer conductors of the cable thus preventing a large load capacitance

from forming and at the same time reducing leakage current (see § 2.2 on page 16). The total voltage difference between the probes, divided by the separation distance between the probes is the vector electric field components, E_x, E_y, and E_z. To make the probe work function of the probe to be uniform, all the five probes were painted with Aquadag paint. To make symmetric ground configuration for the probes all the four sides of the gondola were covered with aluminum plates coated with Aquadag paint.

The electric field instruments measure quasi-dc and VLF ac electric fields. This is done using one measurement with different sampling rates and using two different data acquisition systems. For quasi-dc measurement, electric field instrument was connected to multiplexed encoder with sampling rate at 14 samples per second. The VLF ac electric fields were measured using the onboard data acquisition system called Single Board Reconfigurable Input Output (SBRIO) from National instruments (NI).

2.7 Circuit for Atmospheric Electric Field Measurement in BEENS Experiment

As discussed in one of the earlier sections (refer § 2.1.1 on page 14) , a high input impedance operational amplifier is needed to measure the potential difference between two points in the stratosphere accurately due to high atmospheric resistance. For BEENS experiment, an instrumental amplifier INA116 is used to

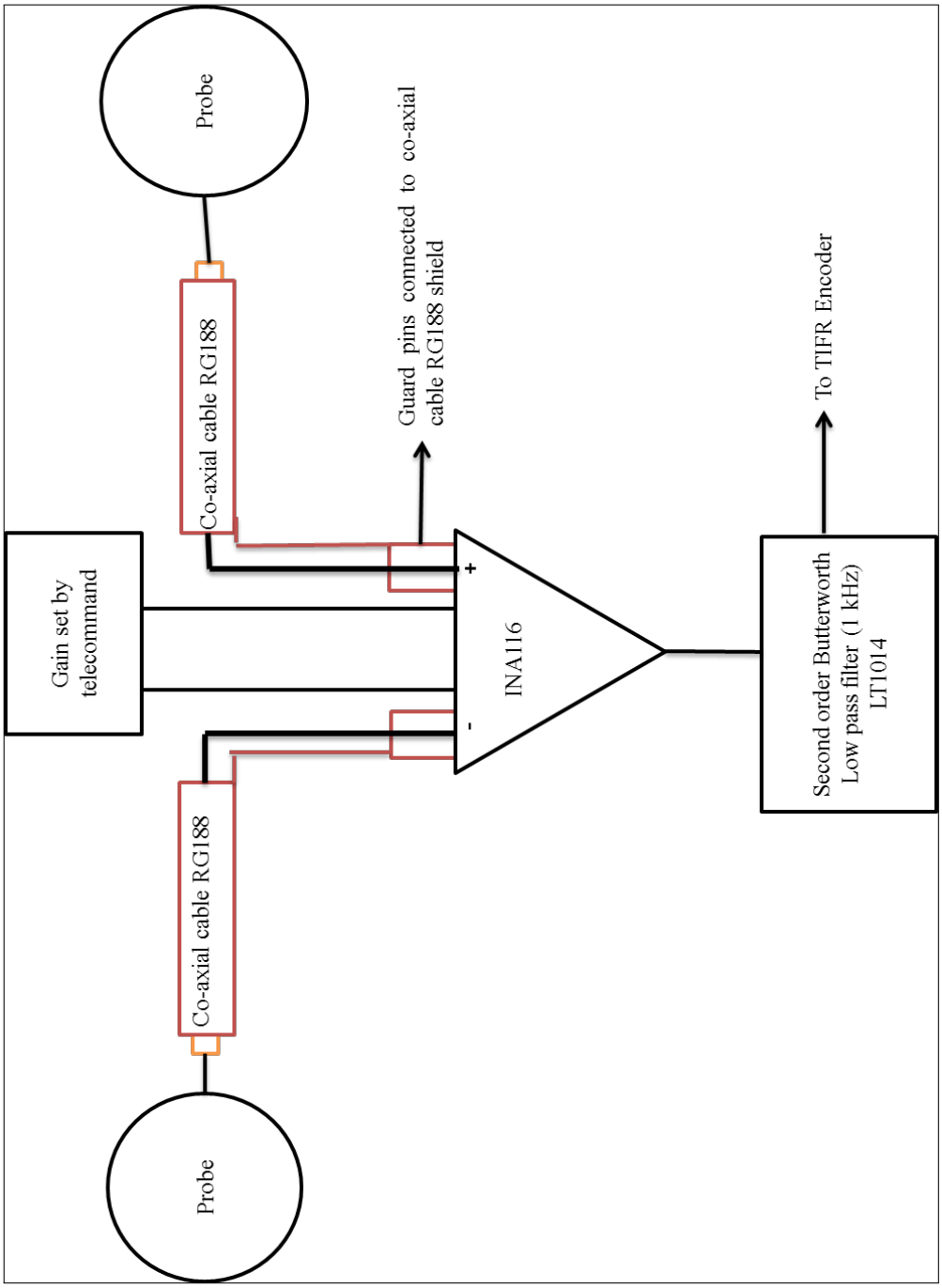

Figure 2.11: Block diagram of electric field experiment in BEENS experiment

measure the potential difference between two points in stratosphere. Its differential input impedance is of the order of 10^{15} ohms which is very much greater than the atmospheric resistance at stratospheric heights. With INA 116 offers voltage follower (with very high input impedance), difference amplifier and guard generator

these entire in one package. This is the first time an instrumentation amplifier is used for the measurement of atmospheric electric field. It is a simple circuit with only one external resistor used for setting the gain. The main advantage in using instrumentation amplifier is there is no external feedback given from the output to the input of op amps. Figure 2.11 shows the block diagram for measuring electric field measurements in BEENS experiment. Appendix A shows the schematics for electric field electronics used in BEENS to measure vector electric field.

2.8 Search Coil Magnetometer

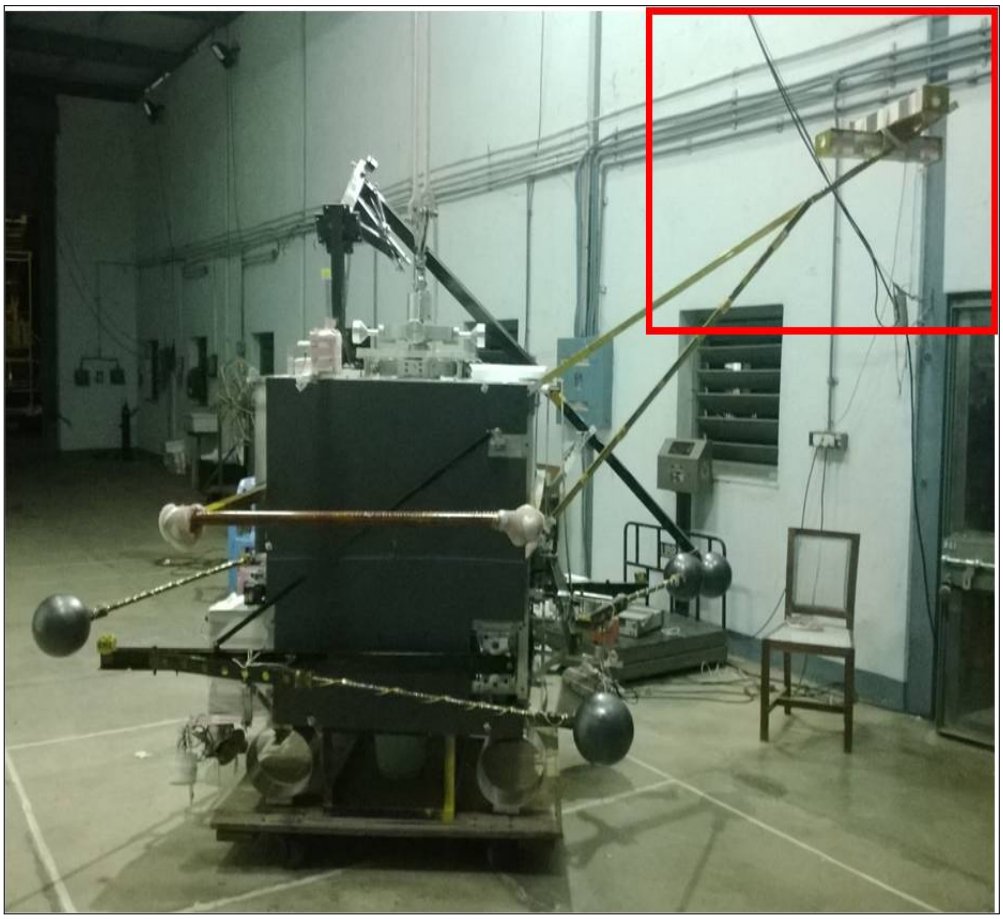

Figure 2.12: Search Coil Magnetometer attached to BEENS payload

The Search coil magnetometer was procured from the Lviv Centre of Institute for Space research, Ukraine. This is a three axes induction coil magnetometer. It is used to study the magnetic field variation in the frequency band of 0.5-50k Hz is space and land conditions. Both electronics and induction coil sensor are housed inside a protective tubular shape made of fiber glass tube with inner electrostatic screen. The magnetic core is made of a number of ferromagnetic high permeability amorphous tapes, insulated one from another. These coils detect changing magnetic fields which induce an EMF in the wire according to Faradays Law. In BEENS experiment the search coil is mounted on the upper portion of the gondola with a 2.0 m boom as shown in figure 2.12 Only two search coils were used for BEENS experiment with one in north south (NS) direction and other in east west (EW) direction with respect to the fluxgate magnetometer. This magnetometer was used to study the electromagnetic energy in the band from 0.5 - 16k Hz. The data obtained from search coil magnetometer will not be discussed in this thesis.

Chapter 3

Experimental Procedure for BEENS

3.1 Introduction

The prime aim of BEENS is to measure the electric fields at stratospheric heights (~35 km). The importance of electric field measurements at stratospheric heights is discussed in the next chapter. The main instruments onboard the BEENS include electric field (Langmuir double probe technique), search coil magnetometer, a flux gate magnetometer, Single board reconfigurable input out board (SBRIO) data acquisition system (DAC), and other circuits responsible for telecommunication and control from the ground. The present chapter provides a brief outline on each one of them and also provides a detailed procedure of launching of BEENS experiment. Boom deployment mechanism used for deploying electric field probes is also discussed in this chapter. Various tests carried out at Tata Institute of Fundamental Research (TIFR), national balloon facility (NBF) are briefed.

The electric field probes are used to measure quasi DC electric field and the search coil magnetometer for magnetic field measurements. Langmuir double probe technique was used for measuring quasi DC electric field ranging from 0.002 V to 4 V. Search coil magnetometer, designed by the Lviv center of institute of Space research,

Ukraine, was used for measuring ac magnetic fields from 5 Hz to 16 kHz. A Fluxgate magnetometer was used to determine orientation of balloon gondola and also for resolving electric field into north south (NS) and east west (EW) components. The orientation of the electric and magnetic fields is measured relative to the direction of geomagnetic field. The electronics are housed within the central gondola along with the other payload electronics like telemetry and other sensors that are responsible for data transmission, communication and control.

3.2 BEENS Balloon Configuration - An Outline

The balloon and the payload were connected by a long load line of about 75 m. The main packages along the load line were a cut-off device situated just below the balloon, a parachute, a GPS radiosonde and a radar reflector. The support packages for the BEENS experiment were a telemetry unit, a telecommand unit, a ballast container, a battery pack and few other housekeeping devices. Several flights have been conducted in the past from the same location during the Indian Middle Atmosphere Program in the 1980s (Gupta and Narayan [1987]; Garg et al., [1989]; Sampath et al., [1989]; Udare et al., [1991], to state a few). Most of these flights were aimed at making measurements of polar conductivities, ion densities and mobilities, though a few of them yielded vertical electric field profiles during the balloon ascents. Figure 3.1 provides a complete schematic of balloon configuration used for BEENS experiment.

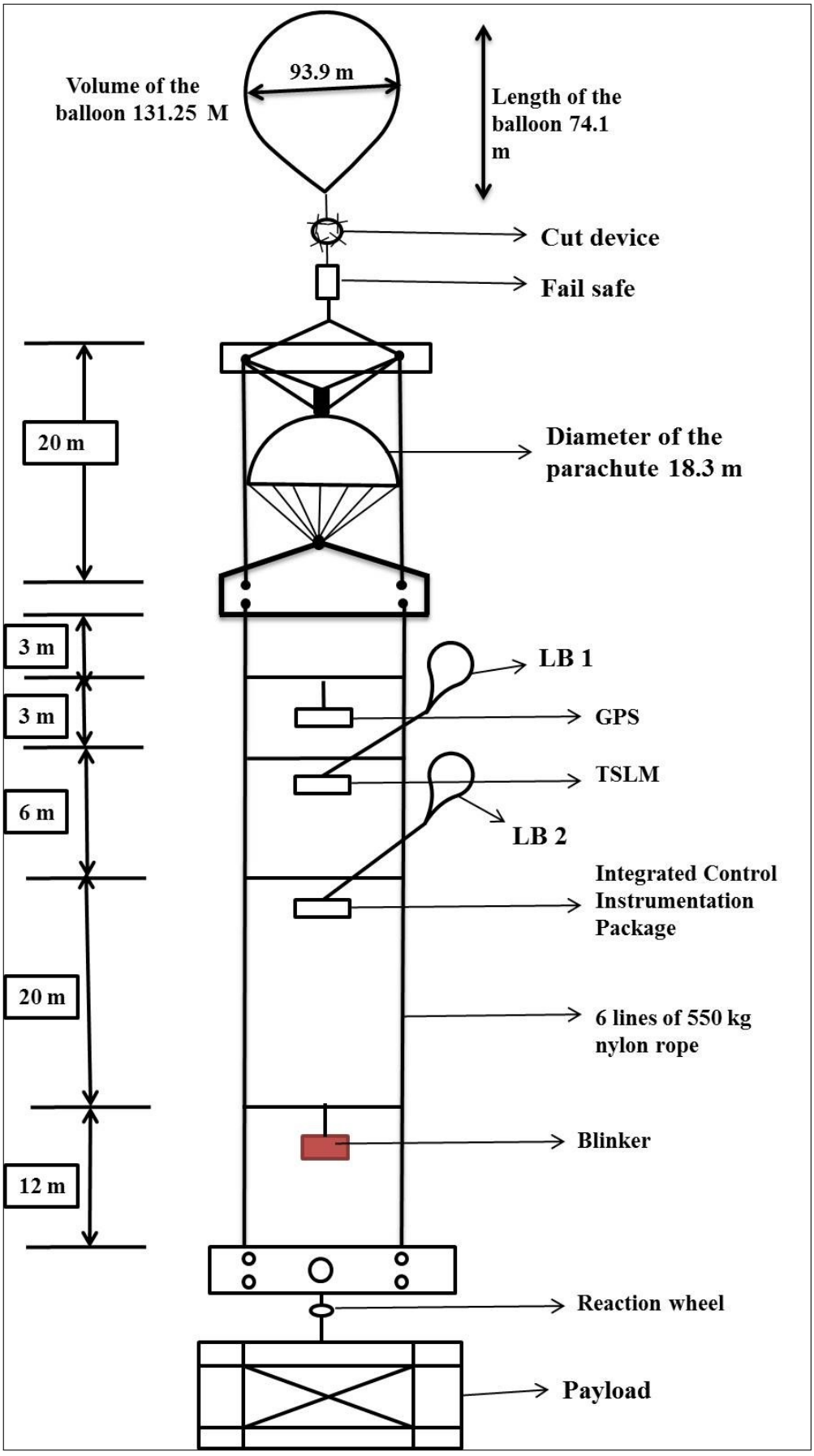

Figure 3.1: Schematic of BEENS Balloon Configuration

3.3 Gondola Design

In simple terms a gondola can be described as a frame that provides a rigid platform for mounting the electronic systems and other sub system required for the successful launch of a balloon flight. In case of BEENS experiment, it is a large

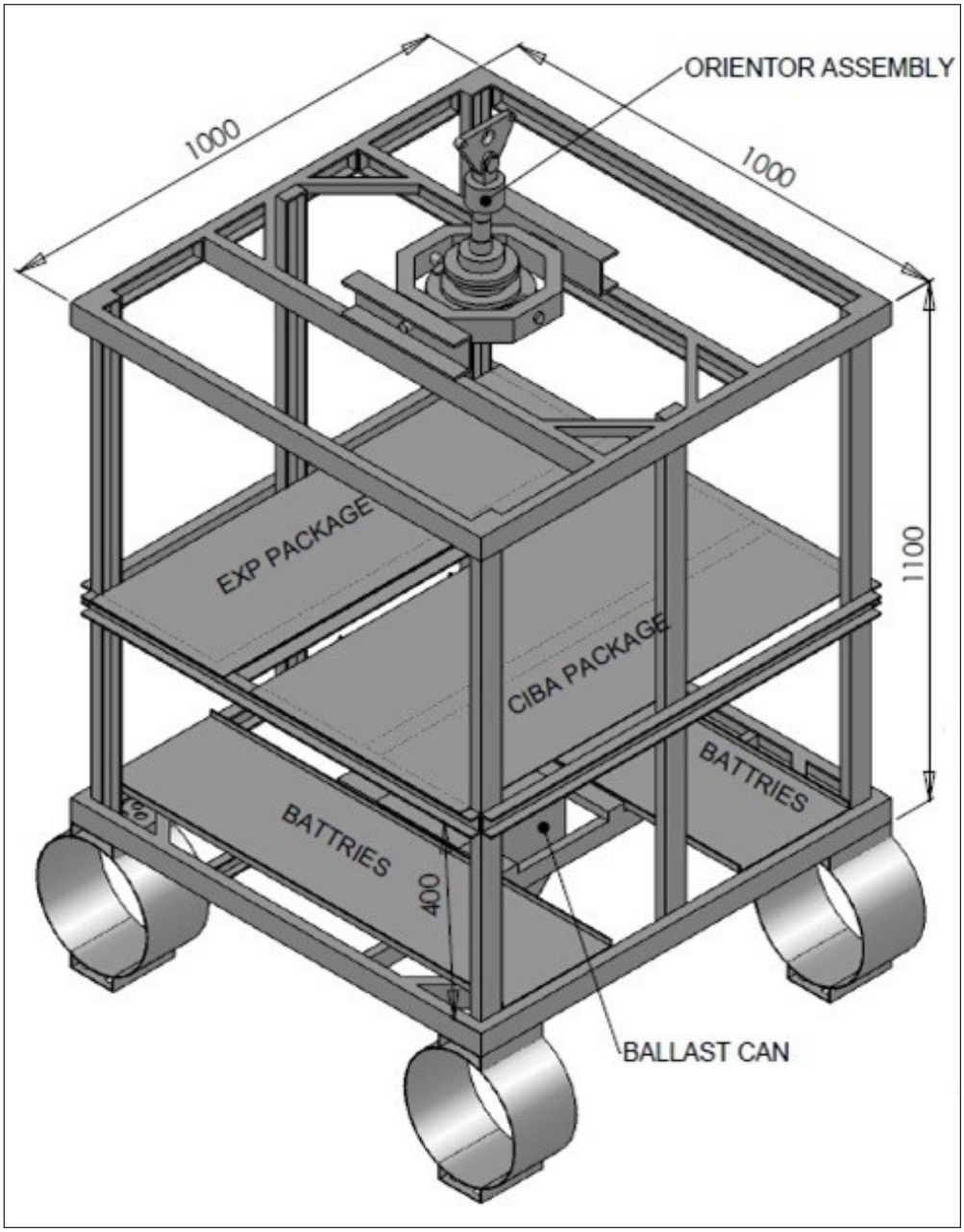

Figure 3.2: Gondola design used for BEENS experiment (dimensions are specified in mm units)

cubic aluminum structure of dimension 1.1m x 1m x 1m. It holds all the electronics and its subsystems which are required for the experiment. Figure 3.2 shows the structure of the gondola used for BEENS experiment. The gondola is divided into different compartments and each compartment is used be to keep a subsystem of the experiment. The top of the gondola is attached to the reaction wheel along with a universal coupler that facilitates the gondola rotation. This universal coupler helps the gondola to rest at vertical position even when there is a drag from the balloon during the flight at float altitude thereby avoiding the tilting of gondola during the flight.

3.4 Boom Design and Deployment Mechanism

The launch vehicle available at National Balloon facility (NBF), TIFR was not suitable for our electric field sensors in deployed condition. Under deployed conditions, a boom of length 3 m would cause problems during the launch. Due to this constraint in the launch vehicle, it was decided to have a deployable mechanism wherein the boom would be in a stowed condition before launching the Balloon. Later using telemetry command booms that bears the electric field probes would be deployed.

Designing a deployable boom for electric field probes was quite a challenging task in the BEENS experiment. The responsibility of manufacturing a deployable

boom, suitable for the electric field measurement of BEENS experiment, was handed over to a private concern. Earlier many prototype designs for the boom were developed and tested for the aforesaid experiment. The first successful one was the "scissor type" mechanism. As the name implies, it uses folding supports that are linked in a criss-cross 'X' pattern. Detailed information about this is available elsewhere as this is a common mechanism used in devices such as lift tables and scissor lifts. The boom designed using this model would be stowed before the launch and after launch, under deployed conditions, the boom would be unfolded and stretched. As a prototype, the scissors mechanism worked well. But considering the fact that the scissors mechanism involved a lot of sagging and with the lateral movement of the entire boom adding to the complication, successful deployment of the booms on-board a balloon seemed difficult with this mechanism. A lateral movement of the boom would always make the measurement of electric field difficult besides the fact that the length of the boom itself was around 2 m. With the boom length being only two meters, electric field sensors would be very close to the gondola increasing the possibility of measuring nothing but the perturbed electric field made by the gondola due to its large metallic structure. Hence, despite the successful working of the model, the scissors mechanism failed to meet the constraints of a design suitable for balloon payload. So, we could not adopt this model for our BEENS experiment to measure electric field at stratospheric altitudes.

The responsibility of developing a boom suitable for balloon experiment was

handed over to a new concern. Having in mind all the setbacks faced in the previous model, this time we settled for the spring and hinge boom deployment mechanism. A hinge is a mechanical term that stands for a type of bearing (machine element that constrains relative motion to only the desired motion) that helps in connecting solid objects, restricting the movement only in limited directions. An example for hinge joints encountered in day-to-day life are elbow, ankle and knee joints in human body and some automatic/semi-automatic door systems. More information on this topic is available elsewhere. A boom based on hinge model designed in combination with a spring mechanism would be ideal for this experiment as it would deploy instantaneously without any additional mechanical parts and more importantly without disturbing other sub system in its vicinity. This mechanism was quite feasible for deploying the electric field sensors. The boom will be in a stowed condition during the launch (Refer to figure 3.3). The stowing of the booms was achieved by a motorized technique where the motor is used to lock the booms to its stowed position (figure 3.4 and 3.5). We had to depend on the remote unlocking of the motorized technique for deploying the boom using the telemetry command once it is launched from the ground (a schematic illustration of the gondola and booms in the deployed condition is given in chapter 4, refer to figure 4.1on page 72).

Figure 3.3: Electric field Booms of BEENS experiment in stowed condition

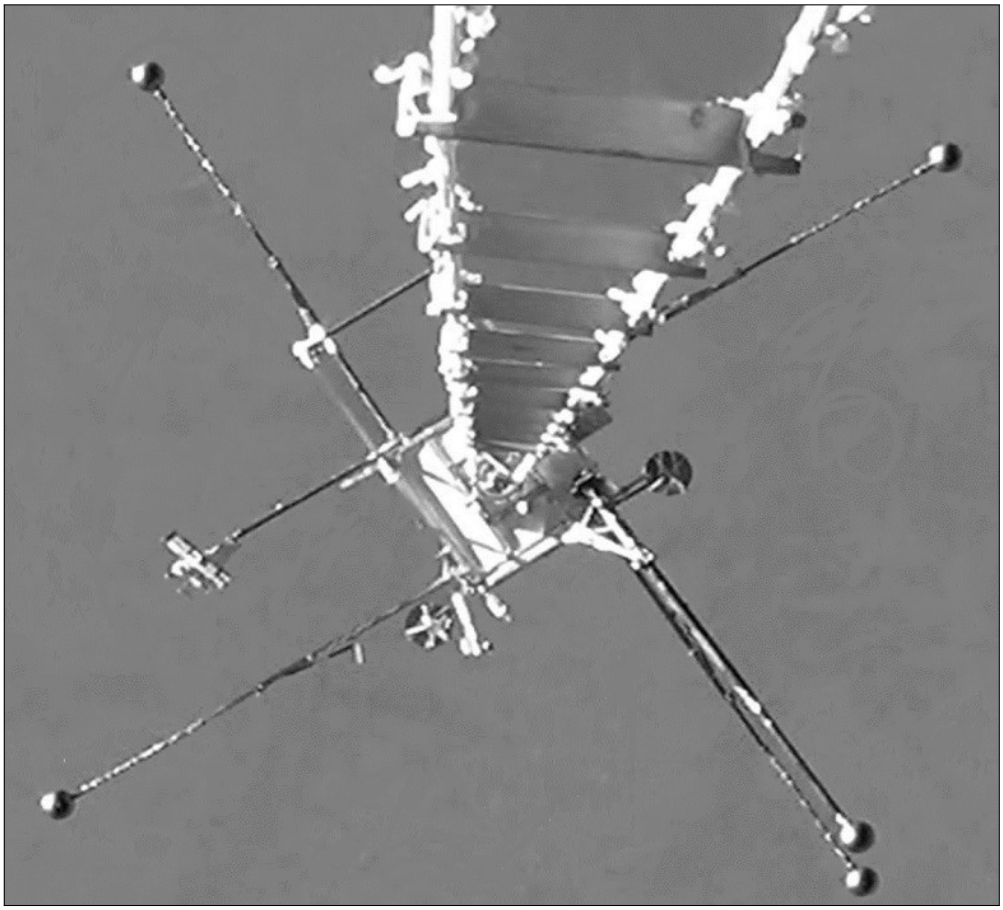

Figure 3.4: Boom in Deployed Condition (Top View) at float altitude

Figure 3.5: Boom in Deployed condition (Side view)

3.5 Cleaning of Booms

For stratospheric balloons, the most important consideration is that one should use preferably nonconducting booms; the outer surface in particular needs to be ultra clean. Even the oil from our finger prints is too conductive, so a pure alcohol cleaner is commonly used to clean the surface of the booms before the launch.

As mentioned earlier, the booms were used for electric field measurements onboard BEENS experiment. Once deployed, the electric field probes (spherical sensors) would be separated from the central payload using both metallic and fiber glass booms. Under stowed conditions, the metallic boom stretched to 1.5 m (length) from the gondola and from the end of the metallic boom, a long fiber glass boom of length 1.5 m was attached. A similar setup was done at all the horizontal sides of the gondola. The metallic booms were isolated from the central payload using Teflon spacers/washers to ensure that there was no actual contact with the gondola. Each Teflon spacers were thoroughly cleaned twice; once initially before fitting and again after fitting to minimize the data error that might contribute to the observed variations in measurements. After completing the mechanical integration of the booms and gondola, the entire boom was wrapped with Kapton Dag tape that provided additional advantages of insulation, and high dielectric breakdown and a complete non conducting surface. Before shifting the payload to the launching site,

all the booms were again cleaned with alcohol and precautions were taken during the launch time to avoid, touching of the booms with bare hands.

3.6 Reaction Wheel

A reaction wheel (RW) is a type of flywheel (a rotating mechanical device that is used to store rotational energy) used primarily by spacecraft or an atmospheric balloon. They are useful when the spacecraft or a balloon is required to be rotated by very small amounts. To minimize the DC offset in the electric field measurement of the BEENS experiment, the reaction wheel was used to rotate the entire payload at a constant period. This rotation technique was earlier used by many researchers for measuring electric field in balloon/rocket/satellite experiments (Mozer and Serlin [1969]; Ogawa et al., [1975]; Holzworth [1989]; Hu and Holzworth [1997]; Holzworth and Bering [1998]). In BEENS experiment the reaction wheel used for rotating the balloon gondola was developed at TIFR, Hyderabad. As mentioned earlier the payload was rotated with a constant period depending on the current supplied from the battery pack. A dedicated battery pack was provided for reaction wheel. At balloon altitude (commonly to as termed as float altitude is the altitude at which the balloon stops ascending and stays close to that altitude. In case of BEENS the float altitude is ~36 km) the reaction wheel achieved 7 rotations per minute (rpm) which was sufficient for minimizing the DC offset and improving the work function of the electric field probe. The reaction wheel is connected to a universal

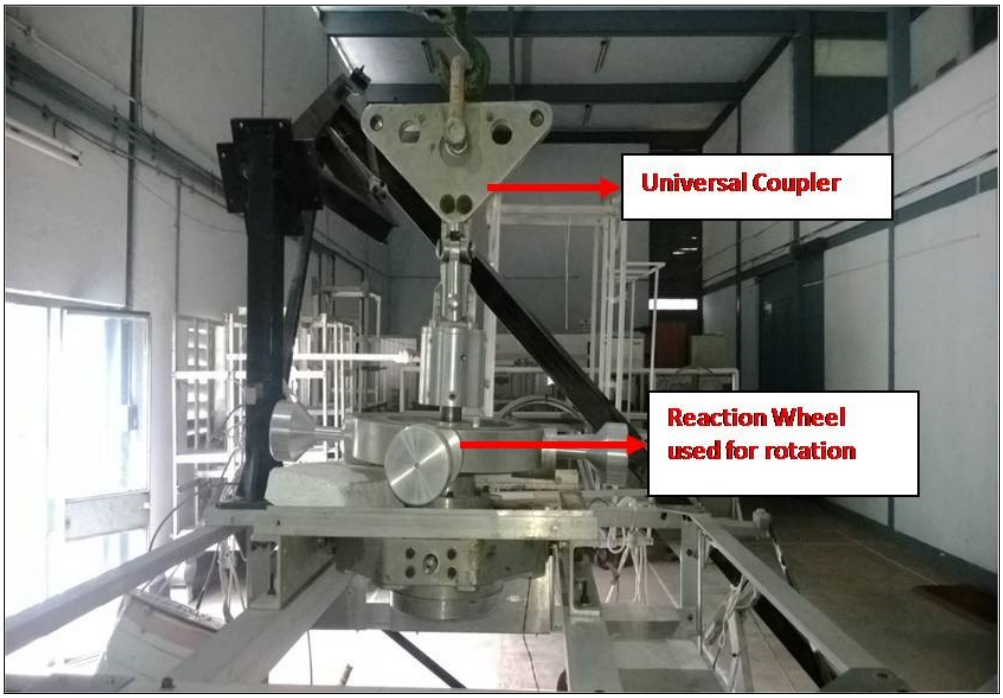

Figure 3.6: Balloon Gondola fixed with reaction wheel and universal Coupler

coupler and in turn connected to the balloon gondola using nylon rope as indicated in figure 3.6. The main use of universal coupler is to make the balloon payload to stay in vertical position irrespective of the drag due to winds in the upper atmosphere. This configuration ascertained that the electric field measurements are done without any inclination error.

3.7 Subsystems in the BEENS Payload

3.7.1 Telemetry system

The analog signal outputs from the pre-amplifier board and fluxgate magnetometer were fed into the telemetry encoder where input signals of voltage ranging

from +4.2 V to -4.9 V can be fed. The raw outputs received from the electric field instrument and fluxgate magnetometer were fed to the pulse code modulator (PCM) encoder for digitizing the analog signals. The PCM encoder used the multiplexer circuit to sample the data. The multiplexed signals are converted into digital data using a 12 bit analog to digital converter (ADC). The digitized data was then fed to the transmitter to transmit the encoded signal to the ground station.

3.7.2 Data Transmission

The output data from the BEENS payload is digitized and then transmitter serially using a radio link. A PCM encoder was used for digitizing the data and later converting it into a coded serial output as mentioned earlier. The encoded data was then passed on to the transmitter that in turn transmitted it to the ground station.

3.7.3 PCM Encoder

The pulse code modulation (PCM) encoder was used for converting data collected from several analog or digital data channels to a single serial digital data channel for convenient and reliable transmission of the data. In case of BEENS experiment, output data from all six channels to be telemetered were provided as input to the PCM encoder and conversion to a single stream of serial data was accomplished. The encoder used can accept both single and differential analog inputs

in the range 0 to 6 V and ±4.5 V respectively.

Sampling of data was done using multiplexer. The sampling frequency is determined for a given channel based on the frequency at which the data were sampled for a given channel. The resolution of data would be determined by the sampling frequency. The sampling frequency for BEENS experiment was around 14Hz (14 samples per second). Any variation in the data faster than 7 Hz would not be observed through this telemetry system according to the Nyquist criterion (Gruenberg [1967]).

The 12 bit analog to digital converter (ADC) converted the analog inputs of the encoder into digital form. The converted voltage was a twelve bit number that ranged between 0 and 4095. The 12 bit number thus obtained was proportional to the voltage output of the given channel computed using the formula

$$\text{Volt} = [(\text{Count X} - 8.909))/4095] + 4.17$$

Where Count is the output from TIFR encoder.

The PCM encoder used a Bi-phase-L format at rates up to 200 kbps to encode the signal. The Bi-phase- L format, commonly known by various names such as Manchester code, phase encoding, or simply PE is a line code in which the encoding of each data bit has at least one transition and occupies

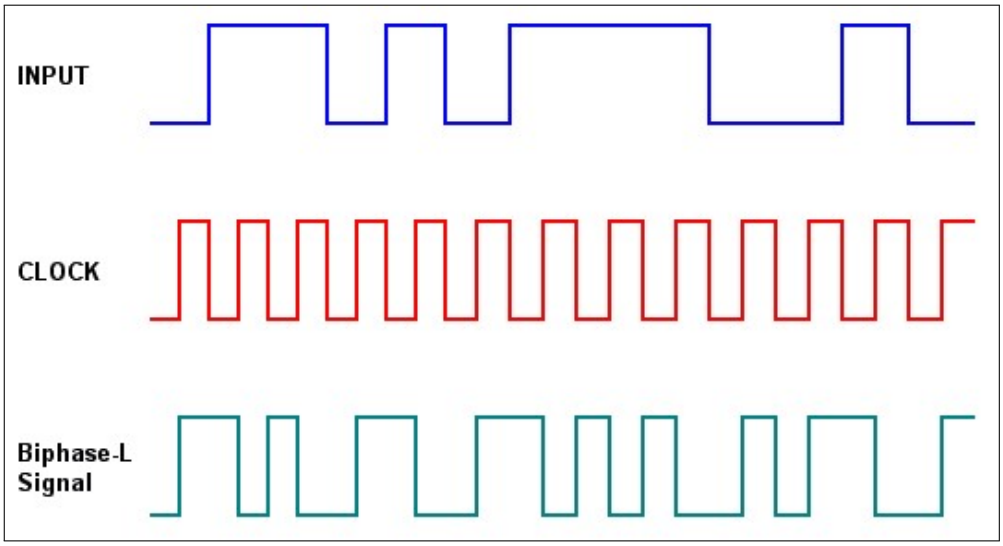

Figure 3.7: Bi-phase-L encoding (reproduced from http://ashish.ideaforge.co.in/electronics/biphase_modem.htm)

the same time. The advantage of this encoding is that it has no DC component, and is self-clocking/self-synchronized. This encoding uses transition at the middle of each bit interval as shown in figure 3.7 (for more information refer to http://ashish.ideaforge.co.in/electronics/biphase_modem.htm, http://en.wikipedia.org/wiki/Manchester_code). A word contains 8 bits with 7 information bits and one parity bit. 32 words form a frame and in turn 8 such frames form a super frame. In other words, each frame contained four words for frame synchronization, and one word as frame counter for the super frame synchronization.

3.7.4 Telemetry Transmitter

An S band (radio waves with frequency range 2-4 GHz) telemetry transmitter operating at a carrier frequency 2259 MHz was used for transmitting data from the PCM encoder. The radio frequency power output of the transmitter was 1 watt. The PCM encoder data were phase modulated by the Bi-phase (L) signal. This modulated signal was subsequently transmitted to the ground receiving station using a radio link.

3.7.5 Telecommand System

A telecommand system provides various commands to be sent from the ground station to various on board subsystems. Telecommand is used for various flight control operations like detaching the small control balloons, dropping the ballast, apex valve opening and closing, timer extension, flight termination, deployment of sensors, operation of motors etc.

The ground segment of a telecommand system consists of a command encoder and a transmitter. The onboard segment consists of a receiver, a command decoder and a command control unit. For BEENS, the transmitter was operated at carrier frequency of 148.25 MHz and its output power was ~35 watts. The transmitter was modulated at subcarrier frequency of 6.25 kHz which was amplitude modulated

by the command signal. The onboard unit received the telecommand signal and decoded it. The command signal unit either activated or deactivated the respective relay switches in response. A Confirmation was sent through the telemetry to the ground station.

3.7.6 GPS Receiver

Figure 3.8: Chapman 12 channel GPS receiver used by TIFR national balloon facility for BEENS (Figure Courtesy: TIFR)

For accurate positioning of balloon during the BEENS flight a Chapman 12 channel GPS receiver was used in the payload (refer figure 3.8) . The GPS receiver provided information on latitude, longitude, altitude and time in NMEA (National Marine Electronics Association) format. The output from this receiver was given to telemetry encoder and was later decoded in the ground station.

3.7.7 Ballast

Ballast unit was used to control ascent rate of the balloon. It used tiny steel shots for in-flight releasing of a controlled load and would be released in case the balloon slowed down due to any change in atmospheric conditions. Tiny steel shots were stored in a container at the bottom of balloon gondola. The outlet of this container was blocked using an energized electromagnet and tiny steel shots could be released by disconnecting the supply to electromagnet through telecommand. The operation was monitored through telemetry and a phototransistor that optically sensed the dropping of steel shots.

3.7.8 Apex Value

The apex valve was fitted at the top of the balloon. It helped in controlling the balloons altitude by releasing hydrogen gas from balloon. It was operated by sending command from the ground station to telecommand unit and was monitored in the ground station through telemetry.

3.7.9 Timer

A timer unit was used in the balloon to terminate the flight. It was programmed before the flight in accordance with flight duration required for the experiment. During the flight, the time for termination of flight either could be advanced or extended using the telecommand depending on the atmospheric conditions.

3.7.10 Beacon

A medium frequency beacon was used in all balloon flights as a safety measure as instructed from civil aviation authorities. It transmitted the signal 'TFR'in Morse code to forewarn approaching aircraft of the descending payload train in space. An AM transmitter at 1.665 MHz along with a half wavelength wire antenna was used for this purpose. The output power of the beacon was 10 Watts. Beacon operation was monitored using a radio receiver.

3.7.11 ATC Radar Transponder

During the balloon flight, detection and location of the balloon should be shared with nearest airport for safety measures. The ATC transponder communicates

with air traffic control radar beacon system of Hyderabad airport. As a result, the position and location of the balloon would be displayed on screen to the on-duty controllers. The balloon transponder was assigned a permanent identification code '2736'which would display the location and altitude of the balloon on the radarscope at the airport air traffic controller tower. For every flight, ATC transponder would be calibrated and re-certified prior to launch.

3.8 Packing of Electronics

The measuring electronics sent to the stratosphere would experience severe temperature changes as it would pass through the troposphere, tropopause and stratosphere during the balloon ascent. So the payload inside the gondola was thermally insulated from the surrounding environment using 1 inch thick thermocole sheets. The entire payload was covered with thermocole. Individual electronics like BEENS electronic instruments, enocoder, and other measuring electronics were convered with thermocole with aluminized mylar film (polymer films coated with a thin layer of aluminum) covered on one side, avoiding loss of heat by radiation and wrapped in polythene film. Over the thermal packing aluminum sheets coated with aquadag covered all the sides of the gondola. These aluminum sheets served as a star point ground (virtual ground) for the measuring electronics.

3.9 Power Supply Unit

The BEENS electric field probe, Search coil magnetometer, Fluxgate magnetometer and Single Board Reconfigurable Input/output (SBRIO) data logger required power supply of ±5 V, ±10 V, ± 5V and 24 V respectively. The required voltages were drawn from the raw output voltage of 24 V provided from the battery. The raw output voltage from battery pack was given to the DC DC converter (XP power). This was a very low noise DC-DC converter that provided the required outputs for the BEENS payload. The DC-DC converter was provided by the reversed diodes for the voltage surge protection. Figure 3.9 provides the picture of power supply unit used for BEENS.

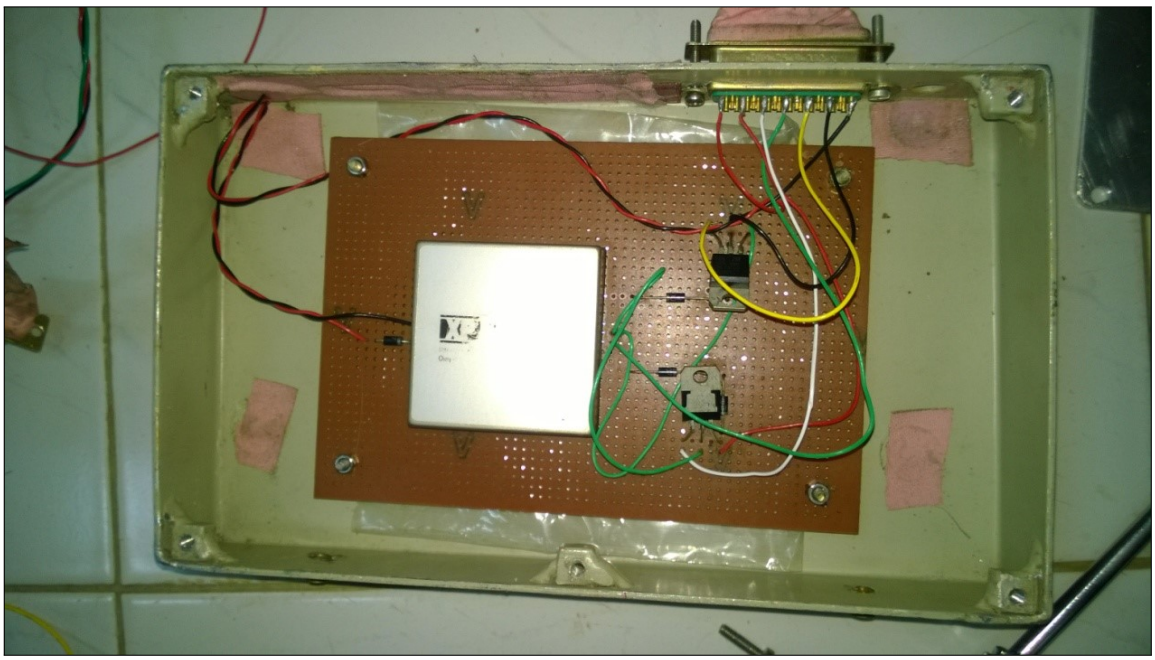

Figure 3.9: Power supply unit used for BEENS experiment

3.10 Battery Packs

Common battery packs were used as power supply to various measuring electronics inside gondola. Lithium ion cells were used for powering electronics inside gondola. Each cells had a working voltage of 2.7 V with 7.5 Ah current rating which was sufficient for our payload. The cells were connected in series and parallel fashion depending on the requirements of the measuring instruments inside gondola. 24 V raw voltage was given as input for BEENS payload, from this regulated voltages (±10V and ±5V) were derived using DC-DC converter. Another separate battery pack was made for the reaction wheel rotation. A high current lead acid battery was used for rotating the motor of the reaction wheel. Current was set to maximum for reaction wheel motor so that it would rotate the entire payload of weight 400 kg. Before the balloon flight all batteries are checked for full capacity.

3.11 Fluxgate Magnetometer

Fluxgate magnetometer was used for determining the orientation of the balloon gondola at a given time. It is a three axis fluxgate magnetometer. The X and Y axes provided magnetic north and east directions and Z axis provided information on the inclination of the gondola for any given time. Fluxgate magnetometer measured the component of the Earth‘s magnetic field parallel to the axis. The

output voltage form the fluxgate magnetometer was proportional to the cosine of the angle between the magnetometer and the magnetic north direction. The output voltage was scaled in such a way that it was nearly + 2.5 V when the magnetometer pointed towards north and - 2.5 V when it pointed towards south. Any inclination/tilt in the gondola was detected using the z axis of the fluxgate magnetometer. The sensitivity of fluxgate magnetometer was ±60000 nT. The output voltage of the fluxgate magnetometer was converted to magnetic field units using the formula provided below

$$B = (\frac{V_o}{S}) - B_o$$

Where B Magnetic field in nT, V_o- output Voltage in V; S Sensitivity in V/nT (36.5 μv/nT); B_o Zero Offset in nT. Zero offset of each component

X Component = -120 nT

Y Component = -68 nT

Z Component = -190nT

3.12 Environmental Testing

Environmental testing was done at TIFR balloon facility before the payload integration with other subsystems for the flight. The experiment payload is tested for operation under the environmental conditions expected at balloon altitudes (Refer Figure 3.10).

The BEENS payload, i.e., electrometer, SBRIO (data acquisition system), was thermally packed along with temperature sensor and was kept inside a thermo-vacuum chamber. In this chamber, the environment at balloon altitude could be simulated. The temperature was set to -50°C and pressure to 10^{-2} mbar inside the thermo-vacuum chamber. The thermo-vacuum chamber was switched on and it took 40 minutes to reach the temperature specified and for one hour it stayed at -50°C. In the next 30 minutes temperature was increased to -40°C and it stayed there for around 11 hours and later thermo-vacuum chamber was switched off and it took around 6 hours to return to normal temperature and pressure. During the whole process BEENS payload was switched on and was continuously monitored for normal performance of the instruments inside the payload. BEENS payload successfully passed environmental test at TIFR national balloon facility.

Figure 3.10: BEENS payload undergoing environmental testing inside thermo-vacuum chamber at National Balloon Facility, TIFR, Hyderabad

3.13 Mechanical and Electrical integration

Mechanical and electrical integration of the gondola was done once the payload successfully passed the environmental test. The placement of different measuring electronics to be integrated to BEENS experiment and BEENS payload were decided based on compatibilities of all electronics. The entire subsystem of balloon and BEENS payload were mounted on the racks provided inside the gondola and finally clamped with screws.

Harnessing of wire was done once the position of different subsystems of balloon and BEENS payload for interconnection within and outside gondola were finalized. The booms were mounted on the corner of the gondola diagonally on all the four sides of the gondola. Care was taken to ensure the electric field probes were not in contact with each other in stowed condition of boom. All the interconnections were checked and the payload was tested for proper function using external regulated power supply unit. Any technical/operational snag during integration was rectified at this point. The final integration of all the subsystems and BEENS payload were tested using the flight battery for a short while.

3.14 Long Duration Test

After completion of environmental, mechanical and electrical integration of balloon gondola, the entire payload is conditioned for flight readiness. The payload is kept in full readiness condition and is tested on external power supplies for a period of twice the planned duration of the balloon flight. At the commencement and at the end of this test, the instrument functioning is checked using the internal battery power supplies for a short period. During this long duration test various commands were given to check the flight readiness of each subsystems and BEENS payload. If all the tests are found to be satisfactory, the instrument is considered flight-worthy.

3.15 Launch Procedure for BEENS Experiment

In general, launching of any balloon experiment is quite complex and it involves a lot of effort to launch the balloon successfully. After the payload has passed all the environmental, mechanical and electrical integration and the long duration test, another complete test of BEENS payload and subsystems of balloon is conducted at the launch pad site. Below is the brief description of the launching of BEENS experiment from TIFR balloon facility, Hyderabad.

3.15.1 Scheduling of Flight

BEENS balloon experiment was scheduled to be launched during the month of April 2013. At the National Balloon Facility (NBF), TIFR, schedule for the launch of balloon flights were allotted between mid-October to mid-April. There would be no launches during the period of pre-monsoon and monsoon weather conditions, as the weather is not suitable for balloon launches.

The experimenter is allotted a specific launch window of about two weeks once the balloon launch is approved by the Balloon board of NBF, TIFR. BEENS experiment was allotted in the month April 2013.As the tropospheric westerly jet speed was very high during the time of April 2013, BEENS experiment was re-scheduled to the month of December 2013. For the balloon to be launched the following conditions have to be satisfied:

i. Surface winds should be less than 5 knots with a steady direction during the time of launch operations (2 to 3 hours)

ii. Cloud cover should not be more than 2-3 octas with no cumulonimbus (CB) clouds around the station.

iii. The tropospheric westerly jet should be less than 35 m/s in the troposphere region which lies from 12 km to 20 km altitude.

iv. The tropopause temperature should be warmer than -85°C.

v. Permission to launch the payload should beobtained from the Airports Authority of India and the nearby Indian Air force stations for the intended launch window.

vi. To find the upper wind conditions, a rubber balloon is initially launched. This gives information on wind at different altitudes and from this the balloon trajectory is deduced. Figure 3.11 show a typical wind profile obtained from the balloon flight.

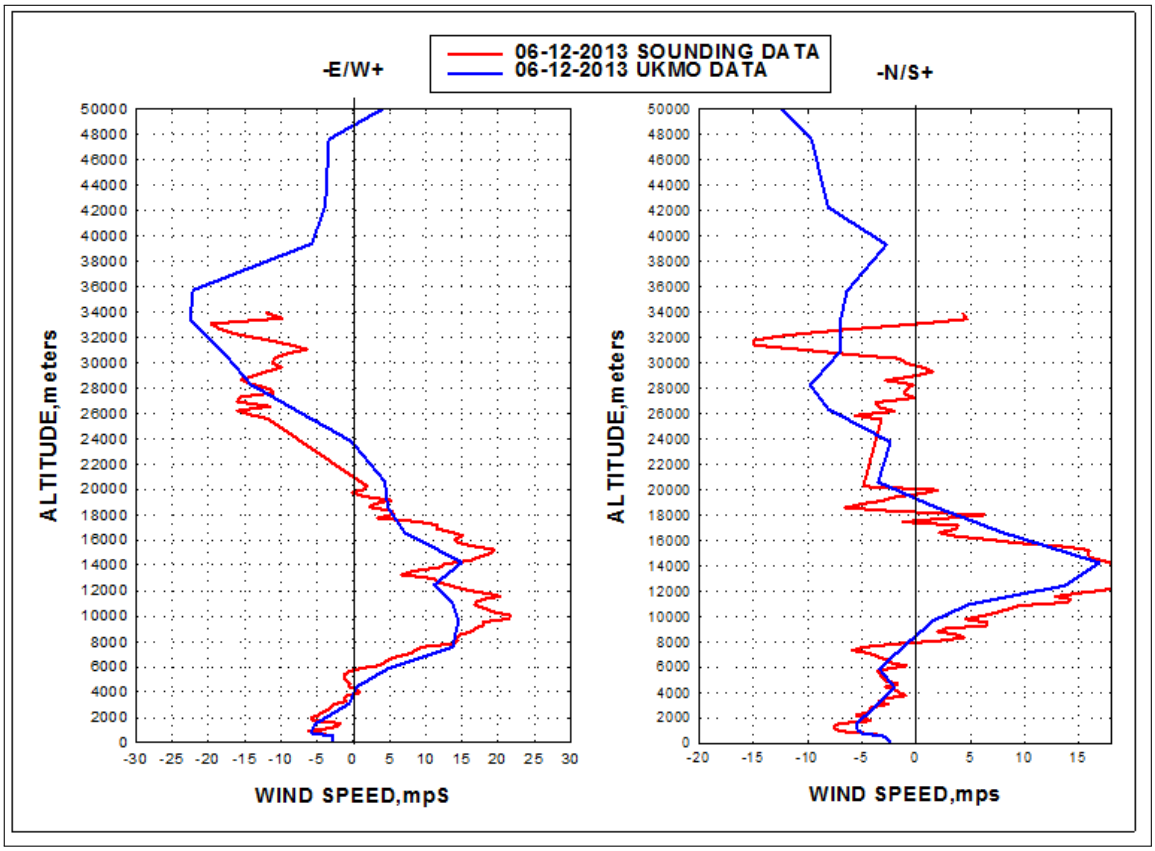

Figure 3.11: Wind profile obtained from sounding balloon and UKMO data

3.15.2 Launch sequence

The balloon gondola was carefully taken out from the payload rigging area and suspended from launch truck in the front side and moved to the center of the launching site three hours before the scheduled launch time. Other units like hydrogen cylinders, balloon spooling truck and other necessary equipment were also brought to the launching site. A pilot balloon would be raised to about 300 m from the ground to find the direction the wind once the main balloon was launched. Depending on the surface wind conditions, the balloon and the load line were laid on the ground and other instruments were hooked to the load line at proper places. Figure 3.12 gives the complete picture of BEENS experiment. The pre-launch tests were conducted with telemetry, experiment payload and all other control systems individually for their certification of instruments working all right. After prelaunch tests were done, filling of hydrogen gas started. The balloon was filled with roughly one tenth of its volume capacity. This was done so as to allow for the expansion of the gas when the balloon reached higher altitudes. Once the filling operation is over, the balloon would be ready for launch. Two pilot rubber balloons were released one after the other to check the wind direction and wind shear as it travels for the first 300 m. Then the main balloon would be released.

Figure 3.12: Panoramic View of BEENS experiment Launch

Figure 3.13: Filling of Hydrogen Gas to the main Balloon

Figure 3.14: BEENS payload group. (From left: K. Emperumal (TO III), Prof. S. Gurubaran (Guide and Principal Investigator (PI) for BEENS experiment), S. Manu (Ph.D Student and Author of this Thesis) and Dr. K. Jawahar (TO III))

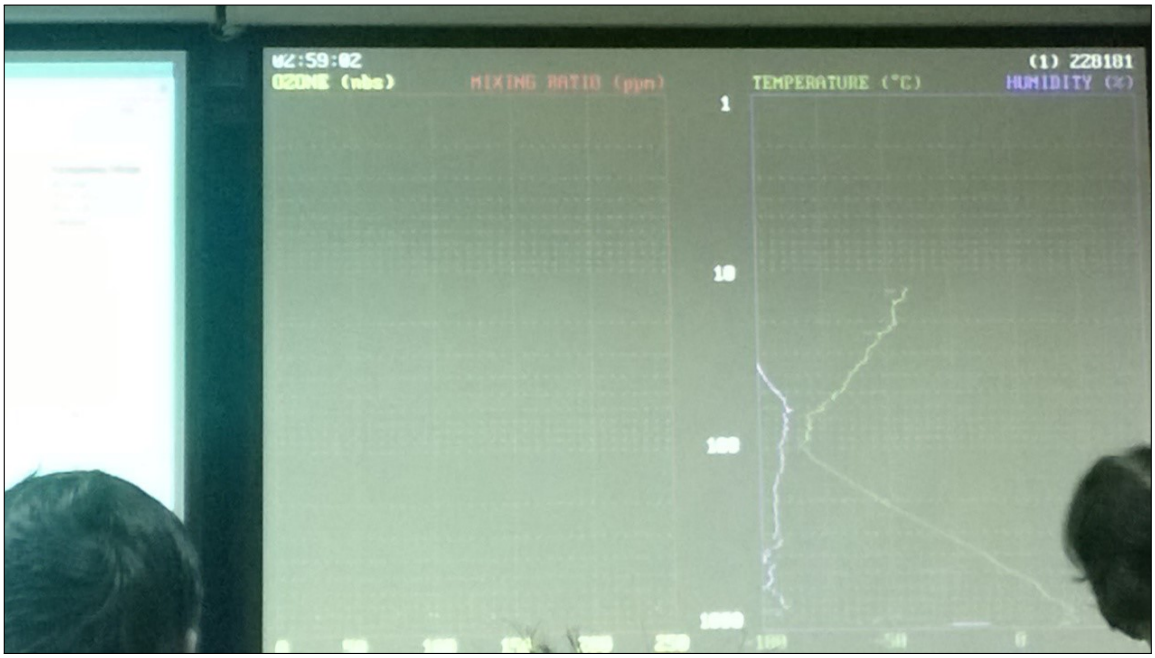

Figure 3.15: On Screen monitoring of temperature and pressure at Ground station of National Balloon Facility, TIFR, Hyderabad

3.15.3 Tracking and Recovery

The balloon was continuously tracked using the onboard GPS receiver after

the launch. An advanced recovery team would be sent for retrieving the payload

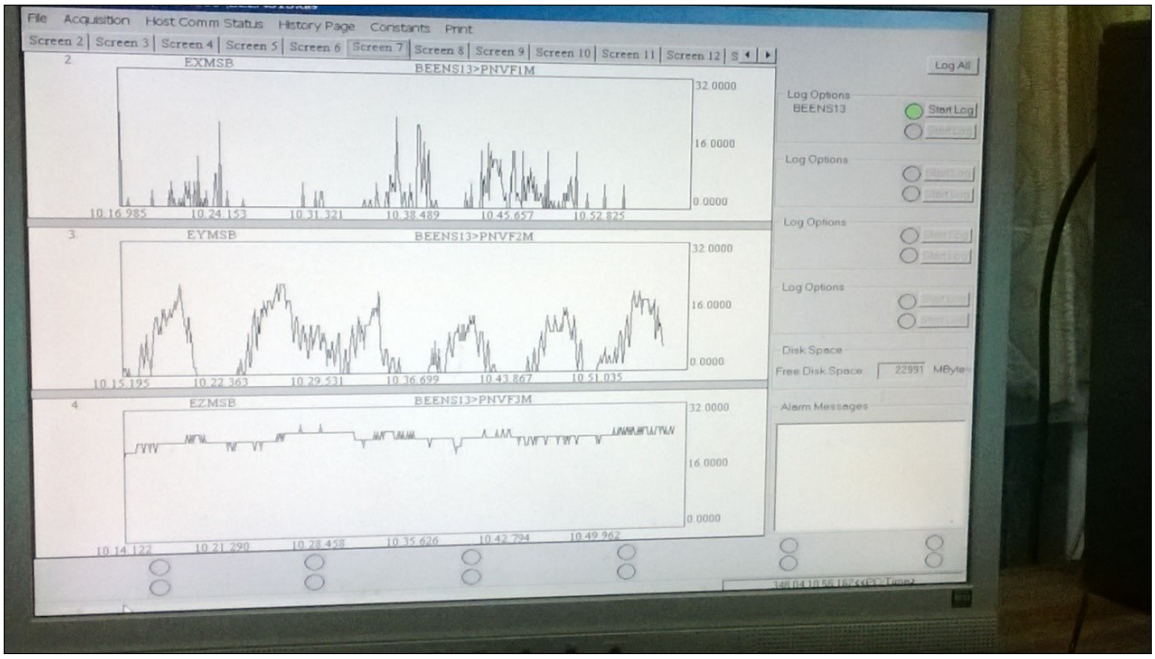

Figure 3.16: Real Time monitoring of BEENS payload data at the ground station of National Balloon Facility, TIFR, Hyderabad

an hour before the launch, based on the wind conditions derived from the balloon sounding prior to launch. Once launched, the balloon is free to drift in the direction of the prevailing wind and there is no control to change the direction of the drift. The Director General of Civil Aviation, Government of India has given the operational corridors for balloon drift and care is taken not to drift balloon over thickly populated area, forest areas thereby endangering the recovery of the scientific payload and accessories of flight. Reward tags are also attached to the payload train for the safe keeping of equipment for the finders with assistance from local police until the arrival of the recovery team.

The advance recovery team is always in touch with the base station once the balloon reaches the ceiling altitude. They were briefed about the trajectory of the

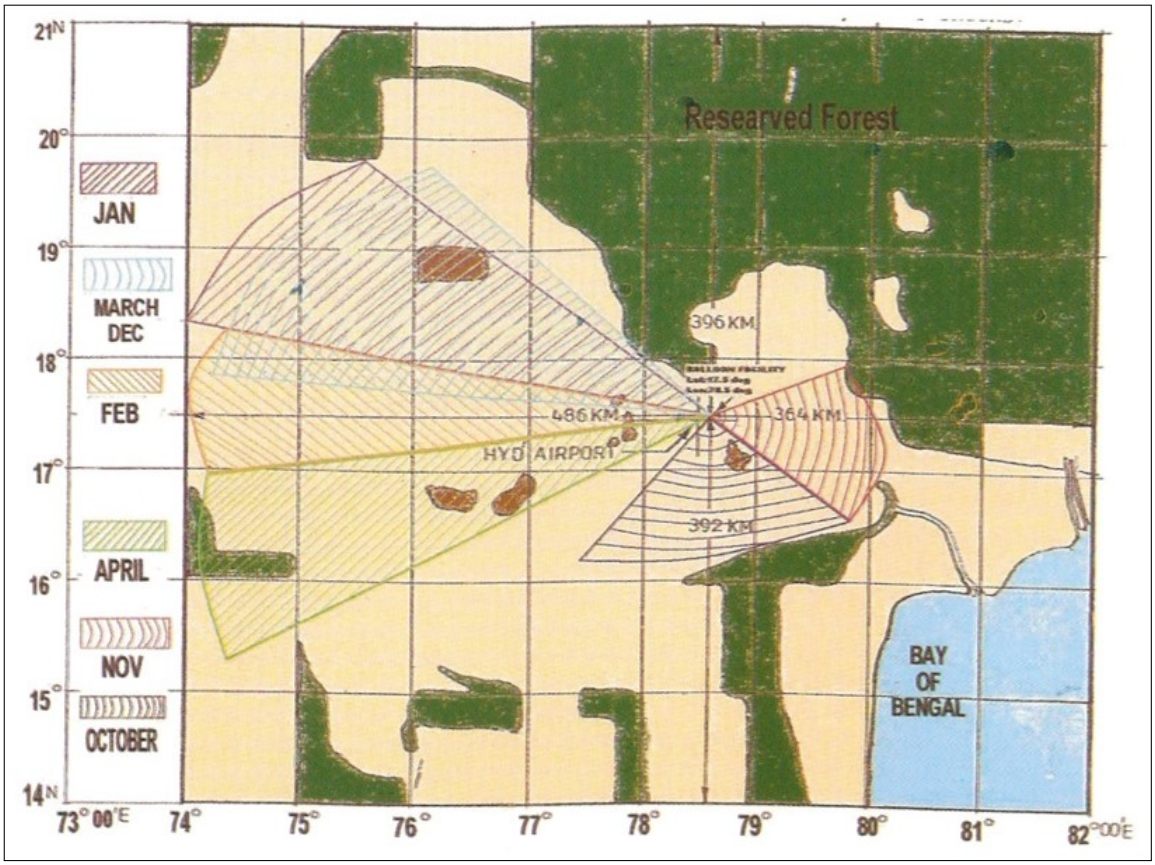

Figure 3.17: Balloon Flight operational corridor (obtained from National Balloon Facility, TIFR, Hyderabad

balloon. The advance team would reach the payload impact point within a couple of hours of touchdown. The advance recovery team takes care of the payload till the arrival of the main recovery team.

The main recovery team leaves the base station after the termination of flight in a recovery truck capable of accommodating the main payload and other accessories of the flight. Snapshots taken at various stages of the balloon experiment. launch and recovery operations in particular, such as fueling the balloon (Figure 3.13), members of the BEENS research group working at lab (Figure 3.14), on-screen (Figure 3.15) and real time monitoring from ground station (Figure 3.16), balloon

flight operation corridor(Figure 3.17) and recovery work (Figure 3.18)are provided in figure 3.13-figure 3.17 for demonstration purpose.

(a) (b)

(c) (d)

(e) (f)

Figure 3.18: Snapshots of recovery of BEENS payload from Jowar field some near Pandharpur, Maharashtra by TIFR crew members

Chapter 4

Results of BEENS Experiment

4.1 Introduction

Balloon borne measurements of electric fields of ionospheric origin are very useful in studying the long term variations of the electric fields unlike from the measurements from rocket and satellite measurements. Rockets and satellites will provide only the snapshots while the balloon experiments make the continuous monitoring possible. The only disadvantage of the balloon measurement of electric fields is, it can provide only the large scale distribution with scales larger than 1000 km.

Meteorological processes in the lower atmosphere give rise to intense electric fields and produce a potential difference between the Earth and the ionosphere of about 300 kV. The ionospheric fields are relatively weak, of the order of 1 - 100 mV/m, but extent over large areas. Thus the potential difference of the order of 50 kV may well occur in the ionosphere during active times. Due to the dominating influence of fields generated by meterological processes, the ionsopheric disturbances are very hard to detect at ground level. The conditions for measuring them are favourable at altitudes of about 30 - 40 km. The disturbances of meteorological

origin are rapidly damped when they propagate upwards into a medium of rapidly increasing conductivity, on the other hand disturbance of ionospheric origin are not all damped rapidly when they propagate downwards into a region of decreasing conductivity. Thus, the horizontal electric fields at balloon altitudes are only from ionsopheric source (Mozer and Serlin [1969]).

The primary goal of the Balloon Experiment on the Electrodynamics of Near Space (BEENS), the first of which was carried out from the National Balloon Facility, Hyderabad (17.5 ° N, 78.6° E, geographic; 8.7° N geomagnetic), India, on December 14, 2013. This experiment is used to probe and understand the processes that drive the various electric field sources at low latitudes and in that process generate a data base on stratospheric electric fields from a low latitude continental site. The experiment was conducted during the early hours of December 14, 2013, using a 110,000 cubic meter balloon that reached a float altitude of 35 km.

4.2 Electric Field Results of BEENS Experiment

The sensor configuration is depicted in Figure 4.1. The BEENS payload comprised of two orthogonal pairs of spherical probes, referred hereafter as 1-2 or x-probes and 3-4 or y-probes (the payload x- and y-axes were referenced with respect to the two orthogonal sensors of a reference magnetometer). The probes were mounted at the ends of deployable booms for horizontal electric field measurements. The fifth probe

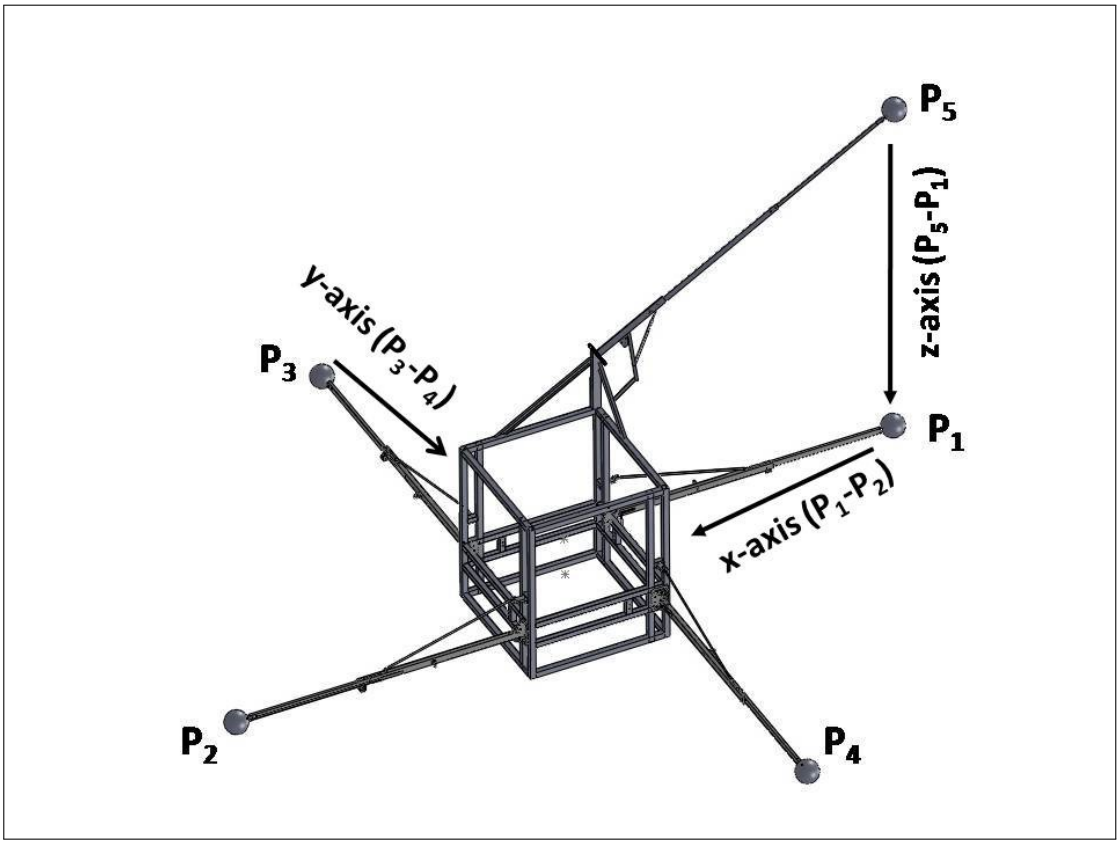

Figure 4.1: A sketch of gondola and the booms shown in deployed condition (not to scale). The directions of the three axes referenced with respect to the probe configuration are indicated

was mounted at the end of another boom that was deployed at an angle of 45° to the horizontal plane, which along with one of the x-probes yielded a measure of the vertical electric field (the third pair would be referred to as 5-1 or z-probes).

The electrometers were tested using a DC DC variable power supply for all the three orthogonal directions. Each pair of the probe marked X-, Y- and Z- axes were chosen. The pair of probes was tested by feeding DC voltage signals to positive probes of each pair and grounding the negative probes. All the pair of probes was tested for both positive and negative DC voltages. The output of this experiment for each axes of the electric field measurements to be carried out is shown in figure 4.2.

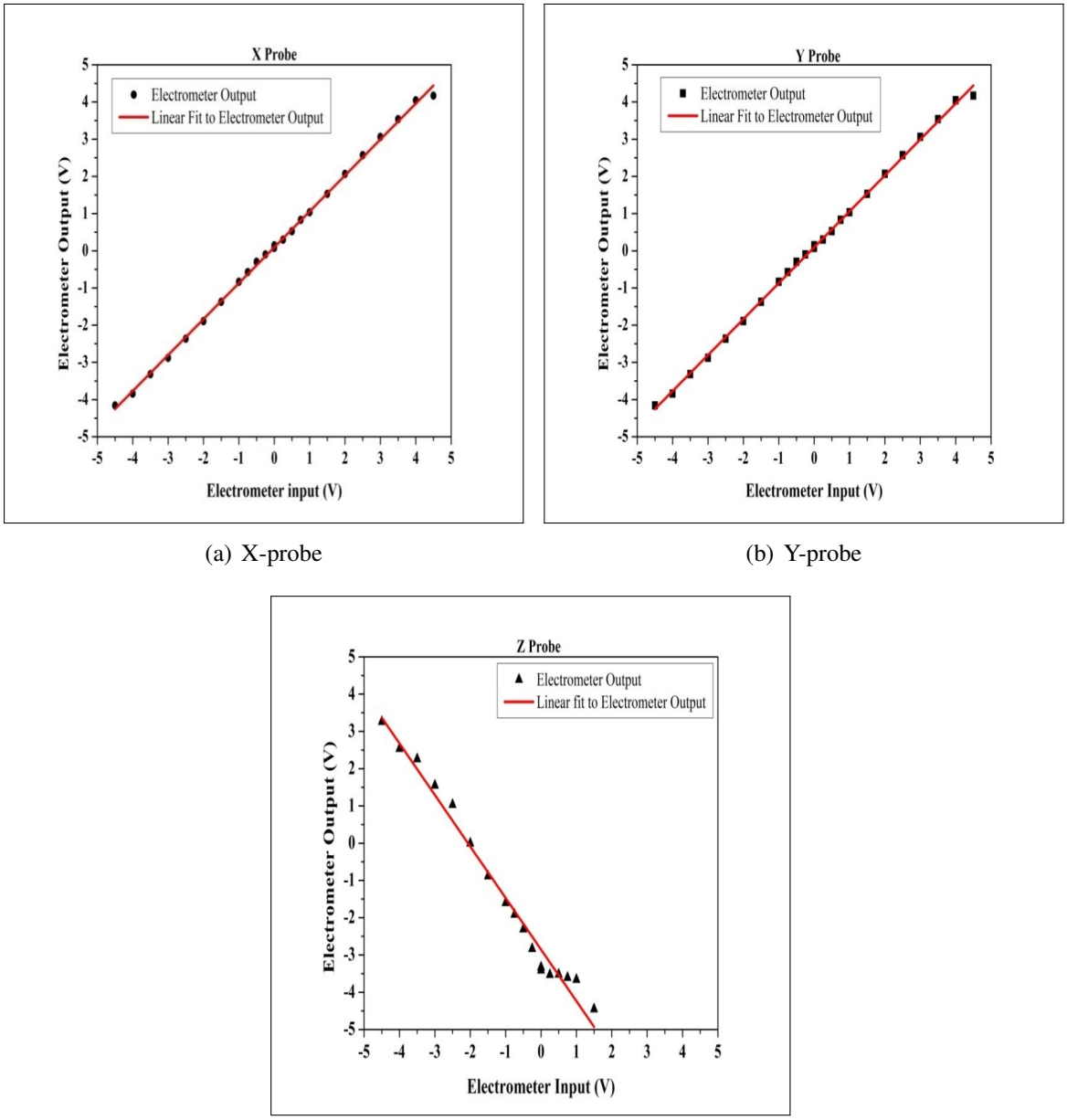

(a) X-probe

(b) Y-probe

(c) Z-probe

Figure 4.2: Performance results for the probe-electrometer system obtained just prior to launch. Known voltages are applied to the x−, y− and z− probes separately in isolation and the electrometer outputs monitored on the respective telemetry channels

From the figure 4.2 it is seen that all probes shows linear variation which is expected for any instrumentation amplifier working. Figure 4.2(c), Z- probe output which is showing negative slope. One reason may be the configuration used to derive for vertical electric field. In BEENS experiment to measure the vertical electric field,

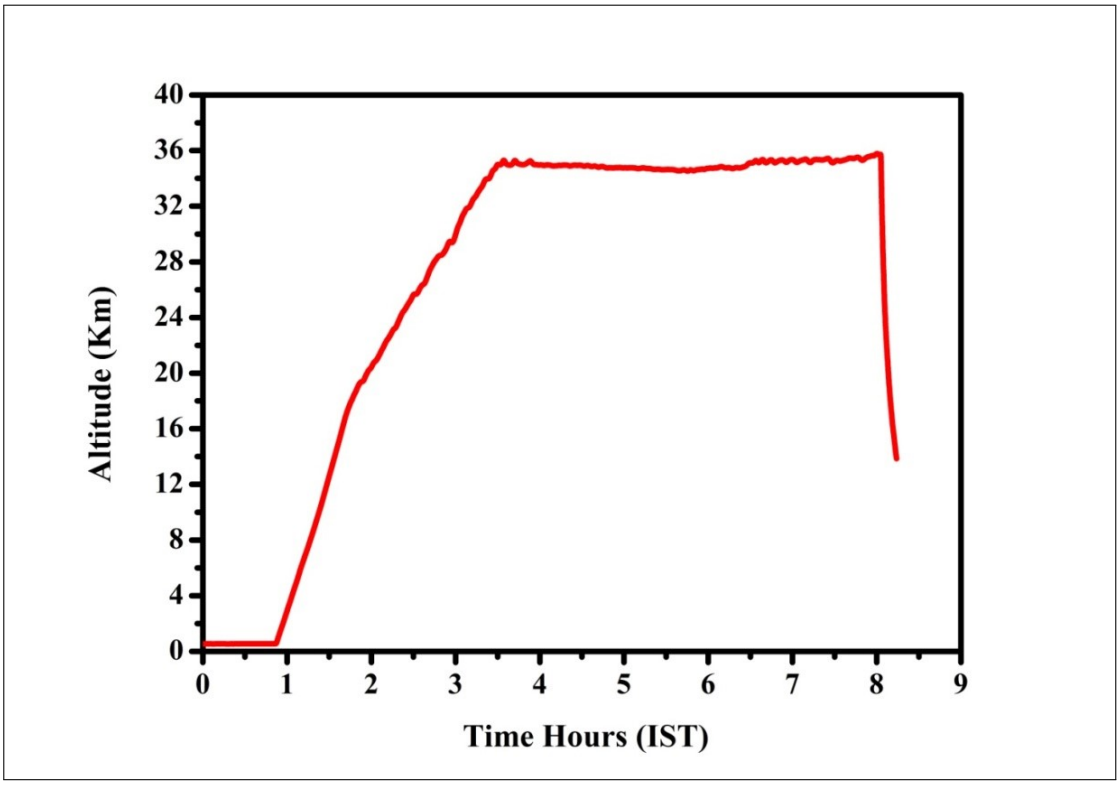

Figure 4.3: Altitude profile of BEENS Experiment

one of the X- probe is coupled with vertical electric field measurement with a 45° angled Z- probe. Due to this, coupling of both X- probe and Z- probe outputs, there may be a feedback from the X- probe electrometer to Z- probe electrometer.

The launch of BEENS balloon experiment took place in the early hours of 14 December 2013 at 00:52 hours Indian Standard Time (IST). After the balloon was released, electric field booms were deployed immediately to make sure booms are released perfectly without any hitch. Figure 4.3 shows the position (altitude) of the balloon borne BEENS payload over time.

When the balloon reached the float altitude of ~35 km, the stratospheric winds

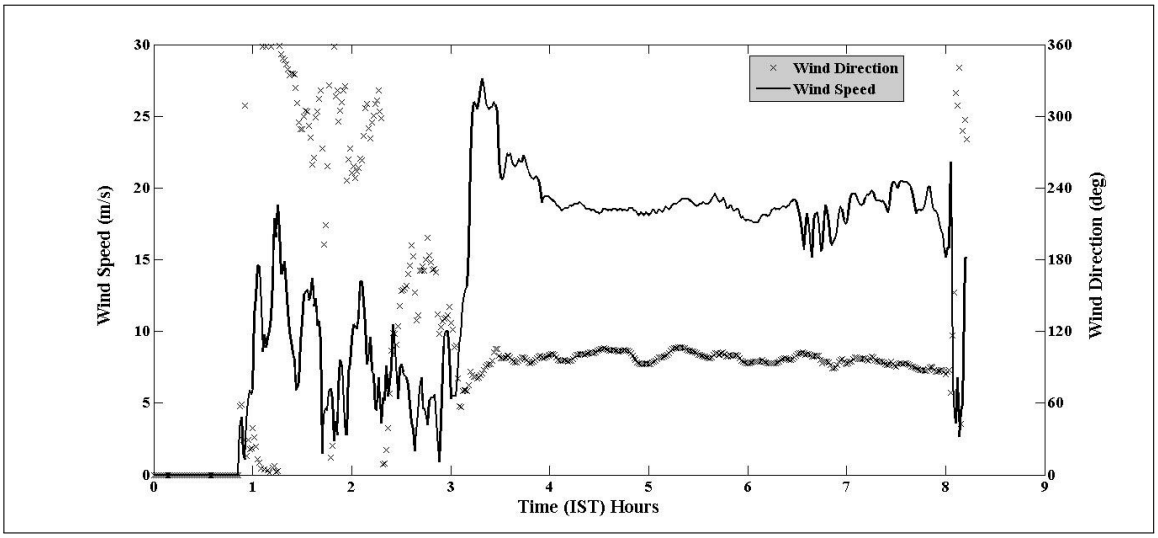

Figure 4.4: spatio-temporal variation of ambient wind speed and wind direction

there were blowing with speeds of ~20 m/s towards west and with the safe flight corridor for the recovery of the payload being about 400 km on the west, the flight had to be terminated at around 08:00 IST after achieving a float duration of slightly more than four hours. Figure 4.4 depicts the GPS radiosonde measured wind speed and wind direction. As noticed here, the wind direction remained at ~90° (which is easterly) between 03:30 and 08:00 IST when the balloon was at the float altitude.

The BEENS payload took two and half hours to reach the float altitude of 35 km. The reaction wheel is switched on as the balloon ascended an altitude of 5 km using telecommand. Gain set and reset command was executed by giving telecommand from ground station to balloon payload to check the correctness of telecommand executed. Figure 4.5 show the execution of gain set and reset, for both x- and y- probes, command from the ground station.

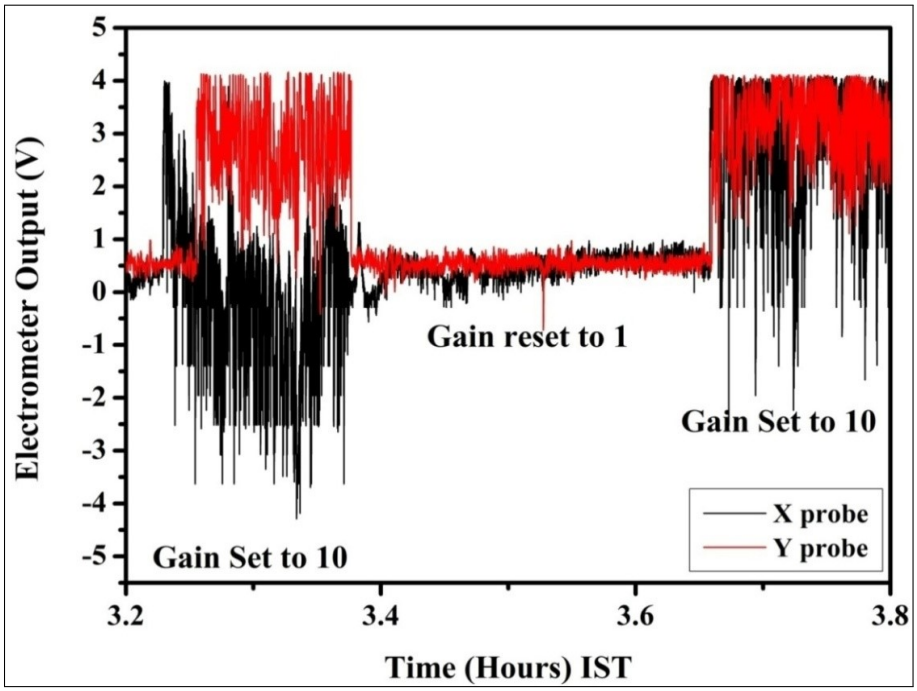

Figure 4.5: Gain set and reset for both x- and y- probes of electric field measurement during the time 03:12 and 03:48 hours IST

The fluxgate magnetometer fixed inside the gondola gave the orientation of x- and y- probes for resolving the Electric field components into two components, i.e., electric field in North-South (NS) direction and East-West (EW) direction. Figure 4.6 shows the fluxgate magnetometer data confirming rotation of the payload.

The raw telemetry data are stored in a binary file. The binary file contains data of time, electric field channels, fluxgate magnetometer channels and other parameters in digital numbers. Time, electric field, and fluxgate magnetometer data are extracted from the binary file and is converted using to Voltage using the formula below.

$$V = -\left\{\frac{\text{count} \quad X \quad 8.906 \ V}{4096}\right\} + 4.17 \ V$$

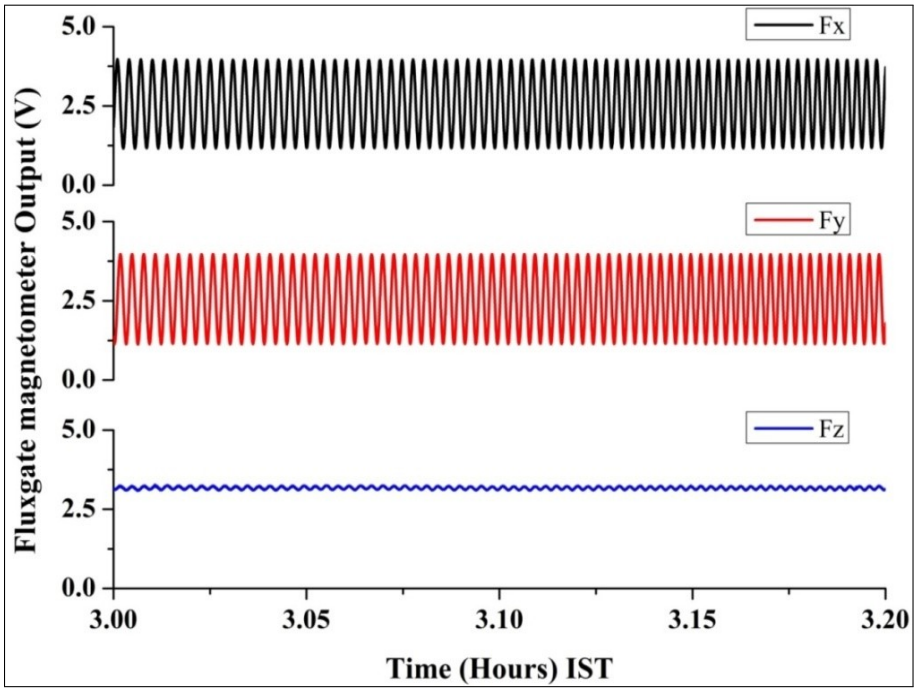

Figure 4.6: 12 minutes of Fluxgate magnetometer output of all three channels between time 03:00 to 03:12 hours

The converted values are used for deriving electric field using the fluxgate magnetometer data by resolving electric field data into two components, i.e., North-South electric field (E_{NS}) and East-West electric field (E_{EW}) .

The orography along the BEENS Balloon drift is contributed by the Deccan Plateau, a region elevated in the range of 300 - 500 m above the mean sea level. There were no mountain ranges with altitudes greater than 1000 m in the vicinity of at least 300 km from the BEENS balloon track on all sides. The EUMETCast dissemination mechanism provides access to the image archives from EUMETSAT fleet of satellites. A thermal infrared (10.2 - 12.5 μm) image of the Indian sub-continent obtained from one such archive is depicted in figure 4.7. Captured at 02:30 IST on 14 December 2013, this image does not reveal any high altitude convective cloud system in the

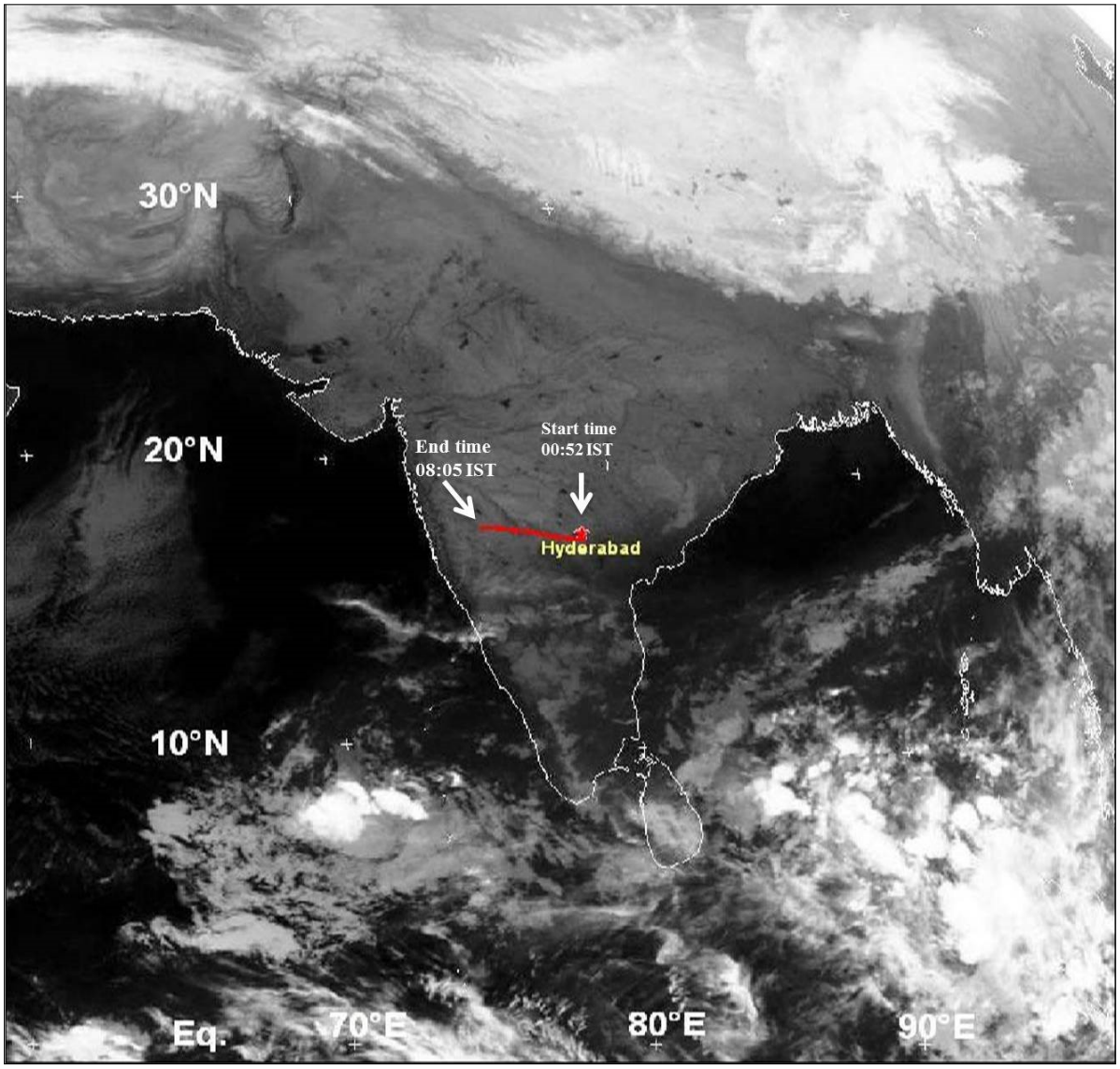

Figure 4.7: A thermal infrared image (10.5-12.5 μm) (corresponding to 02:30 IST) obtained from the EUMETSATs fleet of satellites. The balloon track is indicated in red

vicinity of the balloon path. The balloon trajectory of BEENS experiment is shown as thick red curve.

The sampling rate of electric field measurements was found to be 72 ms/sample. The fluxgate magnetometer data were used to compute the payload rotation rate. Figure 4.8 shows the rotation of the payload was stabilized only after the balloon

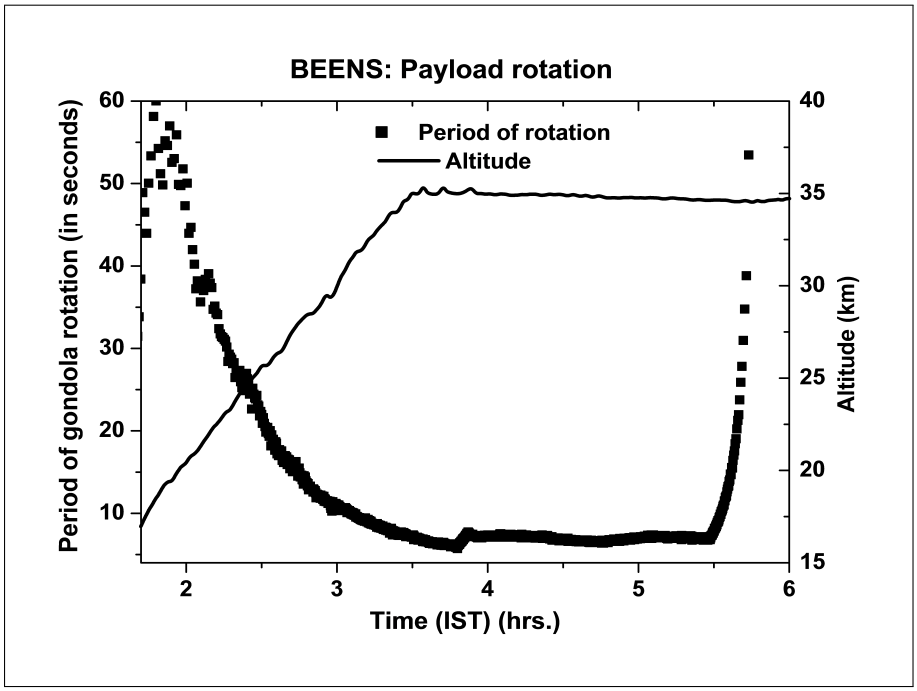

Figure 4.8: The payload rotation rate (squared symbols) computed using the reference magnetometer data and plotted along with the balloon altitude (continuous curve)

attained the float altitude. The period of rotation reached the lowest value of ~6 s (corresponding to ~10 rpm) then as against ~60 s at 02:00 IST. Unfortunately, the orienter responsible for the payload rotation malfunctioned at 05:30 IST following which the rotation was disabled. Further, the large DC offsets in the y- channel saturated the corresponding signal till about 04:00 IST.

4.2.1 Imapct of Using Five Boom Configuration

Due to the five probe configuration there was quite distortion in the measurement of electric field. The boom that was used to deploy P_5 (refer figure 4.1) is made of metallic boom and was isolated from the central payload using Teflon

washer like all other horizontal booms. The potential difference measured in the vertical direction to be greatly influenced by this arrangement. Another issue was to do with the requirement from the probe geometry that one of the x probes was to be used for the vertical electric field measurement. In fact, out of the two x probes, P_1 and P_2, probe P_1 was to be regarded as negative for the P_5-P_1 pair and connected to the negative input of the Z- channel of instrumentation amplifier and positive for the P_1-P_2 pair and connected to the positive input of the X channel instrumentation amplifier. Due to this configuration, there may be some interconnection between the inputs of X- and Z- channels. Thus the gondola noise present in the Z channel might have coupled to the X- channel. Because of the above issues, little useful information could be retrieved from the z channel and to some extent from the x- channel. On the other hand, the y- probes were well isolated electrically and distanced well away from other probes and booms used to deploy them. Indeed, foremost of the 2-hour duration, the data from the y- channel were clean and relatively less noisy.

In figure 4.9, we show the 43-second samples of the raw x- and y-probe outputs, namely, V_{12} and V_{34}, respectively, between 05:18 and 05:30 IST, along with their 25-point running averages. The top three panels depict V_{12} and the bottom three panels depict V_{34}. Having depicted the magnetometer y-sensor output (dash-dot curves) also for identifying the payload rotation, one can easily pick up the near-sinusoidal variations in the electric field channels that occurred at the same period as that of the payload rotation. An immediate difference that could be noticed between the V_{12}

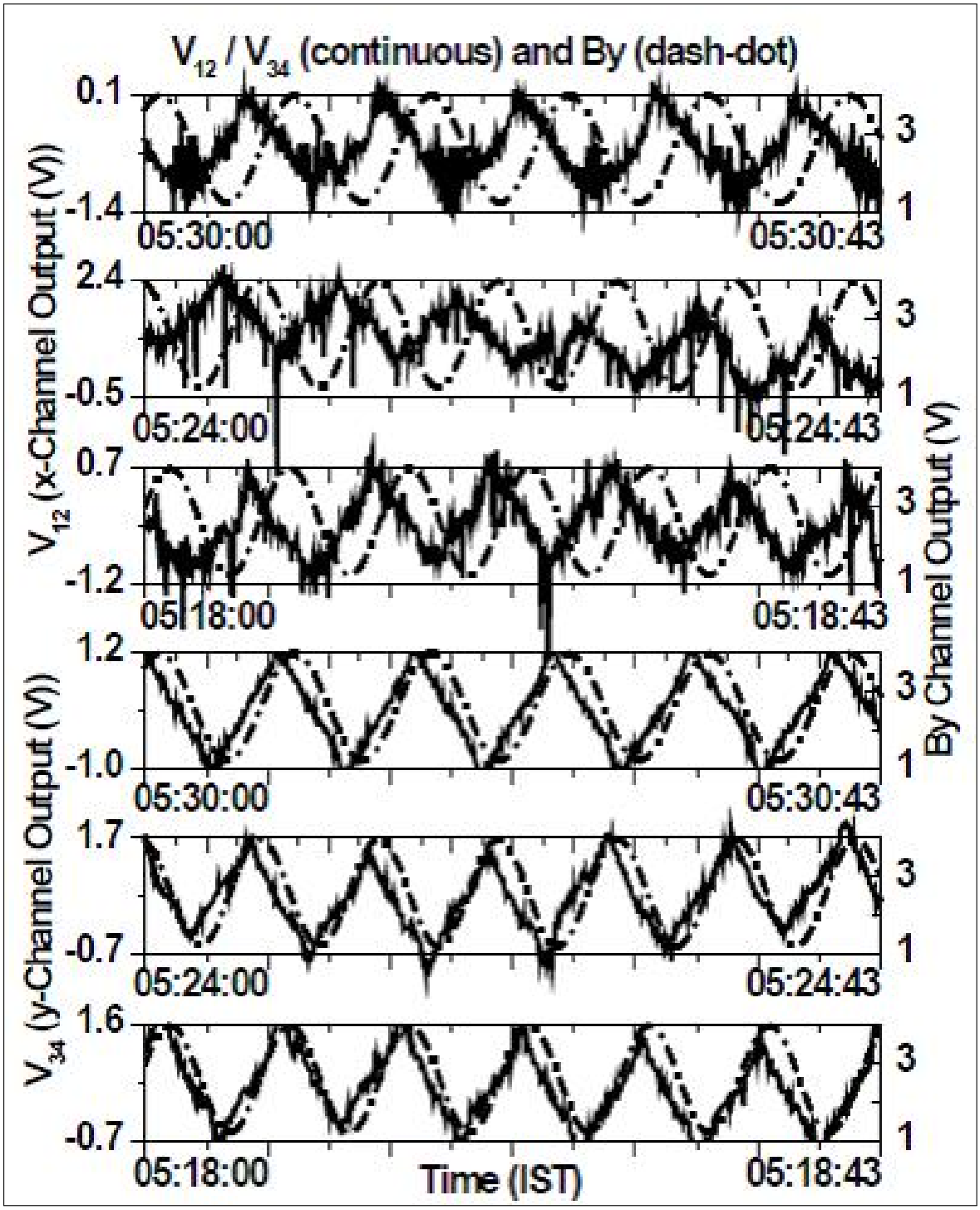

Figure 4.9: The raw x- and y-channel outputs (continuous) along with the magnetometer y sensor output (dash-dot). The top three panels represent V_{12} and the bottom three V_{34}. The time segments are indicated below every panel

and V_{34} outputs is that the y-probe outputs (V_{34}) were quite clean when compared to the x-probe outputs (V_{12}). As explained earlier, the noisiness of V_{12} is due to

the probe geometry chosen for this experiment and the use of a non-conducting boom for deploying the z-probe (P_5), the latter resulting in the gondola related noise fields appearing in the vicinity of one of the x-probes (P_1). In addition, the interconnection between the x- and z-inputs (opposite polarities) of the differential electrometer created noise coupling between the two channels.

4.2.2 Distortion over the Sinusoidal Variation of the Electric Field in the Rotating Platform

The columnar resistance is the electrical resistance of a unit-area column of atmosphere, extending between the surface of the Earth and the ionosphere. It varies with the mobility and concentration of the ions contained within the column. Ion number concentration depends on the balance between ion-production and ion-removal. The ion-production may be due to cosmic ray excitation and ion-removal may relate to aerosols if not through self-recombination (Harrison [2005]).

The spherical probe exposed in this environment acquired the ambient potential that can be measured through electrometer. If the input impedance of the electrometer is higher than the columnar resistance then there is no loading effect and the measured field is more precise.

To avoid various offset voltages involved in the measurement such as offset

voltage of the electrometer, offset voltage generated by unleveled pair of horizontal booms, offset voltage due to uneven surface properties of pair of probes, gondola was rotated at constant rate $\sim$ 6 rotation per minute (rpm). These offset voltages are additive in nature which results on a finite DC voltage superimposed over the atmospheric electric field which produce sinusoid variation. But the observed sinusoidal variation is looks like a distorted triangular wave and that can be attributed to the following reasons,

1. The potential acquired by the probe at an instantaneous position has required some time to discharge before the probes moves and acquire new value. The distortion due to discharge time constant can be avoided by rotating the gondola at very slow speeds. Otherwise we can reduce the electrometer impedance so that the acquired potential can be discharged fast by paying the penalty of adverse loading effect. The Pspice simulation studies can be used to validate this integrator phenomenon, which is shown in Figure 4.10. The sine to triangular distortion has obtained by the virtue of stray capacitance effect.

2. The sampling rate of the ADC should be 5-fold higher than the frequency of the signal against Nyquist criterion. (which, intern related to the rpm as well as frequency of the observed ELF band). For example the sampling rate of the ADC is just two times higher than the signal frequency then a triangular

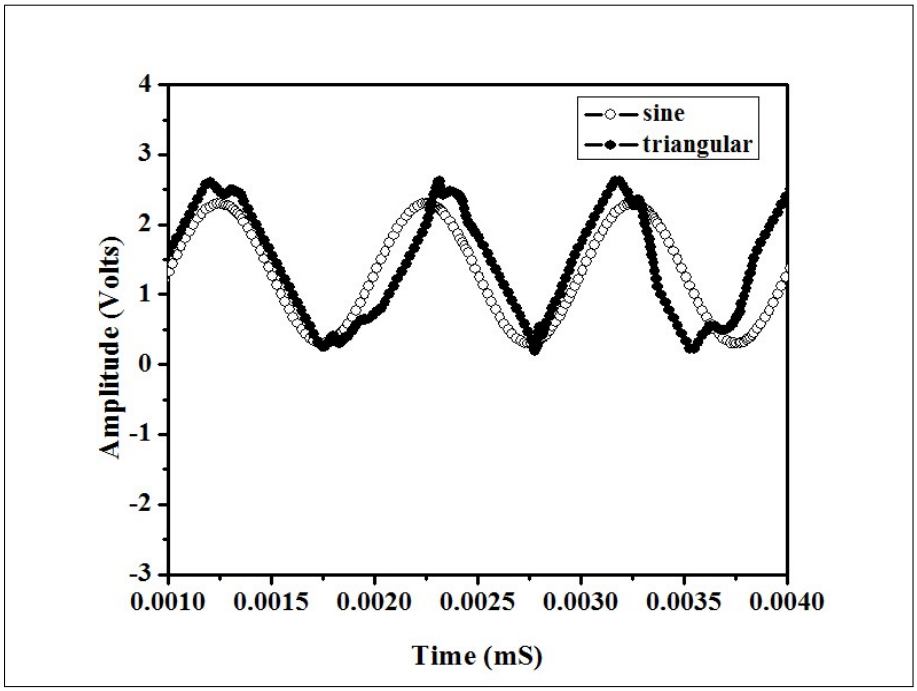

Figure 4.10: Simulation showing the sinusoidal distorted into near triangular waveform due to the effect of capacitance

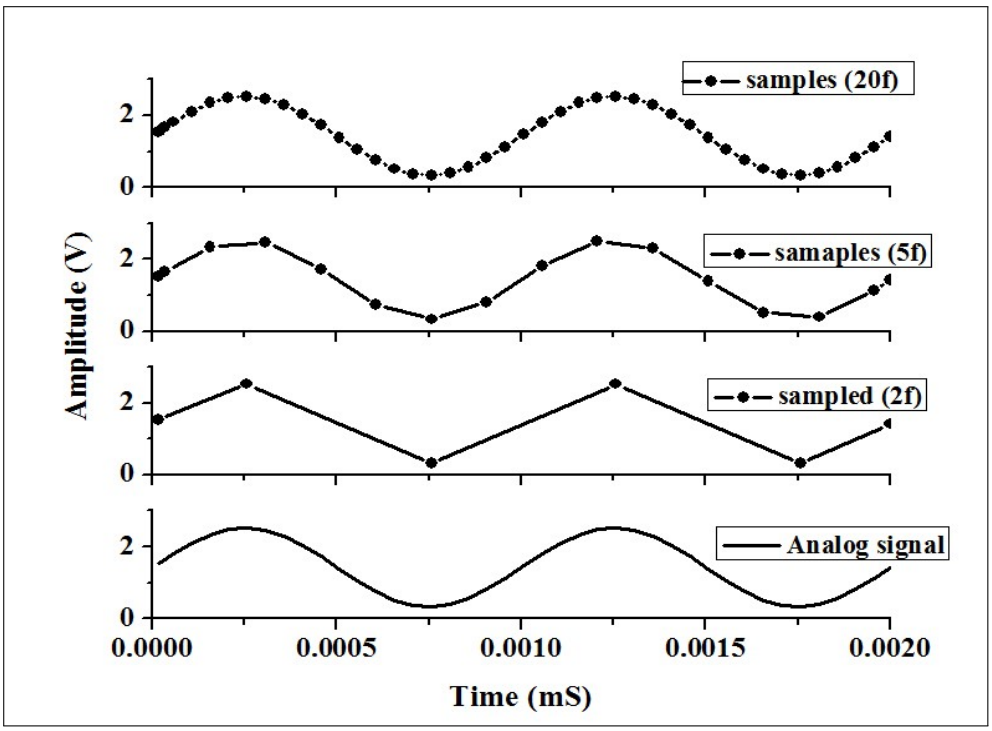

Figure 4.11: Simulation showing the effect of sampling rate on the analog signal under test

wave has been constructed from the digital data instead of sine wave. Hence proper reconstruction of sine wave requires at least 5 fold higher sampling rate then the signal frequency. Distortion due to sampling rate is depicted in Figure 4.11.

3. The high frequency noise spikes leads to the erratic sampling in case of signal embedded into noise situation. In case of very weak sinusoidal variation submerged into the high frequency noise, the sampled signal gives raise a distorted pattern as shown in the Figure 4.12(a). This can be avoided to some extent by using higher order active low pass filter for discriminating high frequency noise from the signal and that can be shown in Figure 4.12(b).

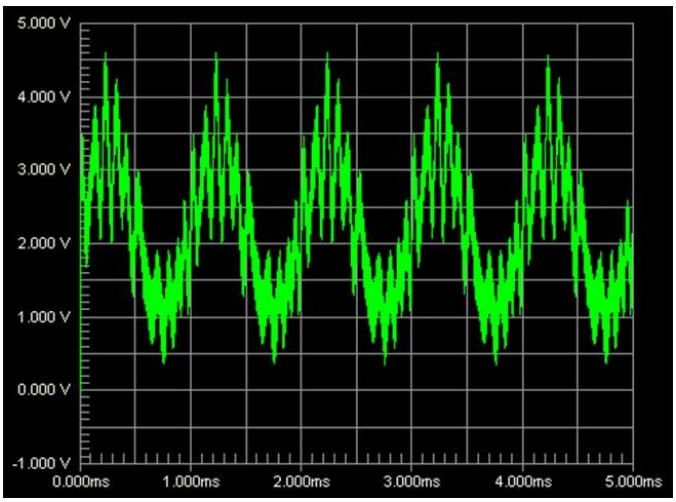

(a) simulation of a sample analog signal embedded in noise

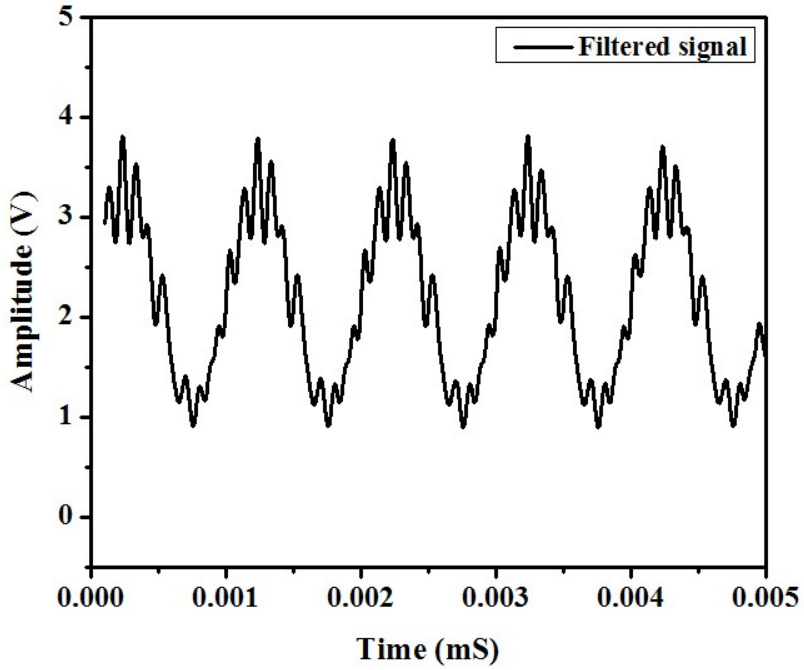

(b) Filtered analog signal which is embedded in noise

Figure 4.12: Effect of high frequency noise superposed on a sinusoid signal of interest

4.2.3 Vertical Electric Field

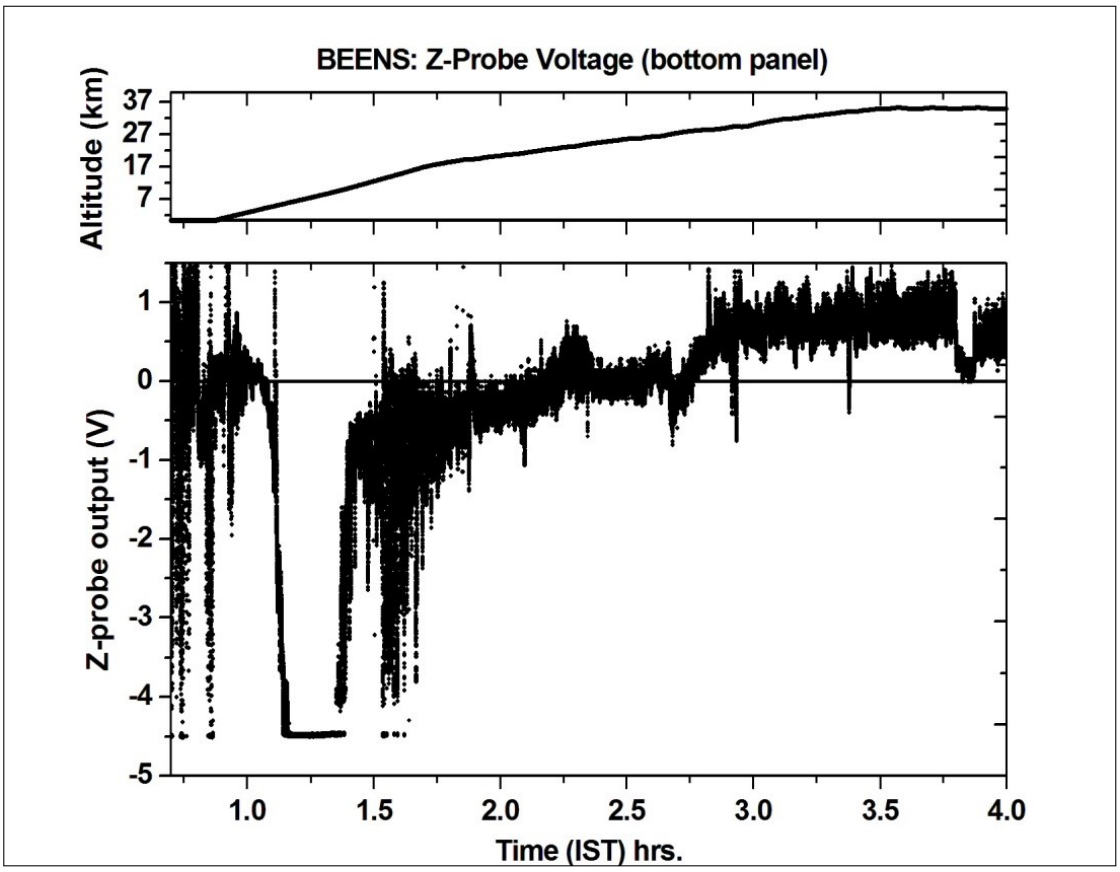

Figure 4.13: Raw output from vertical probes with time (bottom panel) and the altitude of the balloon(top panel)

In Figure 4.13, the raw output from the z- probes (bottom panel) is shown along with the balloon altitude (top panel). The signal saturation at ∼- 4.5 V noticed at 01:06 IST commenced at a time when the rotation of the payload was first enabled. The balloon was at a height of ∼5 km then. Interestingly, there is saturation in the z telemetry channel, which is not observed in the x and y telemetry channels. This will be a matter of further investigation. Between 01:00 and 02:00 IST, several telecommands including those to drop ballast were sent and all channel outputs were fluctuating wildly between their corresponding saturation values at

these times. An interesting revelation in the z-channel output was the gradual increase in the z-probe output as the balloon ascended to its float altitude. This was opposite to what is expected for the vertical electric field. For a conductivity profile exponentially increasing with altitude, the vertical electric field would decrease with altitude (Udare et al., [1991], for example). As already mentioned, the use of a conducting boom with no insulating material of sufficient length at its end is believed to have contributed to the contamination of the z-probe output. Thus the z- channel output will not be analyzed further.

4.2.4 Horizontal Electric Field

As discussed in the section 4.2.1, the use of five boom configuration, especially in x- and z- channel expected science data quality was not retrieved. The y- probes which were well isolated electrically and distanced well away from other probes and the booms used to deploy them. The data from the y channel, for almost 2 hours, were clean and relatively less noisy. One pair of boom is sufficient for delineating horizontal electric fields on a rotating platform.

Figure 4.14 shows the raw telemetry data with 25 point running mean, which corresponds to 1.8 sec time duration. With this process, high frequency noise gets suppressed further. Before estimating the electric fields, the raw data are fitted with a pass band in the range 5.6 - 7.3 seconds corresponding to the range in the gondola

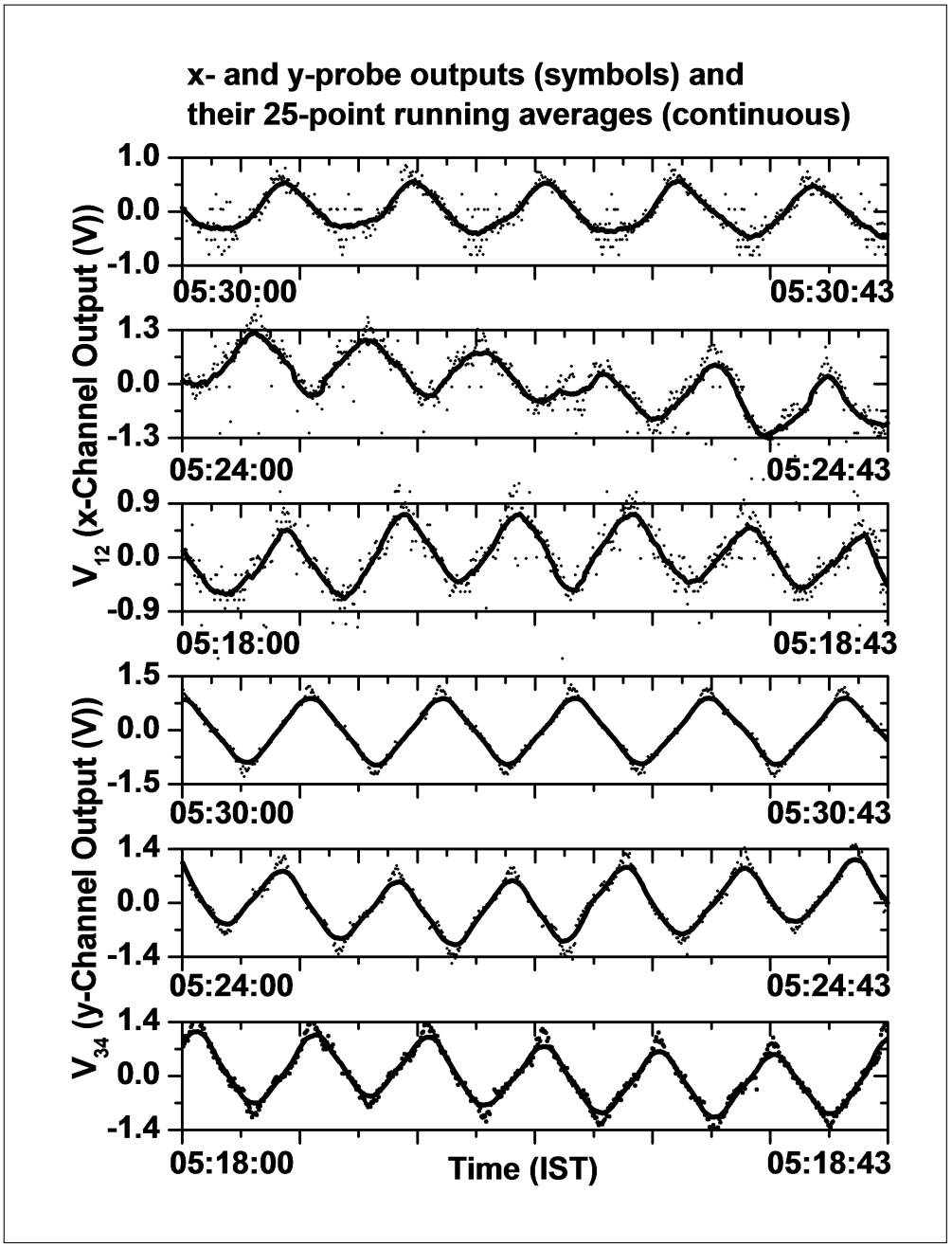

Figure 4.14: The raw x- and y-channel outputs (symbols) along with their 25-point running means (continuous). The top three panels represent V_{12} and the bottom three V_{34}. The time segments are indicated below every panel

rotation rate and so the DC offsets and any of their slowly varying components are removed in advance.

In figure 4.15, the amplitude (top panel) and phase (middle panel) of the

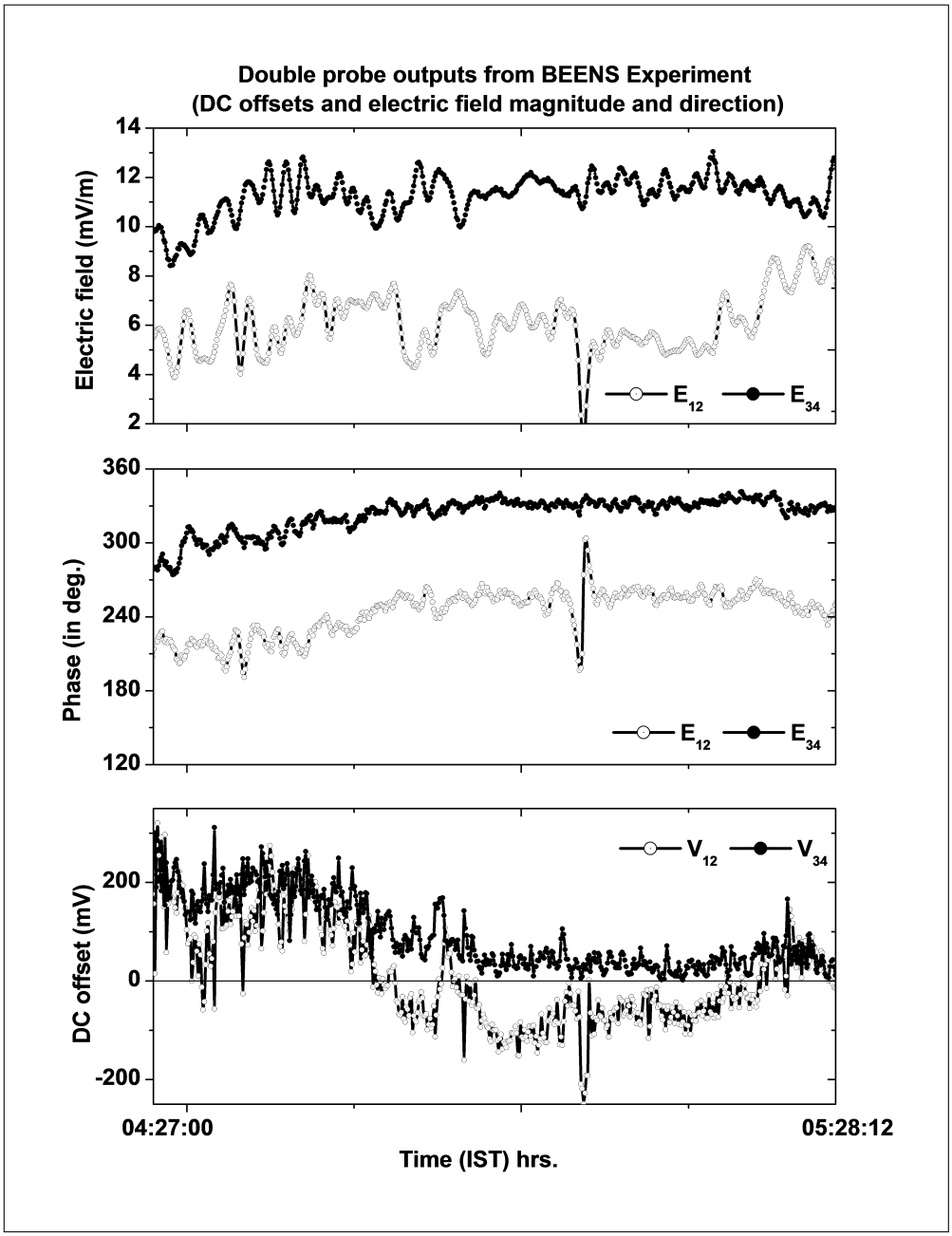

Figure 4.15: The magnitude and direction (top and middle panels) of horizontal electric field at stratospheric altitudes between 04:27 and 05:28 IST and the DC offsets (bottom panel) for the same period, both computed separately for the x- and y-probes

electric field estimated in a least squares sense from the band-pass filtered values of the x- and y-probe outputs between 04:27 and 05:28 IST are depicted. This 60-min duration was chosen considering the fact that the payload rotation was stable and the rotation rate was nearly constant. The amplitude in figure 4.15 represents

the magnitude of the electric field vector for one payload rotation 'event' and the phase represents its direction. There were 535 payload rotations during this one hour period, with each rotation leading to a measurement of electric field vector in the horizontal plane of the payload. The bottom panel of figure 4.12 shows the DC offsets for the x- and y-probe outputs, namely, V_{12} and V_{34}. These were essentially the mean values of the corresponding outputs computed over one payload rotation period. Interestingly, large offsets in the beginning of the experiment (~500 mV) gradually gave way to smaller values in the early morning hours prior to sunrise. The DC offsets are expected to represent primarily the contact potential differences between the two probes in a pair, which are in turn dependent on the differences in the properties of the probe material and how differently the material surfaces have responded to the ambient conditions. The electric field parameters estimated for every payload rotation period, however, were not expected to be affected by the dc offsets, especially at times when the latter varied in time scales much longer than the payload rotation period.

The top and middle panels of figure 4.15 depict the magnitude and direction of the horizontal electric field vector computed separately for the two horizontal probe outputs, V_{12} and V_{34}, for every payload rotation period (~7 s). The phases, plotted in the middle panel, are referenced with respect to north and as expected, the phase quadrature between the two probe outputs is clearly evident between the time period 04:45 and 05:30 IST. As the payload was rotating clockwise, the probe configuration

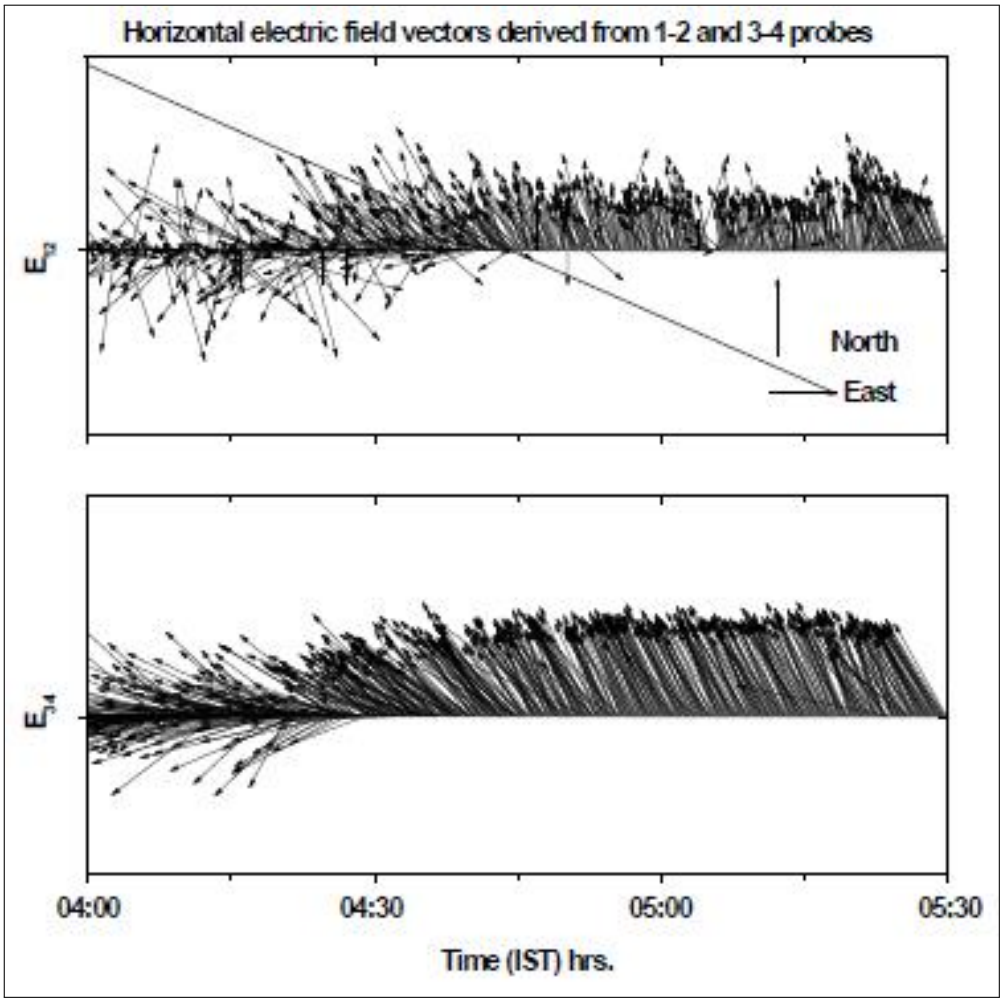

Figure 4.16: The horizontal electric field vectors, E_{12} and E_{34}, computed for every payload rotation period. The directions, north and east, are defined by the arrows

was such that the y-probe output was to lead the x-probe output by 90°. Another important feature noticed in figure 4.15 is the significant difference in the magnitude of the electric field computed for the two probe outputs on most of the occasions. At times when the phase quadrature was noticed between the two, E_{12} was smaller than E_{34} by at least 5 mV/m.

An interesting feature noticed in figure 4.16 is that the electric field, which was predominantly in the zonal direction and directed towards west at earlier times

(prior to 04:30 IST), is seen to turn clockwise between 04:30 and 05:00 IST and point northward during the later times. When the x-probe outputs were more stable during the last one hour of useful electric field observation, one can notice that the electric field derived from the x-probe output, E_{12}, was indeed directed northward and was consistent with the direction of the electric field estimated from the y-probe output.

The north-south (E_{NS}) and east-west (E_{EW}) components of the electric field vector computed for the y-probe outputs between 04:16 and 05:30 IST in figure 4.17. These were the 5-min averages of the estimated electric field components with the error bars representing their standard deviation within the respective 5-min block. The electric fields were largely westward throughout this duration but had changed direction from southward to northward at 04:00 IST and remained northward thereafter. Electric fields in the range of 10-12 mV/m at any instant of the observation duration are clearly evident.

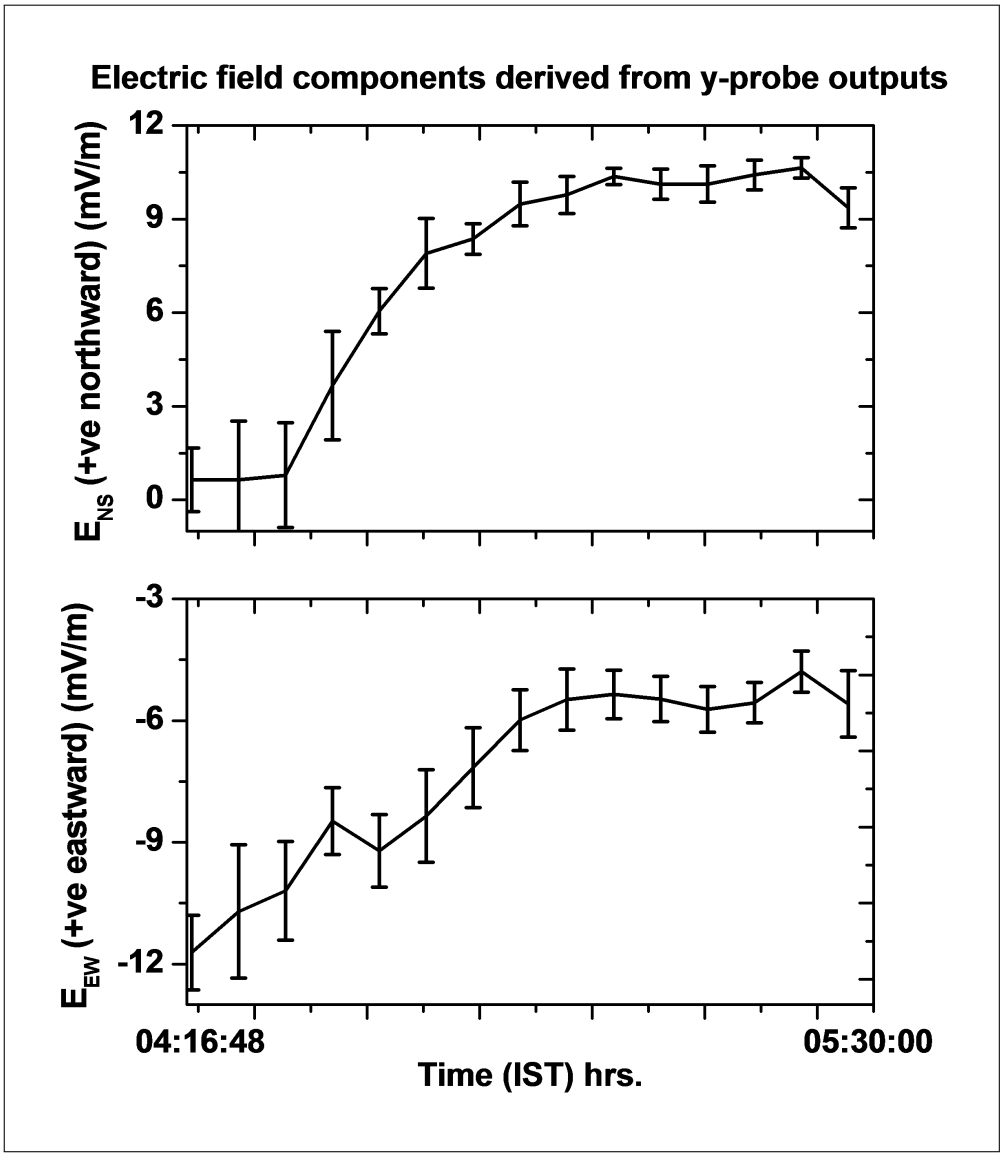

Figure 4.17: The 5-min averages of electric field components derived from the horizontal probe outputs, the northward or ENS plotted in the top panel and the eastward or EEW plotted in the bottom panel. The error bars represent the standard deviation for the electric field estimates made for individual 5-min blocks

4.3 Discussion on Horizontal Electric Field from BEENS Experiment

As mentioned earlier, the intended goal of the BEENS experiment was to capture horizontal electric fields of ionospheric origin at stratospheric altitudes. A

unique configuration of the geomagnetic field at the equator permits a variety of electrodynamical phenomena to occur in the E and F regions of the ionosphere. The plasma fountain that is responsible for the large-scale redistribution of the ionization during daytime, generation of a spectrum of ionospheric irregularities on certain occasions in the dusk sector and the development of intense current system during daytime called equatorial electrojet are the major phenomena occurring in the equatorial region that are of significant interest to the scientific community. Electric fields are the major drivers for these phenomena and it is important to monitor them in order to understand the ionospheric variabilities as this contributes to the subject matter of space weather.

The major electric field drivers for the Earth's giant global electric circuit are the global thunderstorm activity, the solar wind-magnetosphere-ionosphere dynamo and the ionospheric dynamo (Hays and Roble [1979]; Roble and Hays [1979]). In the past, the middle atmosphere was often considered to be electrodynamically passive so that the electric fields observed at stratospheric and mesospheric altitudes could be interpreted as those penetrating from above or from below. Solar wind induced magnetospheric convection, for example, produces large scale fields of several tens of milli-volts per meter in the polar cap and in the auroral ionosphere. These horizontal fields were indeed observed at balloon altitudes with little attenuation (Mozer and Serlin [1969], for example) in accordance with theoretical analysis (Park [1976]). Large-scale ionospheric dynamo fields of a few milli-volts per meter too are expected

to penetrate to stratospheric altitudes with little attenuation (Volland [1972]). It is to be noted that the global thunderstorm activity driven fair-weather electric fields are observed as vertical fields, whereas the upper atmospheric sources induce horizontal fields at balloon altitudes. In the case of the former, the Earth and the ionosphere act as equipotential surfaces and the sources drive electric fields that point essentially downward in the fair-weather regions, i.e., far away from thunderstorm centers. In the case of the latter, the two upper atmospheric generators produce charge separation and hence large-scale electric fields horizontally through the solar wind-magnetosphere-ionosphere dynamo or the ionospheric neutral wind dynamo as the case may be. These horizontal fields map downward as they are to mesospheric and stratospheric altitudes. Observing horizontal fields of ionospheric wind dynamo origin from a balloon platform at low to mid latitudes has always been a challenge because they are smaller (~few mV/m) and are difficult to measure, when the measurement errors themselves are ~1 mV/m. Gonzalez et al. (1982) reported large horizontal electric fields (up to 10 mV/m) in the Brazilian Magnetic Anomaly region. To explain this feature, they invoked the idea that the energetic particle precipitation, associated with enhanced magnetic activity, induced irregularities in middle atmospheric conductivity that in turn produced distortion in the fair weather vertical electric field. Orographic features have been known to produce similar irregularities in the conductivity profile that are capable of explaining large horizontal fields observed on some occasions (Ogawa et al., [1975], for example). Such large

induced fields would clearly overshadow the weak ionospheric fields expected at balloon altitudes.

With the presumption that the electric fields at low latitudes were expected to be small ($\sim$ few mV/m), the payload for the BEENS experiment was designed to enable use of 3 m long booms for the horizontal probes that yielded probe-to-probe separation of $\sim$7 m. For the outer one meter portion of each of the horizontal booms, insulating fibreglass rods were used. However, for the inclined boom used to support the probe intended for vertical electric field measurements, no such insulating arm was used. This, along with the probe configuration that permitted use of five probes instead of six, had placed constraints on the usefulness of the electric fields sensed by x- and z-probes. There were also issues with the gyro motor used for spinning the payload that restricted useful electric field measurements to less than two hours out of possible four and half hours at the float altitude. These deficiencies in the probe configuration and the deployable boom chosen for the z-probes will be addressed in the next flight.

The horizontal electric field measured by the y-probes and these measurements were relatively free of noise due to payload rotation as well as any noise arising in the electronics. The modulation of the potential difference generated from the y-probe outputs at the period of the payload rotation (see Figure 4.14) is quite clear. There is no reason to believe that these measurements were contaminated by gondola noise

or the inclined boom. The latter would contribute to a distortion of the field around the x-probe (P_1) underneath the z-probe (P_5) but not around either of the y-probes (P_3 and P_4) (see Figure 4.1 for the probe geometry). Probes P_3 and P_4 were well away and were electrically isolated from the rest of the probes and their supporting structures.

As noted earlier, there are no marked orographic features in the vicinity of the balloon track and therefore any enhanced electric field due to orographic nature would appear in the experimental data. Further, the results presented in this thesis pertain to a float altitude of ~35 km, well above the altitude region over which orographic effects are expected to be pronounced. Also, fair-weather conditions prevailed throughout the experiment duration on the ground and just above the ground. The Kalpana satellite imagery does not reveal any high altitude convective cloud system over the southern Indian peninsular region at the time of the balloon observations reported herein nor do the infrared images obtained from the EUMETSAT fleet of satellites (refer to Figure 4.7). No orographic or local thunderstorm activity effects seemed to have contributed to the observed electric field signatures.

Now that electric fields in the range 10-12 mV/m cannot be of ionospheric dynamo origin and that observations were made over low latitudes thereby precluding auroral electric fields, other sources capable of generating electric fields of observed

magnitude can be looked over.

Holzworth (1989) first reported large horizontal electric fields at balloon altitudes from campaigns conducted during the austral summers of 1983 and 1984 involving long-duration superpressure balloons. The fields detected then were in the range of 10-20 mV/m during nighttime and 30-70 mV/m during daytime at altitudes of ~27 km. Holzworth (1989) called such fields as HITS implying electric fields that were horizontal, inertial, turbulent and stratospheric. A striking feature of those fields was that the horizontal vector rotated counter-clockwise at a period that matched the inertial period of a class of atmospheric gravity waves present at those latitudes. The existence of such fields was confirmed in a later work by Hu and Holzworth (1997) from an extended data set that covered a wide range of latitudes from South Pole to 28°S.

The measurements from the present experiment were made an hour before local sunrise and therefore would correspond to nighttime conditions. The observed electric fields of 10-25 mV/m are, therefore, of similar magnitude to those reported earlier, but were observed at higher altitudes. Moreover, the period of the inertia gravity waves for this location would be close to ~40 hours. As the data duration was short, we could not decipher any possible influence of shorter period atmospheric gravity waves, especially in the period range of 30 min to 4 hours which are quite common at these latitudes (Gurubaran and Rajaram [2001]; Ramkumar et al.,

[2006], for example). Though there was a gradual turning of electric field from westward towards northward (see Figure 4.16), it was still not possible to construct a complete hodograph for want of extended data sets. For this reason, we are not able to invoke a gravity wave hypothesis for explaining the observed magnitudes of electric fields.

Chapter 5

Schumann Resonances Observed at Maitri, Antarctica

5.1 Introduction

The space between the Earth and the ionosphere is termed Earth-ionosphere cavity. This cavity acts as a wave guide for the propagation of electromagnetic waves. W. O. Schumann in 1952 first predicted the Schumann resonances (SR) are distinct peaks in extremely low frequency (ELF, 3 - 300 Hz) range of electromagnetic spectrum. The resonance phenomenon was then observed by Balser and Wagner (1960). The Earth-ionosphere cavity supports two types of electromagnetic modes:

1. longitudinal modes corresponding to global quasi-horizontal wave propagation around the globe

2. transverse modes related to local, quasi-vertical propagation between the surface and the ionosphere (Nickolaenko and Hayakawa [2002]).

The standing waves whose wavelengths commensurate with planetary sizes. Figure 5.1 gives a schematic view of Schumann resonance circumnavigating around

the globe.

For a thin lossless cavity the Schumann resonance Eigen frequencies, f_n, are approximately given by

$$f_n = (c/2\pi R)\sqrt{n(n+1)}$$

Where c is the velocity of light in free space, R is the radius of the Earth, and n=1, 2, 3,.. is the corresponding eigen mode (Schumann [1952]). In a more general approach, losses in the cavity and variability of the upper boundary due to atmospheric conductivity and ionosphere dynamics, the eigen frequencies are slightly lower (Balser and Wagner [1960]). The average frequencies of the five lowest Eigen modes are approximately, 7.8, 14.3, 20.8, 27.3, and 33.8 Hz, which fall in the Extremely Low Frequency (ELF) range.

The importance of thunderstorms in the coupling of electromagnetic energy to the upper atmospheric region on a global scale is underscored by the fact that the thunderstorms and associated lightning activity are the generators which maintain more than 5 x 10^5 Coulombs of the Earth's charge against the conduction loss due to the total global current of ~1800 A flowing through the conducting atmosphere in fair weather regions (Stergis et al., [1957]). At any given time a total of about 2000 thunderstorms occur worldwide with about 100 lightning strikes occurring

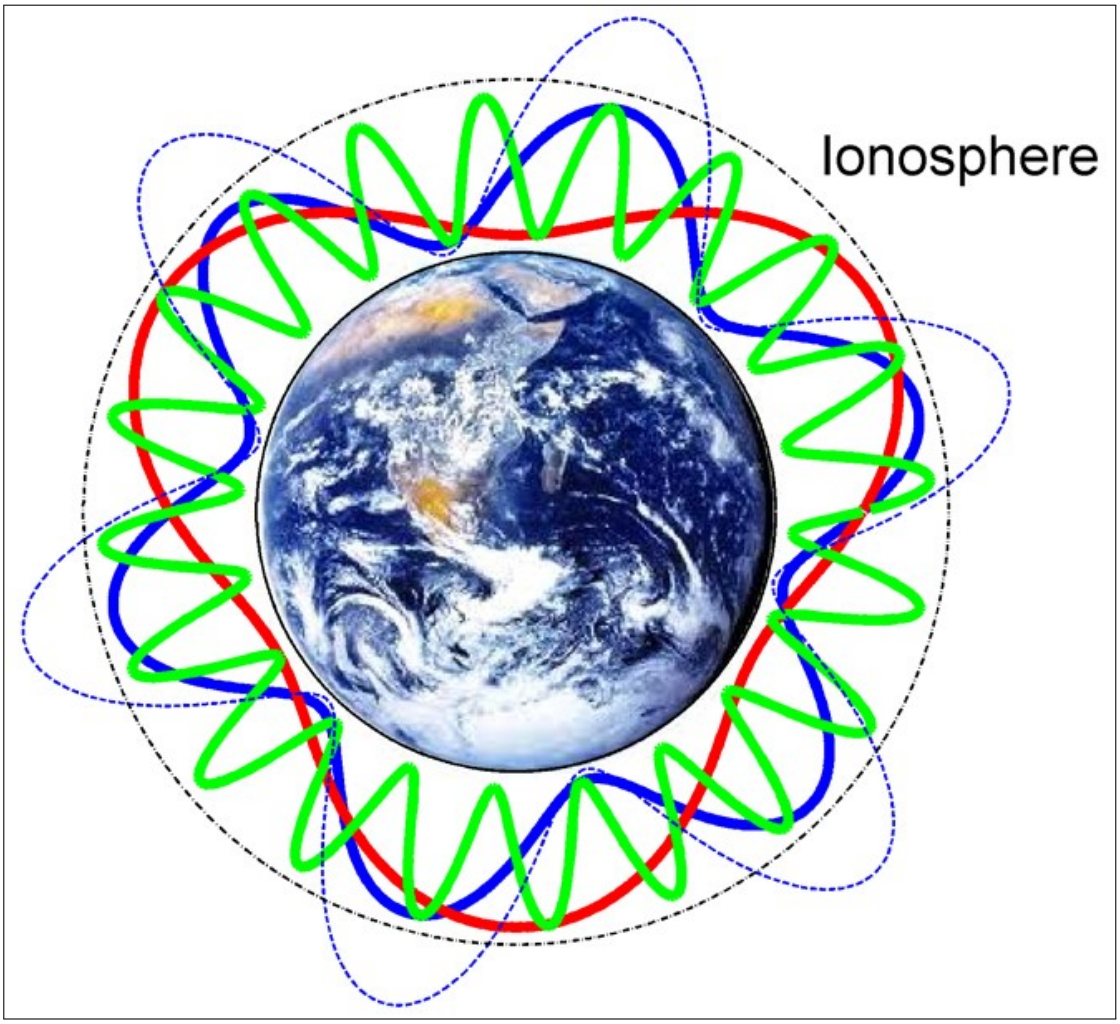

Figure 5.1: Waves created by lightning flashes here shown in blue, green, and red circle around Earth, creating a phenomenon called Schumann resonance. These waves can be used to study the nature of the atmosphere they travel through Credit: NASA/Simoes

every second (Volland [1984]). This large occurrence of lightning strikes keeps the cavity populated with ELF radiation reported by many researchers (Labendz [1998]; Beamish and Tzanis [1986]; Balser and Wagner [1960]; Sao et al., [1973]; Satori and Zieger [1996]; Belyaev et al., [1999]).

Ionospheric asymmetry and inhomogeneous distribution of lightning increase cavity complexity and consequently both data interpretation and cavity characteriza-

tion. The variability in the outer boundary has significant implication on SR spectra. For example, the Eigen frequencies of the cavity were found to be shifted by about 0.5 Hz due to high altitude nuclear explosion (Refer Madden and Thompson [1965] for details). The interaction of solar wind and the ionosphere distorts and modulates the upper boundary and influence cavity Eigen frequencies which respond to solar flares (Reid [1986]). During solar proton events it has shown that the signal amplitude, frequency and Q factor (damping factor) all increased (Schelgel and Fűllekrug [1999]).

Resonances in the Earth‘s cavity are closely related to lightning activity and contain information about the global electric circuit of the cavity. Lightning is the major source of electromagnetic energy in the Earth‘s cavity. Schumann resonances studies are currently directed in three major fields of research specifically climate change, high altitude atmospheric electricity and space weather. The relation between Schumann resonances, lightning, and thunderstorm activity at global scale presents a reliable method to monitoring climate variability and space weather (Williams [1992]; Williams and Satori [2007b]). Correlation between Schumann resonance measurements onboard stratospheric balloons and observation from satellites reveals a promising approach for the investigation of high altitude discharging event such as sprites (Williams et al., [2007a]).

The present chapter discusses on the observations made at Maitri, Antarctica

(70.8° S, 11.7° E). The Schumann resonance measurements at this Antarctica station gives an opportunity to examine the SR parameters, namely, the amplitude and frequency, in the north-south (H_{NS}) and east-west (H_{EW}) magnetic components over the icy continent. The analysis for the first resonant mode presented in this work reveals a strong UT variation in its amplitude in seasonal as well as yearly time scales. The NS amplitude reveals a semi-diurnal variation with peaks at ~10:00 UT and ~21:00 UT, whereas the EW amplitude exhibits a strong diurnal variation with a pronounced peak at 16:00 UT. The diurnal curves for the frequency for both components are similar in nature to those for the amplitude but for a time shift. The diurnal trend in the amplitude is retained irrespective of seasons, whereas significant difference is noticed for the frequency between the summer and winter seasons, especially in the EW component. The observed diurnal variation in the SR intensity is explained in terms of the dominant thunderstorm activity centered over the three convectively active regions: Asia/Maritime Continent (Indonesia), South America and Africa. The diurnal variation in frequency depends not only on the location of the thunderstorm region with respect to the observer but also on the ionospheric day/night conditions and the Earth-ionosphere cavity thickness.

5.2 Precautions to be Taken for the Installation of the Search Coil Magnetometer for Measuring Schumann Resonance

1. The measurement to be carried out in electromagnetically clean place. The sensor to be located as far as possible from power mains lines and large ferromagnetic objects, the minimal distance should be about 200 m. For example, at the sensor outputs one can observe process of opening and closing of the car door at the distance more than 15 meters. Avoid measurement sites near big trees; strong wind will produce soil oscillations too and consequently sensor vibrations. The distance between each of the three sensors should be about 2.5 meters.

2. Sensor should be placed in a stable position. (e.g., the 1"rotation of the sensor in the Earth magnetic field can produce ~250 pT of parasitic signal). For this purpose, the sensor should be buried in the ground and at least the first three-five meters of the cable connected to the sensor has to be buried,. The cover from rain should be foreseen too. This procedure allows avoiding wind blows influence and also decreases sensor temperature fluctuations.

3. A sensor cable should containe 3 twisted wires for power supply, two (or at least one) shielded twisted pairs for signal and one wire for analog ground. The length of the cable to be shorter than 100 m to be prepared.

4. Use of battery will reduce the high frequency noise.

5. If DC-DC transformer is used, it should be make sure that they do not produce noises (spikes) in the input circuits of the equipment.

5.3 Experimental Setup

Measurements made by the three-component induction coil magnetometers (ICM) (Make: LEMI-30i of Lviv Center of Institute for Space Research, Ukraine) deployed at the Indian Antarctic station, Maitri (70.8°S, 11.7°E), were utilized for the present study. Precautions mentioned in above section (§ 5.2) were strictly considered for the SR measurements are carried out at Maitri, Anatrctica. The magnetometer units comprise of three induction coils and a Communication and Measuring (CAM) unit. Two of the coils were installed along geomagnetic north-south and east-west directions to yield the respective magnetic field components (H_{NS} and H_{EW}, respectively) and the third was aligned in the vertical. The magnetometers were designed to capture the desired magnetic field signals in the frequency range 0.01 to 30 Hz. Data gathered by the CAM unit are transmitted for storage to an external PC.

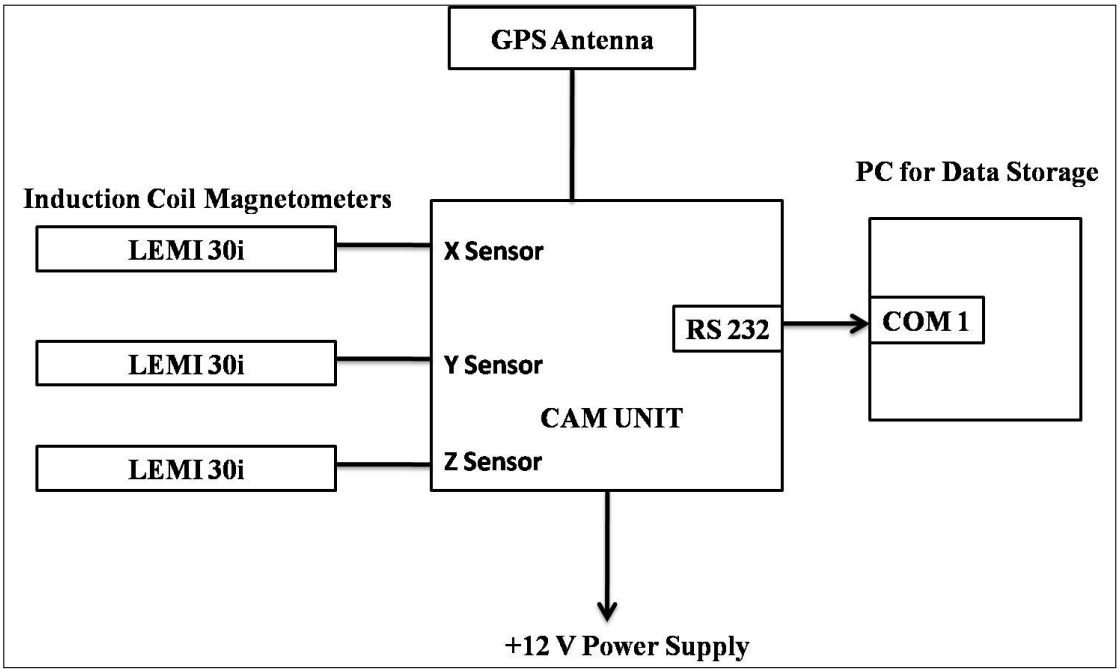

Figure 5.2: Block diagram showing the experimental setup of Schumann resonance measurement at Maitri, Anatarctica

5.4 Results and Discussion of Schumann Resonance Measurement at Matiri, Antarctica

For the present work only the NS and EW magnetic components for the year 2011 is considered. Data were recorded at a sampling rate of 64 Hz. The raw time series data were stored and the SR parameters were obtained during the post processing of the raw data. The raw data were corrected to the geographic coordinates using the transformation equations.

$$X = H\cos(\theta) + D\sin(\theta)$$

$$Y = -H\sin(\theta) + D\cos(\theta)$$

A total of 132 days useful observations for the year 2011 were analyzed after eliminating days with noisy data or when the experiment was not conducted. For the present study, the frequency range from 5 to 30 Hz which includes the first three SR modes recognized at Maitri, Antarctica station.

The model Lorentzian curves Ln(f) with unit amplitude and fixed frequency F_n = (8, 14.3, 20.5) Hz and thee quality factor Q = (6, 6, 6.5) of the first three resonance modes in the frequency range Δ F_n = (F_n-3 and F_n+3) Hz was fitted to the observed Schumann resonance spectra (P_n(f)). Fitting Lorentzian to SR Spectra is a standard method followed by many researchers to obtain the SR parameters (Heckman et al., [1998]; Belyaev et al., [1999]; Hobara et al., [2000]; Shvets et al., [2010]). These parameters considered are (excluding amplitude), on average, experimentally observed values. By calculating the angles between the vectors of model Lorentzians L_n(f) and those representing each resonant peak P_n(f) in the SR spectrum decide whether an experimental spectrum is rejected or not. The angle between two vectors representing the two discrete series characterizes discrepancy between their shapes. The angle between two vectors is calculated in a standard way through the scalar product

$$A_n = \arccos(R_n)$$

Where $R_n = (L_n, P_n) / |L_n| / |P_n|$ is a cross-correlation coefficient between the model Lorentzian L_n(f) and the corresponding part P_n(f) of the spectrum. A rule of

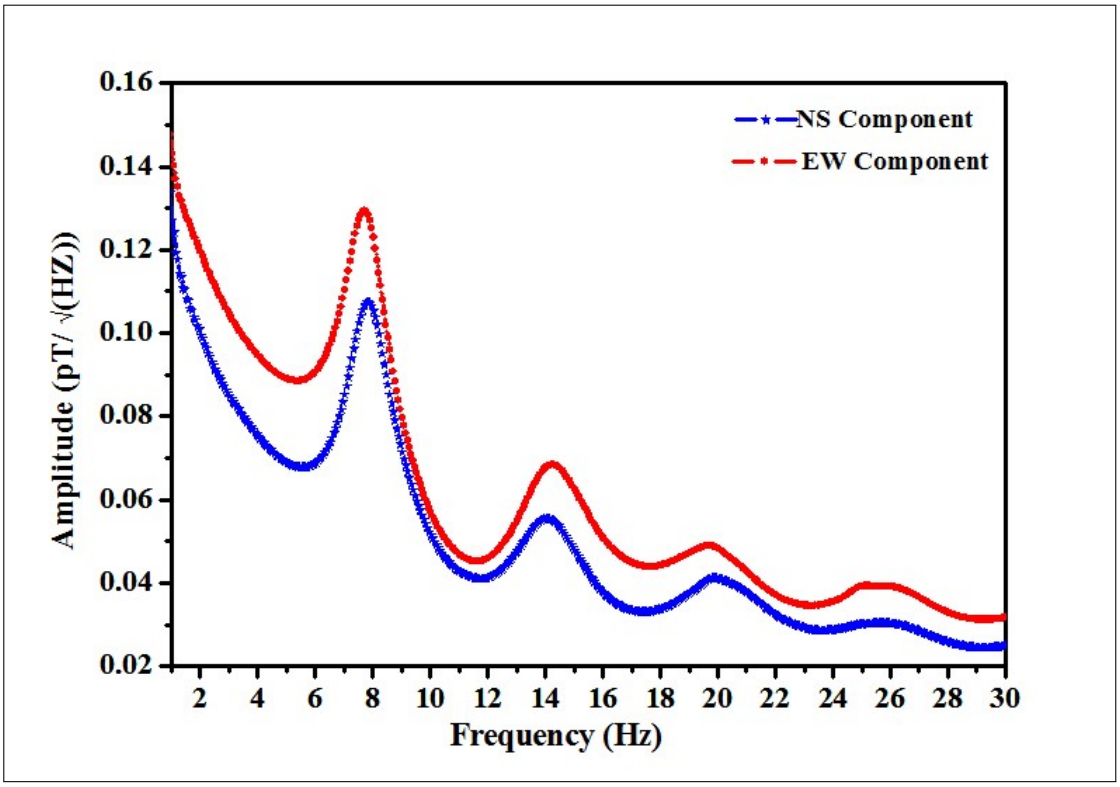

Figure 5.3: Annually averaged amplitude spectra of Schumann resonance over Maitri, Antarctica

selection of a spectrum is proposed as follows: The maximum value of A_n calculated for each three resonance mode must not exceed 40° and the mean value of all three angles must not exceed 22°. Thus the method yields the frequency and the peak power spectral density for each mode.

The power spectra for the SR measurements are obtained by taking 1024 FFT points with 256 point overlapping for every 30 minutes and composite average is taken for the entire year. The 30-min individual spectra for all days were averaged over the whole year. The results from this exercise are depicted in figure 5.3. The amplitudes are expressed in $pT/\sqrt{Hz}$. As expected, the first three modes at 8, 14 and 20 Hz can be prominently seen and the instrument captures well these three

modes. A similar instrument has been used by earlier workers from the low latitude station, Agra, in the Indian sector (Singh et al., [2014]).

5.4.1 Diurnal Variation of the Mode 1 Amplitude and Frequency

A prominent feature of the observations reported here is the strong diurnal variation of the intensities of the SR modes. This was anticipated as the rotation of the Earth changes the location of the observer with respect to major afternoon thunderstorm centers and the propagation conditions for the electromagnetic waves would also vary when part of the ionosphere would lie on the day-side and the rest on the night-side. In figures 5.4 and 5.5, depicts the temporal variation (in UT hours) of the amplitude and frequency variation of the first mode in the two components in the annually averaged sense. Wherever error bars are shown, they represent the standard deviation for the corresponding data point averaged over the selected period. We immediately notice that the diurnal curves of the amplitudes for the two components reveal a very systematic variation. The amplitude of the NS component displays a semi-diurnal pattern having peaks, one around 10:00 UT and the other around 21:00 UT. The EW component shows a small peak around 07:00 UT and a single larger peak, stronger than the NS component, at around 16:00 UT.

From Figure 5.4, it can be infer that the diurnal variation of the NS magnetic

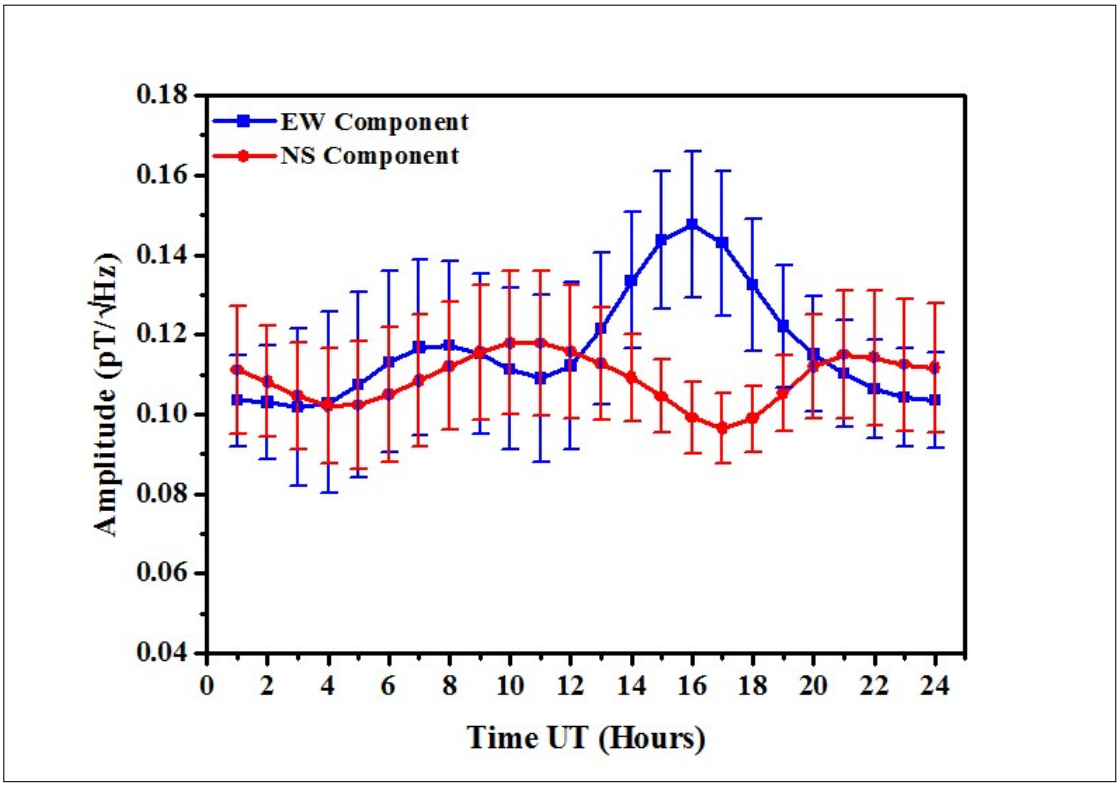

Figure 5.4: Annually averaged diurnal amplitude variation of the first SR mode over Maitri, Antarctica

component, which shows two maxima, is possibly associated with the thunderstorm activity over Asia and South America (the times of occurrence in both maxima correspond to late afternoon local times over these continents with respect to the observing station; for example, peaks between 06:00 and 08:00 UT would correspond to the deep convective activity over the western Pacific region, peaks around 10:00 UT would correspond to the activity over the Indian sector and peaks around 21:00 UT could be related to the thunderstorm activity over the American region). As the magnetic perturbation vector is aligned perpendicular to the propagation wave vector, it can be anticipated that the sensors would pick up those waves whose propagation vector is orthogonal to the alignment of the sensor. For the

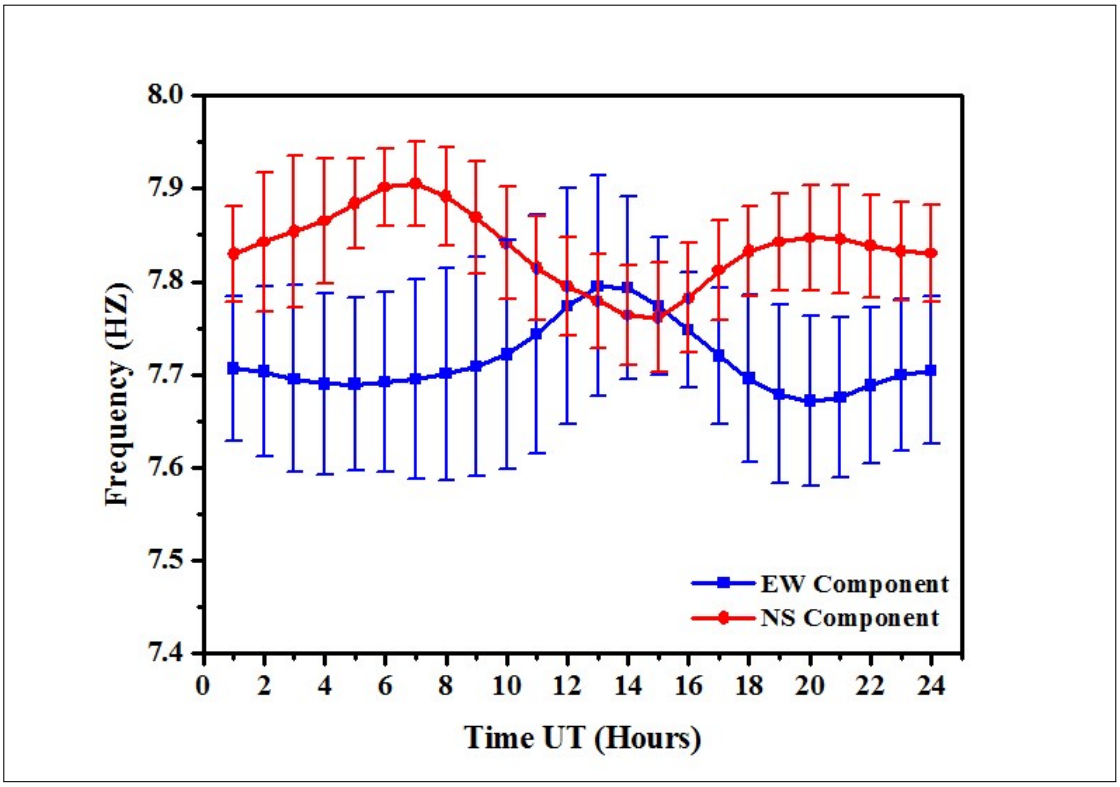

Figure 5.5: Annually averaged diurnal frequency variation of the first SR mode over Maitri, Antarctica

NS component, we expect the waves to arrive at a substantial angle to the observer at Maitri and that implies their sources to be possibly located in the thunderstorm regions far away towards north-east over the Asian sector for the 10:00 UT peak and towards north-west over South America for the 21:00 UT peak. It may be noted that the continental regions in the tropics over those locations would support deep convection during the corresponding local afternoon hours. In the EW magnetic component (H_{EW}), a strong maximum around 16:00 UT suggests an association with the peak thunderstorm activity in Africa (north of Maitri).

Figure 5.5 shows the diurnal frequency variation in the first mode of SR for the whole year. Two prominent peaks are visible in NS and one in EW components.

The reasons for this behavior of the diurnal frequency variation are not known yet but we expect contributions to the diurnal frequency variations to arise not only from the source-observer geometry but also from the ionospheric height movements and conductivity variations.

5.4.2 Seasonal Dependence of the Diurnal Variation of Mode 1 Amplitude

Figure 5.6 shows the diurnal variation of the amplitude of the first SR mode in the NS component during the Southern Hemisphere summer (November, December, January, and February (NDJM)), winter (May, June, July, and August (MJJA)) and Equinox (March, April, September, October (MASO)) during 2011. Larger error bars shown for the equinox months are due to the fact that the results for the two equinox seasons have been combined and also that there were few days available in the month of March. Two peaks are observed in the NS component of SR, one between 08:00 UT and 10:00 UT and the other at around 20:00 UT in all three seasons, which were earlier ascribed to the thunderstorm activity occurring over the Asian/Maritime Continent and the South American continent, respectively. Figure 5.7 shows the diurnal variation of SR in the EW component. Here, it is noticed a strong peak at 16:00 UT in all three seasons with similar amplitudes along with a secondary peak between 06:00 UT and 08:00 UT. Earlier, the results for the annual

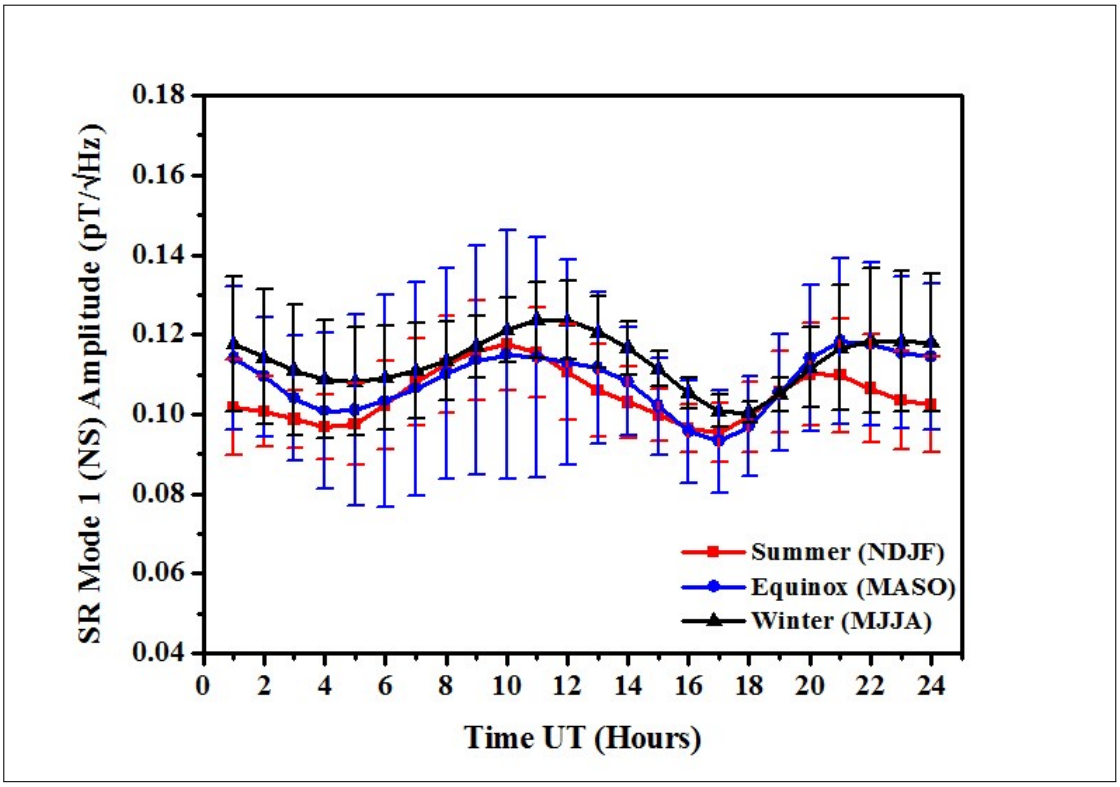

Figure 5.6: Mean Diurnal-Seasonal Amplitude Variation of the First SR mode in NS magnetic components at Maitri, Antarctica

average for this component indicated the potential sources to lie in Africa.

The results for the amplitudes and phases of the diurnal and semidiurnal variations of the SR parameters estimated in the least squares sense are provided in Tables 1 and 2. With regard to the intensity of the SR mode (Table 5.1 and Figures 5.4 and 5.5), one can notice a stronger and dominant diurnal signature in the EW component and a stronger semi-diurnal signature in the NS component. Moreover, the diurnal amplitudes in the EW component are double the amplitudes in the NS component.

The diurnal variation of SR power or amplitude generally has a tendency

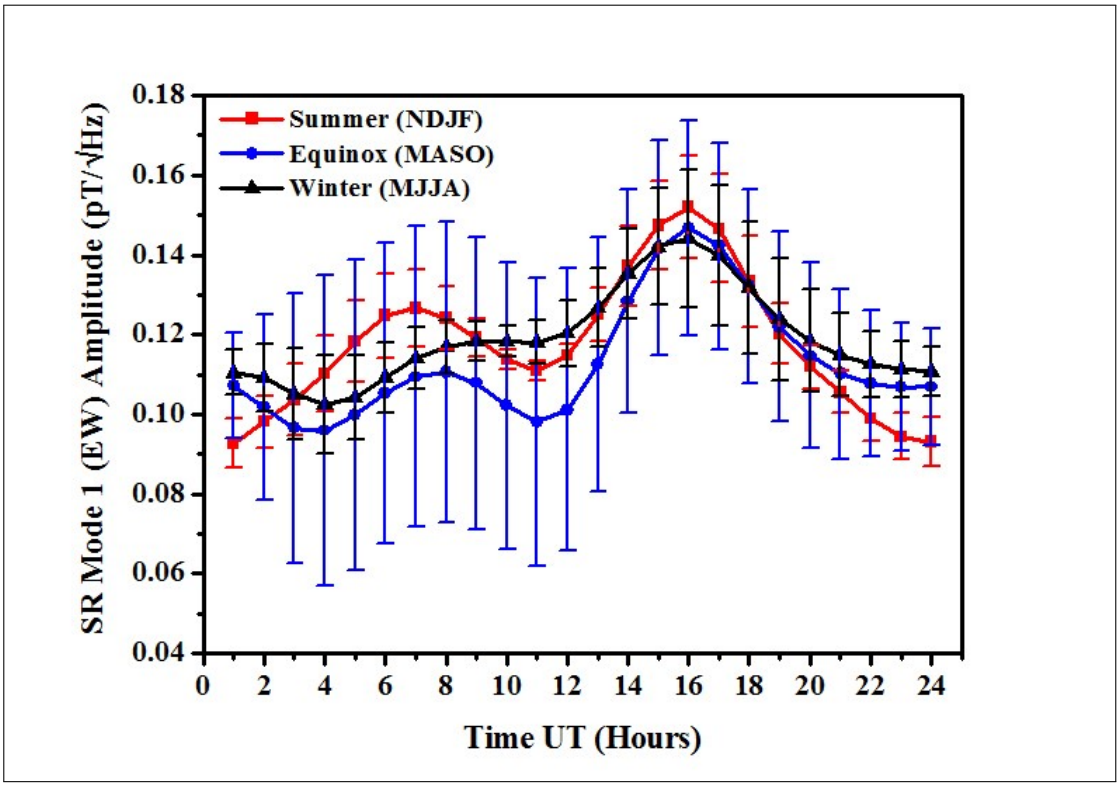

Figure 5.7: Mean Diurnal-Seasonal Amplitude Variation of the First SR mode in EW magnetic components at Maitri, Antarctica

to respond to the thunderstorm activity occurring in the three tropical chimneys, namely, Asia, in particular, over the Indo-Tibetan landmasses as well as the Maritime Continent (Indonesia), Africa and America. The influence of thunderstorm activity over the Asian sector has been shown to be important for the behaviour of Schumann resonance intensities over Kolkata, a tropical station in the Indian sector (De et al., [2009]). In experiments carried out over Negev Desert, Israel, three dominant maxima (08:00, 14:00 and 20:00 UT) were observed in the diurnal variation of SR power (Price and Melnikov [2004]). These maxima were attributed to the thunderstorm active regions over Asia (08:00 UT), Africa (14:00 UT) and South America (20:00 UT). It may be noted that this site is away from the three major thunderstorm active regions

(Asia, Africa and America), zonally all separated from each other by 90°. Whereas for Maitri, the major thunderstorm regions are quite far away from the source regions and the arrival angle for the ELF waves will be ∼45° for the Asian and American thunderstorm regions and 90° for the African thunderstorm region. Therefore, the variation in the amplitude between these stations (Negev Desert and Maitri) will have some similarities for the NS component corresponding to the thunderstorm activity of Asian and American sectors at 08:00 and 20:00 UT, respectively. One can expect similarities in the EW component as well when the respective sensor oriented in that direction responds to the thunderstorm region located in the African sector.

Amplitude monitoring from widely separated stations was also carried out in the past (Fűllekrug and Fraser-Smith [1996]; Roldugin and Vasiljev [2012]). Results from these experiments support the idea that the global thunderstorm activity is concentrated over the continents in the tropical zone and its current peak is located in the zone closest to the dusk terminator (local afternoon hours). Thus, the source-observer distance reaches its minimum near the local time corresponding to the late afternoon hours (Nickolaenko and Hayakawa [2002]). From the SR observations made at Barentzburg (78°06′ N 14°12′ E), Russia, nearly a conjugate station for Maitri, it was noticed that the SR intensity has a double peak in H_{NS}, one at about 08:00 UT and the other at about 20:00 UT (Roldugin and Vasiljev [2012]). However, the east-west component, H_{EW}, shows a prominent single peak at ∼14:00UT and a secondary peak at ∼06:00 UT. The features observed at Maitri are nearly similar to

the observations made from the Northern Hemisphere conjugate station. From the above, one may conclude that the observed diurnal variations in SR amplitude over Maitri are due to thunderstorm activity occurring on a global scale over the three regions located in the Asian/Maritime Continent and the American and African sectors.

SR parameter	season	NS diurnal	EW diurnal	NS semi-diurnal	EW semi-diurnal
Amplitude (x 10^{-3} pT/ $\sqrt{Hz}$)	Summer	3.85 (10.3)	17.8 (13.7)	7.74 (9.7)	14.5 (5.1)
	Winter	1.97 (2.3)	16.2 (16.6)	9.34 (10.6)	9.0 (4.8)
	Equinox	2.66 (8.2)	15.1 (15.4)	8.41 (11.4)	4.16 (4.1)

Table 5.1: Diurnal and semi-diurnal amplitudes and phases of the SR parameters of the first mode (phases given in brackets)

5.4.3 Seasonal Dependence of the Diurnal Variation of Mode 1 Frequency

The resonance frequency for Mode 1 undergoes a very systematic and consistent diurnal pattern during different seasons. The diurnal pattern of frequency variation for both magnetic components is shown in Figures 5.8 and 5.9.

SR parameter	season	NS diurnal	EW diurnal	NS semi-diurnal	EW semi-diurnal
Frequency (x 10^{-2} Hz)	Summer	4.07 (5.0)	1.89 (14.1)	4.27 (7.4)	3.74 (2.1)
	Winter	3.34 (3.5)	4.92 (13.7)	3.28 (6.9)	3.0 (1.5)
	Equinox	5.28 (3.8)	4.95 (11.7)	3.44 (7.9)	3.3 (0.7)

Table 5.2: Same as in Table 5.1 but for frequency

In spite of the large scatter, especially for the equinox seasons, we see in all three seasons two peaks near 06:00 UT and 20:00 UT in the NS component and a single peak near 13:00 UT in the EW component, a clear semi-diurnal variation of the frequency in the NS component and a diurnal type variation in the EW component with time similar to the variations observed in the mode amplitude (refer to Figures 5.6 and 5.7). The maximum occurrence time of one of the components is almost coincident with the minimum occurrence time of the other. For example, the occurrence of the minimum at 14:00 UT in the NS component coincides with that of maximum in the EW component. Another feature to be noted is that there are greater seasonal changes of mean frequency in the EW component than those in the NS component. The diurnal mean frequencies for the EW component are larger during winter and comparatively smaller during summer. It may be noted that the results for the mean frequency reported for Negev Desert reveals greater seasonal change in the NS component with the time of occurrence of maximum varying with time and season. Further, a comparison of Figures 5.6, 5.7, 5.8 and 5.9 the results presented in tables 5.1 and 5.2 for Maitri reveal that the frequency variation leads the amplitude variation by 2-4 hours.

The diurnal variation of the resonance frequency was earlier hypothesized to be caused by the motion of the thunderstorm active centres around the globe (Balser and Wagner [1962a,b]). Later, it was speculated that the diurnal variation of SR frequencies was due to the combined effect of day-night asymmetry and the

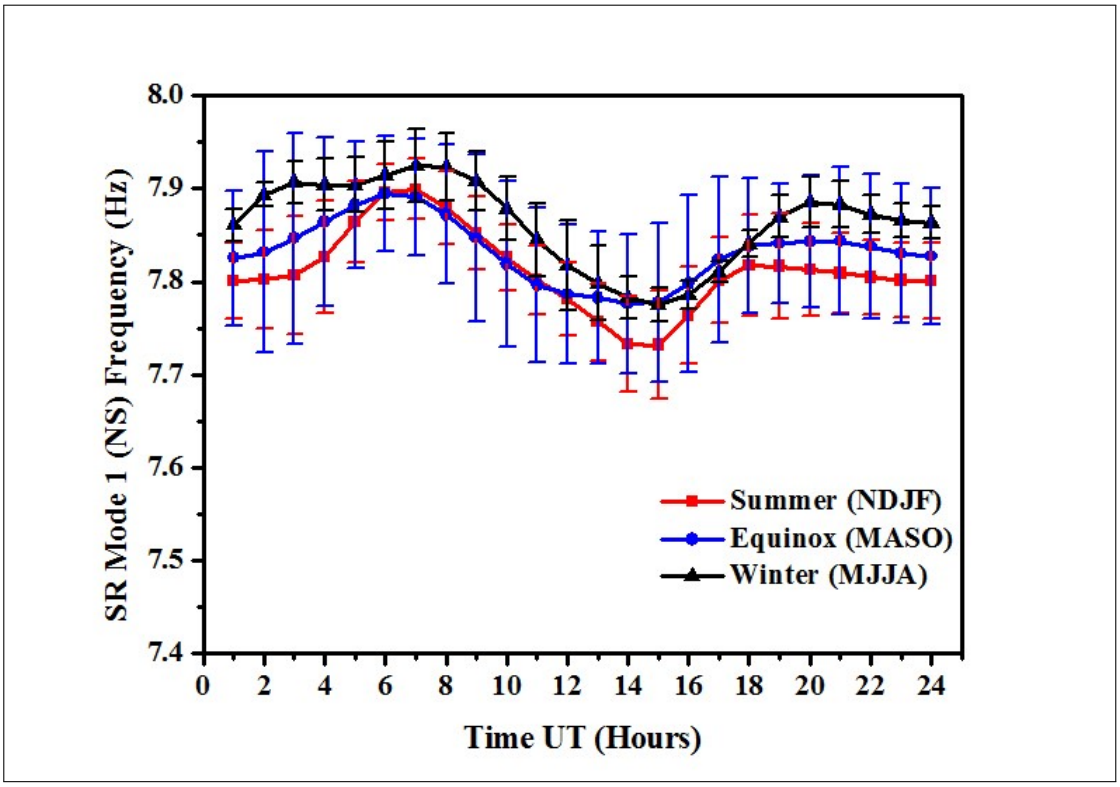

Figure 5.8: Mean diurnal-seasonal frequency variation of the first SR mode in NS magnetic components at Maitri, Antarctica

eccentricity of the geomagnetic field, since the ionospheric parameters are different for day and night sides of the globe (Bliokh et al., [1968]). The magnetic dipole component is stronger on one side of the globe than on the other side. Further, the dipole is closer to the centre of the night hemisphere during noon (UT), where the effective height of the ionosphere is greater and later as the dipole moves towards the day hemisphere, the ionosphere gets lower. Thus, the periodic modulation of the thickness of the Earth-ionosphere cavity was suggested to drive the frequency variation of the global resonance. The mode frequency was shown to depend not only on the zenith angle of the Sun along the signal propagation path from a lightning source to an observer point, but also on the planetary magnetic disturbances (Bliokh

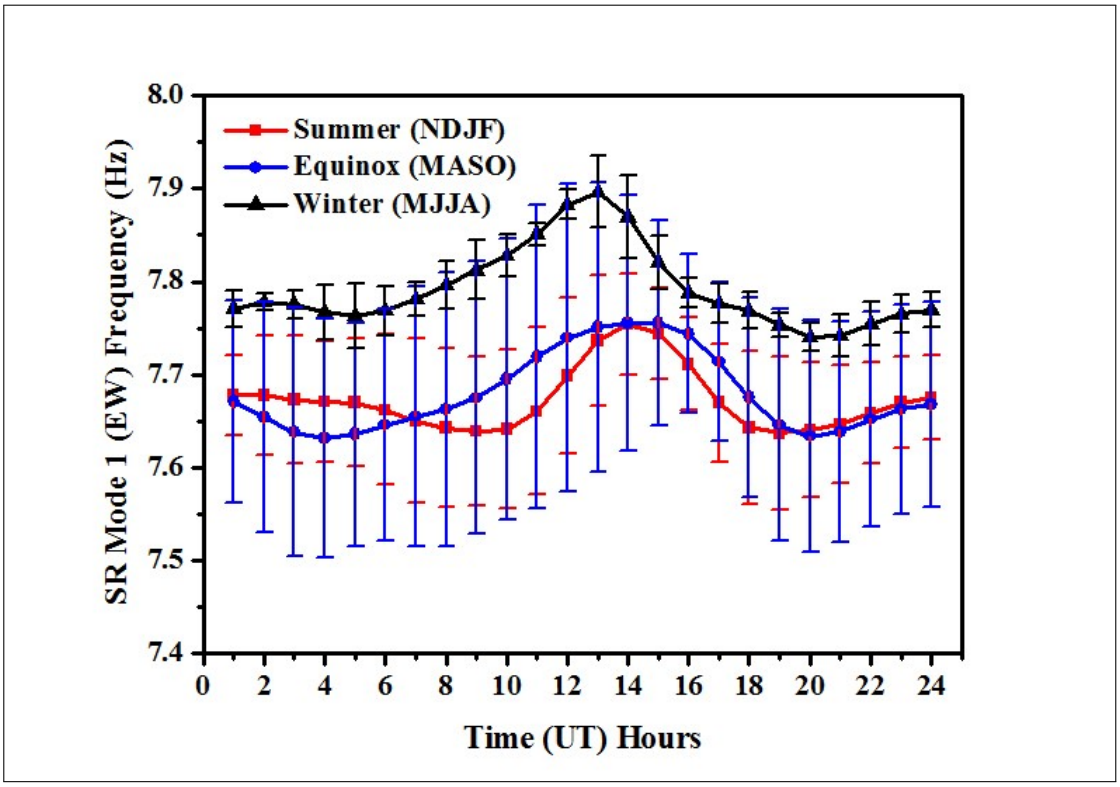

Figure 5.9: Mean diurnal-seasonal frequency variation of the first SR mode in EW magnetic components at Maitri, Antarctica

et al., [1968]). The variation of frequency on any day has been attributed to the solar proton events (Roldugin et al., [1999, 2004]). Measurements in the Himalayan region indicate that the resonance frequency is determined by the effective size of the thunderstorms and associated ionospheric conductivity (Chand et al., [2009]). Results from Agra, in the Indian sector, demonstrated a variation in the mode frequency with solar cycle that is believed to occur essentially through the conductivity and the subsequent ionospheric height changes (Singh et al., [2014]).

It was also suggested that the shifts in the frequency are due to leakage of power in the dissipative medium. The power leakage is primarily dependent on the distance of the excitation source, as late afternoon thunderstorm regions vary with time for an

observer fixed to the Earth. This is an artifact of the source-observer geometry and is not related to the properties of the Earth-ionsophere cavity (Sentman [1995]).

All these investigations clearly reveal that the diurnal variation in frequency can significantly be altered by the ionospheric parameters in the propagation path of the signal as well as the distance between the source and the observer. Since the source of the resonance is the thunderstorm activity over the respective three tropical chimneys separated by 90° longitude, i.e., between Africa and Asia and Africa and America, the peak of the resonance frequency is expected to have a complicated diurnal pattern owing to these conditions.

Returning to the discussion pertaining to the present observations, the steady rise in the diurnal frequency of H_{EW} component in Figure 5.9 suggests that the thunderstorm activity in the tropical Asian and African regions resonates the cavity with the frequency rise attributed to the increase in the energy of the cavity. At about 12:00 UT, it attains its maximum and thereafter a steady fall is seen despite the continuation of energy in the cavity. This is probably due to the rise in the conductivity in the propagation path between the source and the observer. The decreasing trend continues till 18:00 UT with the lowest value occurring around this time. Thereafter, it rises as the conductivity decreases. It is to be remembered here that though the H_{EW} component is dominated by the African thunderstorm activity, it is also influenced by the other two tropical chimneys located in Asia and America,

as the angle between the source and observer is more than 0°. An inverse of the above pattern is seen in the H_{NS} component which can be understood based on the reasoning provided above but taking into account the other two thunderstorm generators.

Chapter 6

Summary and Scope for Future Work

6.1 Electric Field Measurements from BEENS Experiment

The global electric circuit (GEC) is formed due to the presence of conductive Earth and ionosphere between them exists insulating air. This geometry provides the DC global circuit and the AC global circuit (Roble and Tzur [1986]; Williams [2003, 2009]; Markson [2007]; Rycroft and Harrison [2011]). The thesis deals with both DC global circuit measurements and Schumann resonance which is an ac part of GEC.

Chapter 4 of this thesis deals with the DC part of GEC measured at stratospheric height using balloon borne measurements. For the first time vector electric fields at low latitudes are measured using the Langmuir double probe technique over Hyderabad. The large scale electric fields, like Sq, that generates in ionosphere due to the dynamo action at E region maps down to lower atmosphere. The mapping down of the electric field is due to the decreasing conductivity downward. Volland (1972) estimated theoretically the large scale ionospheric dynamo value of about few mV/m. Many researchers have done electric field measurement at high latitudes mapping the vector electric field form auroral activity

which map down to the low altitudes without much attenuation. (e.g. Mozer and Serlin [1969]; Holzworth and Mozer [1979]; Holzworth and Bering [1998]; Saba et al., [2000]). The electric field of auroral activity which map downs to the stratospheric heights is about few orders higher than the fields mapping down at low latitudes. The Balloon Experiment on the Electrodynamics of Near Space (BEENS) which was carried out from the National Balloon Facility at Hyderabad just prior to the wee hours of 14 December 2013. The primary goals of the experiment were to observe stratospheric electric fields at these low latitudes and understand their relationship to the known electric field drivers. As discussed in chapter 4 some of the shortcomings of BEENS experiment is the boom used for vertical electric field measurements and the probe geometry adopted restricted the observation to only single pair of horizontal booms out of two (discussed in section 4.2.3). A malfunctioning of the orienter further restricted the observation duration to 90 min at the balloon float altitude of 35 km.

In spite of these shortcomings, a major and significant outcome from this experiment is the demonstration of the presence of 10-15 mV/m horizontal electric fields that exhibited a tendency to rotate clockwise (figure 4.16 and 4.17). The magnitude of electric field reported here is 3-4 times higher, at stratospheric heights, than the expected ionospheric electric field (~few mV/m) calculated by Volland (1972). The results discussed in section 4.3 (chapter 4), corroborates with earlier observations by Holzworth (1989) and Hu and Holzworth (1997). The magnitude

of the observed electric field are compareble with those earlier observations. The observations from BEENS experiment serve to emphasize once again that the middle atmosphere is not a passive medium transmitting electric fields generated elsewhere but may respond actively to the electrodynamical forcing imposed by atmospheric waves. Future balloon experiments of this kind will be able to throw more light on the nature of the coupling between the stratospheric electric fields and winds and waves of local origin.

6.2 Schumann Resonances Measurement from Maitri, Anatarctica

Chapter 5 discusses on the results obtained from the ground measurements of ac part of global electric circuit i.e., Schumann resonances from Maitri, Antarctica. Maitri station is quite away from the three thunderstorm chimneys (Maritime continent, African continent and American continent). From the SR observations carried out from Maitri, Antarctica, it is evident that it is the lightning flash density along with an alignment of the resonance cavity with respect to the sensor that determines the strength of the detected power or amplitude. Chapter 5 deals on the characteristics of the AC component of the global electric circuit, namely, the amplitude and frequency of the SR parameters. It has been shown that the NS and EW induction coils reveal maximum intensity of signal when the signal propagation

path is 90° to the direction of orientation of the sensor and nearly half the intensity when the signal propagation direction is inclined to about 45°. The geographical location of Maitri, in Antarctica, is just south of Africa. The signal propagation path from Africa to Maitri is nearly 90° and the maximum intensity at 16:00 UT revealed by the observations made by the EW sensor could very well be in response to a source in the African continent. The H_{NS} sensor reveals two maxima, one at around 10:00 UT and the other at 21:00 UT. The amplitude of SR (H_{NS}) is nearly half of that of the signal detected by EW sensor as the source of the thunderstorm activity (MC and American sector) is nearly at 45° bearing. Considering the signal strength and occurrence of these maxima, it is evident that these features are consequences of the thunderstorm activity over the Asian and the American sectors. In accordance with the earlier reports, it can be concluded that the variation of the resonance frequency in Mode 1 is related to the variation in the intensity of the thunderstorm activity as well as the behaviour of the Earth-ionosphere cavity.

6.3 Scope for Future Work

The BEENS experiment conducted from National Balloon Facility (NBF), Hyderabad gave a promising results in the measurement of vector electric field at stratospheric heights. Even though we had shortcomings in areas like data acquisition system, material used for boom to deploy the electric field probes, orienter problem and boom configuration used for vector electric field measurement. With all these

drawbacks in the first BEENS experiment, it was able to capture the electric field signatures at stratospheric altitude. However, the conclusion of the thesis do tell that it may be due to some in-situ generated electric field or generated by the gravity waves still needs to be understood. By improving the measurement system of BEENS and duration of flight data collected, one can have some conclusion about the magnitude of electric field observed at stratospheric heights.

The BEENS II experiment is the future balloon experiment planned to be launched during the December 2015 with many modifications in the system. In BEENS II, the boom used to deploy the electric field will be completely replaced by the fibreglass rod. Instead of 3m boom, it is planned that electric field probes will be 4m away from the central payload/gondola. The electrometer IC (INA 116) used during the BEENS experiment will be replaced by OPA 440 a high input impedance operational amplifier with supply voltage of ±40 V. The gondola structure used in BEENS experiment of 1m x 1m x 1.1m will be further reduced by 20 cm on each side making the gondola small and disturbance of natural electric field due to the presence of large metallic body (gondola) will be reduced. The orienter used in BEENS experiment will be replaced with another orienter in which the rotation of the gondola can be controlled.

The retrieval of vertical electric field data from BEENS experiment could not be achieved due to the boom configuration used as discussed in section 4.2.3 of chapter

4. In BEENS II experiment, a separate boom is being provided for measuring the vertical electric field. From the BEENS experiment, it is clear that one set of double probes is enough for deriving the north-south and east-west electric field components. So in BEENS II experiment, the electrometer used in BEENS experiment is also used in one of the orthogonal pair and a new set of electrometer which is under progress will be used for another set of orthogonal pair. The new set of electrometers will have input impedance of 10^{13} ohms whereas the electrometer used in BEENS experiments had input impedance of 10^{15} ohms. One of the reasons caused the distortion in sinusoidal variation mentioned in section 4.2.2 of chapter 4, due to high input impedance of instrumentation amplifier discharging electric field through the electrometer was delayed. Thus, BEENS II experiment can be used for testing the electrometers to measure the electric field at stratospheric height. By doing this, the results from both the experiments can be studied and compared with the results derived from both the balloon experiments. .

During the BEENS experiment, the use of 1 kHz low pass filter for measuring vector electric field proved very costly for us. As the data was very noisy due to high frequency noise could not be filtered by 1 kHz low pass filter. In BEENS II experiment 10 Hz low pass filter will used so the complete cut off high frequency noise and very clean raw data can be recorded. The encoder provided by NBF, Hyderabad could not sample the data simultaneously and also sampling rate could not be set. In BEENS II experiment, a standalone data acquisition system for the

measurement of vector electric field with 16 bit ADC is planned. We can sample the data simultaneously and also the sampling rate can be varied depending upon the need of the experiment. The conductivity measurement during accent was not done during the BEENS experiment as it was not planned earlier. In BEENS II experiment conductivity measurement during accent period is planned and for every five minutes the conductivity measurements will be recorded.

With all the modifications, BEENS II experiment will be well equipped to measure the large scale ionospheric horizontal electric field which maps down to stratospheric height and also the vertical electric field.

The results of Schumann resonances studies from Maitri, Antarctica gives an overall insight about diurnal and seasonal changes observed in southern hemisphere. In the present thesis only the amplitude and frequency variation of Schumann resonances parameters are studied with their diurnal and seasonal changes. The study can be extended for the disturbances of the lower ionosphere arise from solar porton precipitation (Reid [1986]; Roldugin et al, [2003]), solar wind-magnetosphere interaction and auroral activity (storms and substorms). The Schumann resonances parameters changes during the above disturbances. Since Maitri, Antarctica is a high latitude station, the response of Schumann resonance frequency during X ray flux enhancement and solar proton event can be studied by comparing it with a low latitutde station in Shillong (geographic 25.57° N, 91.88° E, geomagnetic, 16.30° N,

165.12°E). By comparing the results from low and high latitudes station, one can study latitudinal dependence of amplitude and frequency of SR parameters.

6.4 Conclusion

The sources of electric field and currents in the global electric circuit are the thunderstorms situated in the troposphere and the dynamos located in the ionosphere and magnetosphere. Thunderstorms couple the troposphere to the magnetosphere through electromagnetic waves generated from lightning discharges. Ground based measurements of DC global electric circuit are dependent on the atmospheric columnar resistance. Approximately 95 % of the atmospheric columnar resistance lies below 10 km altitude. Atmospheric columnar resistance dependents on aerosol concentration and cloud cover. The greatest effect of aerosol concentration is found in the continental boundary layer. Thus, ground based measurements of DC global electric circuit involves local continental affects on the observations made. Measurements made over oceans or mountains (above the boundary layer) are considered to be free of aerosols prevalent in the continental areas. For monitoring ionospheric potential of thunderstorm generated vertical electric field and large scale horizontal electric fields generated in the ionosphere and magnetosphere mapped to middle atmosphere, long-duration balloon flights provide an excellent platform. It is also known that the global electric circuit is affected by transient luminous events such as sprites, climate change and space weather effects. The effects of transient

luminous events produced by lightning discharges from cloud top to ionosphere and the mechanism which couple the lower troposphere to ionosphere are yet to be understood. Future balloon campaigns must try to accomplish the goal of measuring the electromagnetic environment to study sprite producing thunderstorm. Finally, it is important that future efforts combine ground-based measurements of air-earth current and vertical potential gradient with Schumann resonances as they essentially represent the dc and ac components of global electric circuit, respectively. with Such measurements will provide useful complementary data whenever long-duration balloon flights are conducted.

Bibliography

Aggson, T. L. and D. S. Evans. (1968), Reaction of auroral precipitation on the magnetospheric electric field. Talk presented at the Int. Symp. Phys. Magnetosphere, Washington, D.C.

Balser, M. and C. A. Wagner, (1960), Observation of Earth-ionsophere cavity resonances, Nature, 188, 638-641.

Balser, M., and C. A. Wagner (1962), Diurnal power variations of the Earth-ionosphere cavity modes and their relationship to worldwide thunderstorm activity, J. Geophys. Res., 67(2), 619-625.

Balser, M., and C. A. Wagner, (1962b), On frequency variations of the Earth-ionosphere cavity modes, J. Geophys. Res., 67(10), 4081-4083.

Beamish, D., and A. Tzanis, (1986), High resolution spectral characteristics of the Earth-ionosphere cavity resonances, J. Atmos. Terr. Phys, vol. 48, Iss. 2, 187-203.

Belyaev, G. G., A. Yu. Schekotov, A. V. Shvets, and A. P. Nickolaenko, (1999), Schumann resonances observed using Poynting vector spectra, J. Atmos. Solar-Terr. Phys., 61, 751-763.

Bering, E., T. Rosenberg, J. Benbrook, D. Detrick, D. Matthews, M. Rycroft, M. Saunders, and W. Sheldon (1980), Electric fields, electron precipitation, and VLF radiation during a simultaneous magnetospheric substorm and atmospheric thunderstorm, J. Geophys. Res., 85(A1), 55-72.

Bering III, E. A., (1995), The global circuit: Global thermometer, weather by-product or climatic modulator?, Rev. Geophys., 33(S2), 845-862.

Bliokh, P. V., A. P. Nickolaenko, Filippov YuF, (1968), Diurnal variations of the natural frequencies of the Earth-ionosphere resonator in relation to the eccentricity of the geomagnetic field. Geomagn. Aeron. 8(2):198-206.

Chand, R., M. Israil, and J. Rai, (2009), Schumann resonance frequency variations observed in magnetotelluric data recorded from Garhwal Himalayan region India, Ann. Geophys., 27, 3497-3507.

Coroniti, F. V., (1968), Turbulent conductivities in the magnetosphere. Presented at the Int. Conf. Atmospheric and Space Electricity, Tokyo, Japan.

De, S. S., B. K. De, B. K. Sarkar, B. Bandyopadhyay, D. K. Haldar, Suman Paul and S. Barui, (2009), Analyses of Schumann resonance spectra from Kolkata and their possible interpretations. Indian J. Radio & Space Phys., 38, 208-214.

Everett, J. D., (1868), Results of observations of atmospheric electricity at Kew Observatory, and at Kings College, Windsor, Nova Scotia Phil. Trans. Roy. Soc. Lond. A. 158, 347-361.

Főppl. H, G. Haerendel, L. Haser, R. Lst, F. Melzner, B. Meyer, H. Neuss, H. H. Rabben, E. Rieger, J. Stcker, and W. Stoffregen, (1968), Preliminary results of electric field measurements in the auroral zone, J. Geophys. Res., 73(1), 21-26.

Fűllekrug, M. and A. C. Fraser-Smith, (1996), Further evidence for a global correlation of the earth ionosphere cavity resonances, Geophys. Res. Lett., 23, 2773-2776.

Garg, S. C., T. John, K. S. Zalpuri, P. Subrahmanyam, and Y. V. Somayajulu (1989), Measurement of stratospheric electrical conductivity using balloon-borne Langmuir probe, Indian J. Radio & Space Phys., 18, 285-289.

Gonzalez, W. D., A. E. C. Pereira, A. L. C. Gonzalez, I. M. Martin, S. L. G. Dutra, O. Pinto, J. Wygant, and F. S. Mozer, (1982), Large horizontal electric fields measured at balloon heights of the Brazilian magnetic anomaly and association to local energetic particle precipitation, Geophys. Res. Lett., 9, 567-570.

Gringel, W., J. M. Rosen, and J. D. Hofmann, (1986), The Earths Electrical Environment, Ch. 12, Studies in Geophysics, National Academy Press, U. S. A.

Gruenberg, E. L., (1967), Handbook of Telemetry and Remote Control, Mcgraw Hill.

Gupta, S. P., and A. Narayan, (1987), Balloon-borne measurements of ion conductivity over low latitude stratosphere, Planet. Space Sci., 35, 439-443.

Gurubaran, S., and R. Rajaram (2001), Mean winds, tides, and gravity waves during

the westward phase of the mesopause semiannual oscillation (MSAO), J. Geophys. Res., 106, D23, 31,817-31,824.

Hale, L.C. (1984), Middle atmospheric electrical structure, dynamics, and coupling, Adv. Space Res. (COSPAR), 4, 175-186.

Hargreaves, J. K., (1992), The solar-terrestrial environment, Cambridge Press.

Harrison, R. G. and K. L. Aplin, (2002), Mid-nineteenth century smoke concentrations near London, Atmospheric Environment, 36 (25), pp. 4037-4043.

Harrison, R. G., (2005), Columnar resistance changes in urban air, J. Atmos. Solar-Terr. Phys., Vol. 67, Iss. 8-9, P. 763-773.

Hays, P. B., and R. G. Roble (1979), A quasi-static model of global atmospheric electricity, 1. The lower atmosphere, J. Geophys. Res., 84(A7), 3291-3305.

Heckman, S. J., E. Williams, and B. Boldi (1998), Total global lightning inferred from Schumann resonance measurements, J. Geophys. Res., 103(D24), 31775-31779.

Hobara, Y., N. Iwasaki, T. Hayashida, N. Tsuchiya, E. R. Williams, M. Sera, Y. Ikegami, and M. Hayakawa (2000), New ELF observation site in Moshiri, Hokkaido Japan and the results of preliminary data analysis, J. Atmos. Electr., 20, 99-109.

Holzworth, R. H., and F. S. Mozer (1979), Direct evidence of solar flare modification of stratospheric electric fields, J. Geophys. Res., 84(C1), 363-367.

Holzworth, R. H., M. C. Kelley, C. L. Siefring, L. C. Hale, and J. D. Mitchell (1985), Electrical measurements in the atmosphere and the ionosphere over an active thunderstorm: 2. Direct current electric fields and conductivity, J. Geophys. Res., 90(A10), 9824-9830.

Holzworth, R. H., K. W. Norville, P. M. Kintner, and S. P. Powell (1986), Stratospheric conductivity variations over thunderstorms, J. Geophys. Res., 91(D12), 13257-13263.

Holzworth, R. H., K. W. Norville, and P. R. Williamson, (1987), Solar flare perturbations in stratospheric current systems, Geophs. Res. Lett., 14, 852.

Holzworth, R. H. (1989), A new source of horizontal electric fields in the mid-latitude stratosphere, J. Geophys. Res., 94(D10), 12795-12802.

Hozworth, R. H., and E. A. Bering, III (1998), Ionospheric electric 425 fields from stratospheric balloon-borne probes, in Measurement Techniques in Space Plasmas: Fields, Geophys. Monogr. Ser., vol. 103, edited by R. F. Pfaff et al., pp. 79-84, AGU, Washington, D. C.

Hu, H., R. H. Holzworth, and Y. Q. Li (1989), Storm related variationsin stratospheric conductivity measurements, J. Geophys. Res., 94, 16429.

Hu, H., and R. H. Holzworth (1997), An inertial wave-driven stratospheric horizontal electric field: New evidence, J. Geophys. Res., 102, D16, 19,717-19,727.

Keithley (2004), Low Level Measurements, 6th edition, Keithley Instruments Ltd.

Kelley, M. C., F. S. Mozer, and U. V. Fahleson, (1968a), Auroral-zone electric field measurements on a sounding rocket (abstract), Trans. Am. Geophys. Union, 49, 739.

Kelley, M. C., F. S. Mozer, and U. V. Fableson, (1968b), D.C. and A.C. electric field measurements in the daytime auroral zone Inter. Sym. Phys. of the Magnetosphere Washington, D. C.

Kelley, M.C., C.L. Siefring, R.F.Pfaff, P.M. Kintner, M. Larsen, R. Green, R. H. Holzworth,, L.C. Hale, J.D. Mitchell, and D. LeVine, (1985), Electrical measurements in the atmosphere and ionosphere over an active thunderstorm I. Campaign overview and initial ionospheric results, J. Geophys. Res., 90, 9815.

Kelley, M. C., J. G. Ding, and R. H. Holzworth, (1990), Intense ionospheric electric and magnetic electric field pulses generated by lightning, Geophys. Res. Lett., 17, 2221.

Kellogg, P.J., and M. Weed, (1969), Balloon measurements of Ionospheric electric fields, in Planetary Electrodynamics (Eds. S.C. Coroniti and J. Hughes) Vol. 2 p. 431. Gordon and Breach Science Publ.

Kumar, S., A. Deo, and V. Ramachandran, (2009), Nighttime D-region equivalent electron density determined from tweek sferics observed in the South Pacific Region. Earth, Planets and Space 61, 905-911.

Labendz, D. (1998), Investigation of Schumann resonance polarization parameters, J. Atmos. Solar-Terr. Phys., 60, 1779-1789.

Madden, T. and W. Thompson, (1965), Low frequency electromagnetic oscillations of the earth-ionosphere cavity, Rev. Geophys., 3, 211-254.

Mářcz, F., G. Stori, and B. Zieger, (1997), Variations in Schumann resonances and their relation to atmospheric electric parameters at Nagycenk station, Ann. Geophys. 15, 1604-1614.

Markson, R., (1986), Tropical convection, ionospheric potentials and global circuit variation. Nature 320, 588-594.

Markson, R., (2007), The global circuit intensity: its measurement and variation over the last 50 years. Bull. Am. Meteorol. Soc.. doi:10.1175/BAMS-88-2-223, 223-241.

Mozer, F. S., and P. Bruston, (1967), Electric field measurements in the auroral ionosphere, J. Geophys. Res., 72(3), 1109-1114.

Mozer, F. S., and U. V. Fahleson, (1968), Parallel and perpendicular electric fields in an aurora Space Sciences Laboratory, University of California, Berkeley, 1968.

Mozer, F. S., and R. Serlin, (1969), Magnetospheric electric field measurements with balloons, J. Geophys. Res., 74, 4739-4754.

Mozer, F.S., (1971a), Balloon measurements of vertical and horizontal electric fields, Pure and Appl. Geophys. 84, 32.

Mozer, F.S., (1971b), Power spectra of the magnetospheric electric field, J.Geophys.Res. 76, 3651.

Mozer, F.S., (1971c), Origin and effects of electric fields during isolated magnetospheric substorms, J.Geophys.Res.76, 7595.

Mozer, F.S., and R. H. Manka, (1971), Magnetospheric electric field properties deduced from simultaneous balloon flights, J. Geophys. Res., 76, 1697.

Mozer, F. S. (1972), Simultaneous electric-field measurements on nearby balloons, J. Geophys. Res., 77(31), 6129-6132

Nickolaenko, A.P. and Hayakawa, M., (2002), Resonances in the Earth-Ionosphere Cavity, Kluwer Academic Publishers, Dordrecht/Boston/London, 380pp.

Norville, K. W. and R. H. Holzworth, (1987), Global circuit variability from multiple stratospheric electric field measurements, J. Geophys. Res. 92, 5951.

Ogawa, T., Y. Tanaka, A. Huzita, and M. Yasuhara (1975), Horizontal electric fields in the middle latitude, Planet. Space Sci., 23, 825-830.

Park, C. G. (1976), Downward mapping of high-latitude ionospheric electric fields to the ground, J. Geophys. Res., 81, 168-174.

Pinto, I. R. C. A., O. Pinto, Jr., W.D. Gonzalez, S. L. G. Dutra, J. Wygant, and F.S. Mozer, (1988), Stratospheric electric field and conductivity measurements over

electrified convective clouds in the South American region, J. Geophys. Res. 93, 709.

Potter, W. E., L. J. Cahill Jr., (1968), Measurements near an auroral electrojet (abstract), Trans. Am. Geophys. Union, 49, 738.

Price, C. and A. Melnikov, (2004), Diurnal, seasonal and inter-annual variations in the Schumann resonance parameters. J. Atmos. Solar-Terr. Phys., 66, 1179-1185.

Ramkumar, G., T. M. Antonita, Y. Bhavani Kumar, H. Venkata Kumar, and D. Narayana Rao (2006), Seasonal variation of gravity waves in the equatorial middle atmosphere: Results from ISROs Middle Atmospheric Dynamics (MIDAS) program, Ann. Geophys., 24, 2471-2480.

Reid, G.C., (1986), Electrical structure of the middle-atmosphere, in Study in Geophysics: The Earth's Electrical Environment. In: Krider, E.P., Roble, R.G. (Eds.), National Academy Press, Washington, DC, pp. 183-194.

Roble, R. G., and P. B. Hays (1979), A Quasi-static model of global atmospheric electricity 2. Electrical coupling between the upper and lower atmosphere, J. Geophys. Res., 84(A12), 7247-7256.

Roble, R. G., and I. Tzur, (1986), The global atmospheric electrical circuit. Study in Geophysics, The Earth's Electrical Environment. National Academy Press, Washington, D.C., pp. 206-231.

Roldugin, V.C., Y. P. Maltsev, A. N. Vasiljev, and E. V. Vashenyuk, (1999), Changes of the first Schumann resonance frequency during relativistic solar proton precipitation in the 6 November 1997 event, Ann. Geophys., 17, 1293- 1297.

Roldugin, V. C., Y. P. Maltsev, A. N. Vasiliev, A. V. Shvets, and A. P. Nickolaenko (2003), Changes of Schumann resonance parameters during the solar proton event of 14 July 2000, J. Geophys. Res., 108(A3), 1103.

Roldugin, V. C., Y. P. Maltsev, A. N. Vasiljev, A. Y. Schokotov and G. G. Belyajev, (2004), Schumann resonance frequency increase during solar X-ray bursts, J. Geophys. Res., 109, A01216.

Roldugin, V.K. and A. N. Vasiljev, (2012), Variations in the Schumann Resonance Polarization Ellipse in the Horizontal and Vertical Planes according to Observations at the Barentsburg and Lovozero Observatories. Geomag. Aeron., 52, 68-76.

Rycroft, M. J., S. Israelsson, and C. Price, (2000), The Global Atmospheric Electric Circuit, Solar Activity and Climate Change, J. Atmos. Sol.-Terr. Phys., 62, 1563-1576.

Rycroft, M.J., R. G. Harrison, K. A. Nicoll, and E. A. Mareev, (2008), An overview of Earths global electric circuit and atmospheric conductivity. Space Science Reviews 137, 83-105.

Rycroft, M.J., and A. Odzimek, (2010), Effects of lightning and sprites on the

ionospheric potential, and threshold effects on sprite initiation, obtained using an analog model of the global atmospheric electric circuit, J. Geophys. Res. 115, A00E37.

Rycroft, M.J.,and R. G. Harrison, (2011), Electromagnetic atmosphere-plasmacoupling: the global atmosphericn electric circuit, SpaceScienceReviews,1-22,

Saba, M. M. F., O. Pinto Jr., I. R. C. A. Pinto, and O. Mendes Jr., (2000), Stratospheric balloon measurements of electric fields associated with thunderstorms and lightning in Brazil, J. Geophys. Res., 105, 18091-18097.

Sagalyn, R. C., and D. R. Fitzgerald, (1965), Atmospheric electricity, in Handbook of Geophysics and Space Environments, Office of Aerospace Research, U. S. Air Force.

Sampath, S., S. Murali Das, and V. Sasi Kumar (1989), Electrical conductivities, ion densities and mobilities in the middle atmosphere over India - Balloon measurements, J. Atmos. Terr. Phys., 51, 533-540.

Sao, K., M. Yamashita, S. Tanahashi, H. Jindoh, H., and K. Ohta,(1973), Experimental investigations of Schumann resonance frequencies, J. Atmos. Terr. Phys., 35, 2047-2053.

Satori, G. and B. Zieger, (1996), Spectral characteristics of Schumann resonances observed in Central Europe. J. Geophys. Res., 101, 29,663-29,669.

Schegel, K. and M. Fűllekrug, (1999), Schumann resonance parameter changes during high-energy particle precipitation, J. Geophys. Rev., 104, A5, 10,111-10,118.

Schumann, W. O., (1952), On the free oscillations of a conducting sphere which is surrounded by an air layer and an ionsophere shell, Z. Naturforschanftung, 7a, 149-154 (in German)

Sentman, D., (1995), Schumann resonances, Handbook of Atmospheric Electrodynamics, vol. 1, edited by H. Volland, pp. 267- 295, CRC Press, Boca Raton, Fla.

Shvets, A. V., Y. Hobara and M. Hayakawa, (2010), Variations of the global lightning distribution revealed from three-station Schumann resonance measurements, J. Geophys. Res., 115, A12316.

Siingh, D., V. Gopalakrishnan, R. P. Singh, A. K. Kamra, Shubha Singh, Vimlesh Pant, R. Singh, A. K. Singh, (2007), The atmospheric global electric circuit: An overview, Atmos. Res., vol. 84, Iss. 2, 91-110.

Singh, A. K., D. Siingh, R. P. Singh, and Sandhya Mishra, (2011), Electrodynamical coupling of Earths atmosphere and ionosphere: an overview, International Journal of Geophysics.

Singh, B. and D. Pundhir, (2014), Shift of effective lightning areas during pre to post period of solar cycle minimum of 2008-2009 as determined from Schumann resonance studies at Agra, India. Annals Geophys., 57, 6.

Stergis, C. G., G. C. Rein, and T. Kangas, (1957), Electric field measurements above thunderstorms, J. Atmos. Terr. Phys., vol. 11, Iss. 2, Pages 83-90.

Udare, R. S., R. Rajaram, T. Ogawa, and M. Yashuhara (1991), Height profile of vertical electric field and conductivity over Hyderabad, Indian J. Radio & Space Phys., 20, 307- 309.

Volland, H. (1972), Mapping of the electric field of the Sq current into the lower atmosphere, J. Geophys. Res., 77, 1961-1965.

Volland H., (1984), Atmospheric Electrodynamics, Springer-Verlag, New York.

Wescott, E. M., J. Stolarik, and J. P. Heppner, (1968). Electric fields in the vicinity of auroral forms from motions of barium vapor releases (abstract), Trans. Am. Geophys. Union, 49, 155.

Williams, E.R., (1992), The Schumann Resonance: a global tropical thermometer, Science, 256, 1184-1188.

Williams, E. R., and S. J. Heckman. (1993). The local diurnal variation of cloud electrification and the global diurnal variation of negative charge on the earth, J. Geophys. Res., 98.

Williams, E.R., (1994), Global circuit response to seasonal variations in global surface air temperature, Mon. Weather Rev. 122, 1917-1929.

Williams, E.R., (2003), The global electrical circuit, In: Holton, J.R., Pyle, J., Curry, J.A. (Eds.), Encyclopedia of Atmospheric Sciences, vol. 2. Elsevier, pp. 724-732.

Williams, E. R., V. C. Mushtak, R. Boldi, R. L. Dowden, and Z.-I. Kawasaki (2007a), Sprite lightning heard round the world by Schumann resonance methods, Radio Sci., 42, RS2S20

Williams, E. R., and G. Stori (2007b), Solar radiation-induced changes in ionospheric height and the Schumann resonance waveguide on different timescales, Radio Sci., 42, RS2S11

Williams, E.R., (2009), G.C. Simpson versus C.T.R.Wilson: fifty years of controversy in atmospheric electricity, Atmos. Res. 91, 259-271.

Wilson, C. T. R. (1920), Investigations on lightning discharges and on the electric field of the earth, Philos. Trans. R. Soc. London, Ser. A., A221:73 115.

APPENDIX

Appendix A

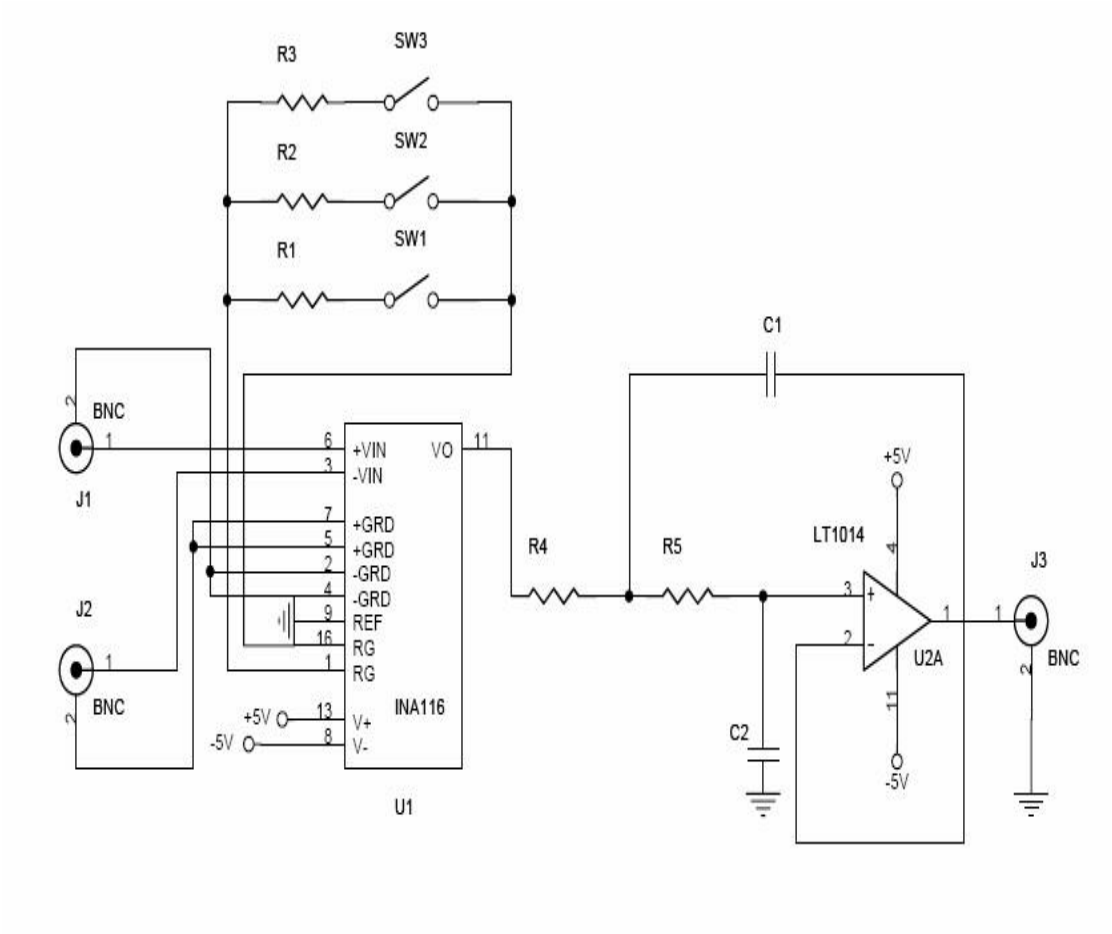

Figure A 1: Circuit diagram for a single-channel differential electrometer that shows the INA116 instrumentation amplifier whose output is connected to a low pass second order Butterworth filter implemented through the IC LT1014.

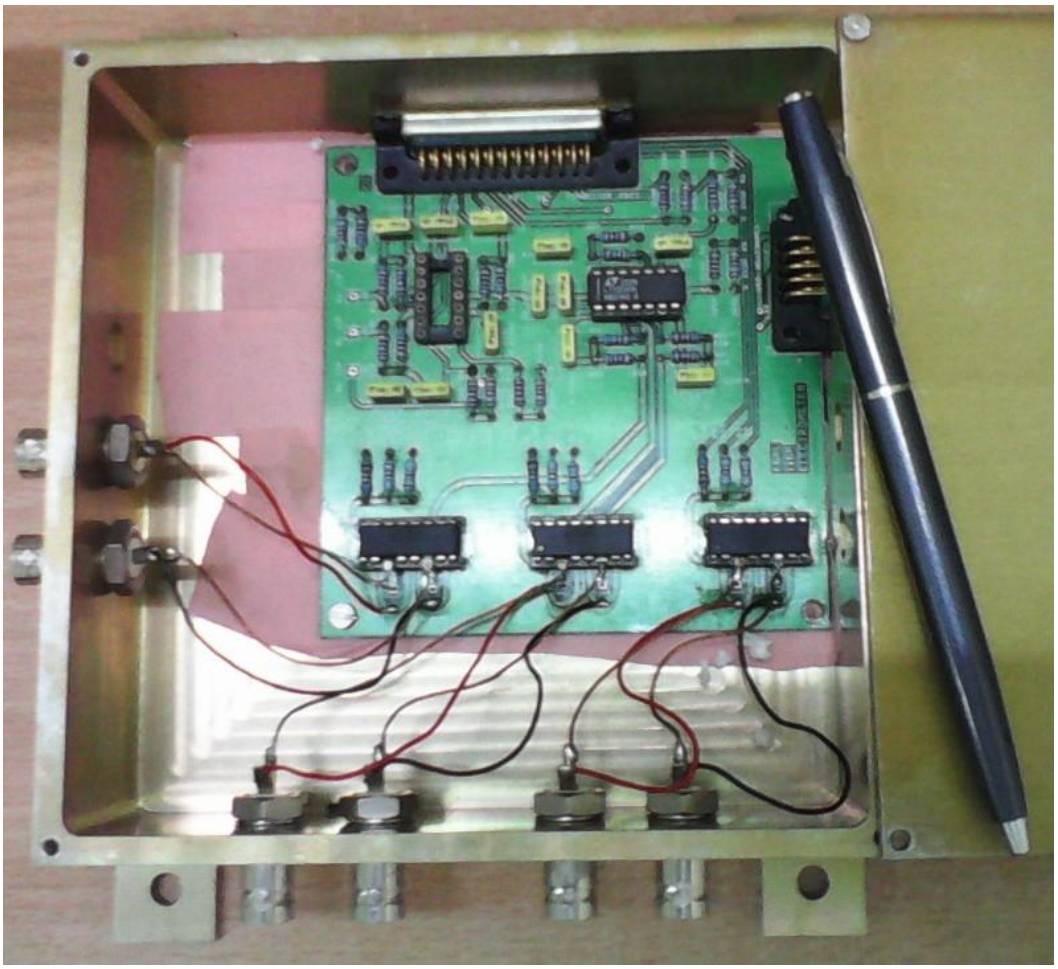

Figure A2: The flight model of a 3-channel differential electrometer used for BEENS experiment.

Appendix B

List of Conference/Symposium/Schools attended

1. Attended the DST - SERC School on "Electrodynamical coupling of atmospheric region" held at Indian Institute of Geomagnetism, New Mumbai, 6 -19 January, 2010.

2. Presented a poster paper entitled "Observations of Schumann Resonances in Low Latitude Regions" at16th National Space Science Symposium held at Saurashtra University, Rajkot, February 24 - 27, 2010

3. Participated in "Embedded Systems Conferences India 2010" held at Bangalore, July 21 - 23, 2010.

4. Attended a 3-day Familiarization workshop on Scientific Ballooning, at National Balloon facility, TIFR Hyderabad, 13-15 December, 2010

5. Participated in "Workshop on Data Utilization for Ionospheric Studies and Hands-on Training" at Space Physics Laboratory, VSSC Trivandrum from October 14-15, 2011.

6. Poster presentation entitled "Simultaneous Observation of DC and AC Components of Global Electric Circuit Parameters over Maitri, Antarctica" at AOGS 2013 held at Brisbane, Australia, June 24 - 28, 2013.

List of Publications

1. Design and fabrication of an electrometer for the measurement of atmospheric potential. **S. Manu**, C. Panneerselvam, K. U. Nair, S. Gurubaran, Environmental Science an Indian Journal, Volume 8 Issue 11,2013 [442-452], ISSN: 0974 - 7451. (copy of the published reprint attached in Appendix C).

2. Schumann resonances observed at Maitri, Antarctica: Diurnal variations and their interpretations in terms of global thunderstorm activity. **S. Manu**, R. Rawat, A. K. Sinha, S. Gurubaran and K. Jeeva. (Accepted for publication in current science). (copy of the accepted manuscript enclosed in Appendix C and proof of acceptance attached at the end of Appendix C).

3. Stratospheric electric fields over low latitudes: Results from the Balloon Experiment on the Electrodynamics of Near Space (BEENS). S. Gurubaran, **S. Manu**, K. Jawahar, K. Emperumal and P. Mahavarkar. (Communicated to Journal of Geophysical Research - Under revision).

Appendix C

Copy of Published/Accepted

Reprints Attached.

ISSN : 0974 - 7451 Volume 8 Issue 11

Environmental Science
An Indian Journal
Current Research Paper

ESAIJ, 8(11), 2013 [442-452]

Design and fabrication of an electrometer for the measurement of atmospheric potential

S.Manu, C.Panneerselvam*, K.U.Nair, S.Gurubaran
Equatorial Geophysical Research Laboratory, Indian Institute of Geomagnetism, Krishnapuram, Tirunelveli 627 011, (INDIA)
E-mail: panneer.iig@gmail.com

ABSTRACT

The vertical atmospheric electric field may be sensed by using a passive antenna, which is charged slowly by exchanging the charges in the atmosphere. The potential of the atmosphere is obtained by the measurement of potential difference between the antenna and earth's surface, which is same as the atmospheric potential. In case of a passive antenna at 1m above the surface, the voltmeter system attached with the antenna system and it is operated over a typical input range of ± 500V. This voltage is generated by a floating voltage generator. The input bias current used in this system is of the order of nearly 10^{-14}A with an input resistance of ~10^{15} Ω. This combination must be considered in this circuit is to provide an appreciably higher resistance than atmospheric resistance. In this passive antenna system a high voltage guard is also desirable. A direct method for measuring the atmospheric electric field is used by Electric Field Mill (EFM -100) and Field Mill. The Field Mill needs 230 V AC for running the motor, regular maintenance is required. The above instruments coast high and cannot be used during severe weather condition like high wind speed, rain, lightning snowfall and drifting sand. The passive antenna can be operated any meteorological conditions with 24V battery-powered in any remote place with minimum maintenance. Damages to the electrometer due to severe electrical storms can be cheaply repaired.
© 2013 Trade Science Inc. - INDIA

KEYWORDS

Atmospheric electric field;
Global electric circuit;
Fairweather;
Air-earth current.

INTRODUCTION

The scientific study of atmospheric electricity began in the 18th century, with investigation into the electrical nature of thunderstorms such as that famously undertaken by Benjamin Franklin, producing a spark from his aerial apparatus in 1750. Realisation that the atmosphere was electrified even in fair weather was made by the French botanist and physicist L.G. Le Monnier[21] who reproduced Franklin's experiment with an aerial in 1752 (although he removed the grounding pole from the aerial and placed some dust particles near the apparatus to investigate electrostatic attraction). This positive atmospheric charge was also found by John Canton in 1753. Le Monnier later went on to demonstrate the clear-sky electrification of the atmosphere and the diurnal variation

of atmospheric electricity, by observing changes in the electrostatic attraction of a suspended wire insulated from the ground and exposed to the atmosphere. The English physicist Benjamin Wilson visited Le Monnier in Paris in 1753, who stated in a letter to the President of the Royal Society: The regular diurnal variation of electric field found by Le Monnier was also found by the Italian physicist Giambatista Beccaria[2]. An advocate of the scientific ideas of Benjamin Franklin, Beccaria determined that the atmosphere was positively charged with respect to the Earth during fair weather in 1775. Ten years later the French physicist Charles Coulomb discovered that atmospheric air was not a perfect electrical insulator as previously thought, but was in fact weakly conductive. Unfortunately however, this aspect of his work was ignored at the time.

In the 1860s William Thomson (later Lord Kelvin) invented the water-dropping discharger[19]. With this instrument it was possible to transport charge induced by an insulated tube in equilibrium with the atmosphere on water droplets from a reservoir, being collected by a metal funnel that was connected to an electrometer. That way charge could be measured from a collector whilst still being electrically isolated from the ground, allowing the atmospheric potential (and therefore electric field, given a further reference potential) to be determined. Kelvin recognized the necessity for regular recordings of atmospheric electricity, preferably simultaneously at different locations in the study of atmospheric electricity, following what was described by Kelvin as the "incessant" recordings by Beccaria a century before[20]. Almost fifty years later, C.T.R. Wilson developed a method to measure the air-earth conduction current density (J_C) at the surface in Kew Observatory, London[22]. By this time the presence of ions in the air was known and the Wilson instrument could also measure total air conductivity (σ) and potential gradient (PG) simultaneously, as described in detail by Harrison and Ingram[9]. This invention permitted the beginning of regular measurements of all three major variables in atmospheric electricity in the United Kingdom: air-earth current density, potential gradient and air conductivity. In addition to knowledge that natural radioactivity had sources in the ground that ionized the air, a balloon flight in 1912 by Austrian physicist Victor Hess carrying an ionization chamber demonstrated that ionization rate actually increased with height (after an initial decrease), demonstrating that the ground was not the only source of ionization[11]. The extra-terrestrial source of this ionization was determined to be cosmic radiation, with ionization rate increasing with height as the absorbing mass of atmosphere above decreased. The cosmic origins that produced an increased ion production rate (and therefore air conductivity) with height offered an explanation in addition to decreased aerosol concentration with height for the results from previous balloon flights measuring atmospheric electrical parameters (e.g. Gerdien[5,6]), that noticed an increase in conductivity and decrease in potential gradient with height.

Worldwide thunderstorm activity is believed to maintain the global electric potential between the ionosphere and the earth's surface[24]. Tropical thunderstorms are considered as the main source for the electric field in the lower atmosphere, drawing current upward to the ionosphere. In this way, the global thunderstorm activity is able to maintain a time varying electric potential difference of nearly 300 kV, directed downward between the equipotential surfaces of the ionosphere and the ground[1]. The atmospheric vertical electric field, conductivity and total current density are the three closely related parameters of atmospheric electricity that are required to obtain an adequate description of the fairweather atmospheric electric circuit[12].

The study of Global Electric Circuit (GEC) can help in understanding the electrical environment of the earth's atmosphere. This approach can provide a good framework for exploring interconnections and coupling of various regions of the atmosphere. It can also provide information on the solar-terrestrial weather relationship and offers possibilities for exploring one of the traditional scientific problems, namely, that of associating changes in surface weather with the solar output[10]. Thunderstorms are electrical generators whose global activity provides a current output that maintains a vertical potential difference between the ground and ionosphere. Willson's classical model of global electric circuit is shown in Figure 1.

There is no thunderstorm activity at high latitudes; therefore atmospheric currents at these regions can be regarded as a closure segment of the global electric circuit. The global circuit involves lower atmosphere generators and the upper atmospheric generators, the most important of which are in polar caps. It is a desert like climate with clear skies, very low atmospheric aerosol content. In summer the prevailing winds are light,

flowing in a nearly constant direction, and are relatively free of turbulent and convective motions[13]. Thus the sources of conductivity fluctuations that produce space charge fluctuations and meteorological noise on the measured atmospheric electrical parameters when moved by winds are minimized compared to low-latitude measurements. The vertical atmospheric electric field leads to a potential difference between the surface and any point in the air vertically above. In fair weather the atmospheric electric field is nearly 150 V/m at 1m above the surface and the potential increases positively with increasing in height.

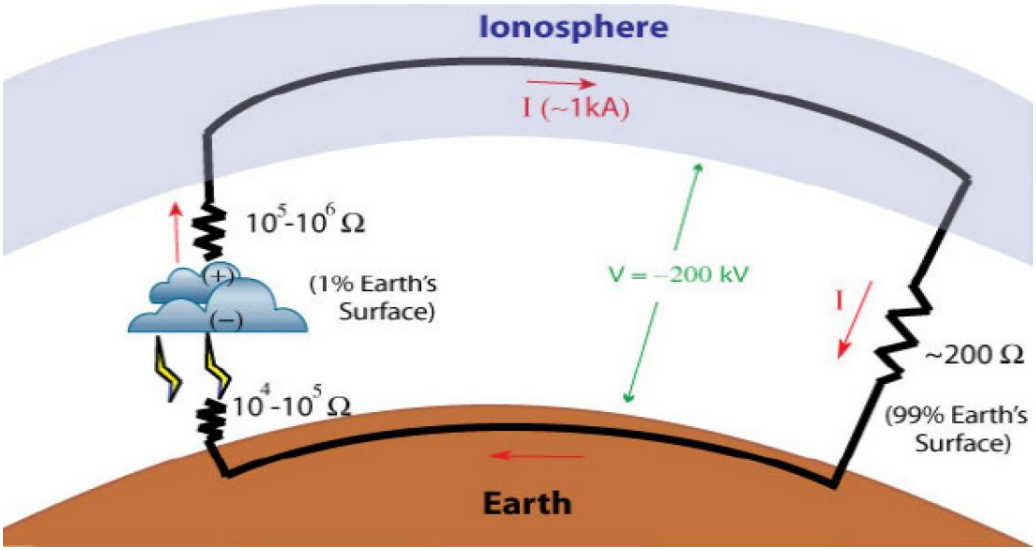

Figure 1 : The global electric circuit model by C.T.R.Wilson.

A device for sensing the atmospheric potential close to the surface is called passive antenna system. This introduces very little distortion only. This is a tensioned, long (20m) and fine (1mm diameter) horizontal wire, which is well insulated at each end. The passive antenna offers spatial averaging and requires no geometrical corrections. But it requires an ultra high input impedance and low leakage current from the measurement circuitry attached.

SITE DESCRIPTION

The passive antenna system initially tested at Equatorial Geophysical Research Laboratory (EGRL), Indian institute of Geomagnetism, Tirunelveli. After successful satisfactory functioning of the system we have installed the passive antenna system at Tirunelveli and at Maitri, Antractica, which is a high latitude station. Presently we are operating the passive antenna system simultaneously at both the stations.

Measurements of the potential gradient (PG), air-Earth conduction current density (J_C) and total conductivity (σ) made at Equatorial Geophysical Research Laboratory (EGRL), Tirunelveli (8.7°N, 77.8°E), which is a regional center of Indian Institute of Geomagnetism, Mumbai under Department of Science and Technology, Government of India. All of these parameters have been recorded simultaneously since 1995 onwards[17]. The environmental and meteorological conditions at the measuring site and the orography relevant observation on atmospheric electricity and data selection reported below One of our experimental site is EGRL (35 m above mean sea level) is more than 12 km from the twin towns of Tirunelveli and Palayamkottai towards the southeast. The site is about 35 km from the Bay of Bengal and the nearest hills of Western Ghats are at distances of nearly 45 km towards the west. The crustal part of the earth over the site is fixed on solid rocks, and hence does not support vegetation. The landscape is nearly flat and there are no trees in the vicinity of the sensors. The experimental site receives rainfall normally during the months of October and November when the northeast monsoon is active. Occasional rains occur during the summer when the southwest monsoon prevails in the Indian subcontinent. Scanty rainfall over most of the year in this region permits a large number of atmospheric electricity measurements to be made. Being in the tropics, this region is under the influence of con-

vection that is expected to be severe during the late spring and early summer months (April–June).

In 1999 we have started GEC experiments at Maitri, Antarctica with the same instruments which is operational at EGRL. The Indian Antarctic station, Maitri is located in the Schirmacher oasis in the Dronning Maud Land, East Antarctica (117 m above the mean sea level). Antarctica has only around 2% of its area that is free from ice. The nearest steep cliff of the east-west trending glacier on the southern side of the station is more than 700 m away from the station and is 300 m in height. The snow-covered surface during summer season was more than half a kilometer away from the station. The instruments were installed on barren land near the station. The surface of the station area is mainly covered by sandy and loamy sand types of soil. The solar zenith angle at Maitri varies from 48° to 88° during summer months. There was no sunset till the third week of January, but periods of short nights slowly increased during February. The variations in surface meteorological parameters were measured by automatic weather station which is installed during this expedition. The cloud cover over the station occurs mainly under the influence of subpolar low-pressure systems and shows an alternating sequence of the sky changing from overcast to clear as the system moves away[3]. The passive antenna system installed at Maitri during 2008 and it is operated continuously round the year. From these atmospheric electrical measurements and those of standard meteorological parameters using Automatic Weather Station (AWS) data, it is possible to resent both an electrical "climatology" of the EGRL and a comparison work carried out between electrical and meteorological parameters. Additionally, inter-comparison of electrical parameters will be made and results compared to other instruments which one is measuring the same parameters with some other technique.

INSTRUMENTATION

The vertical atmospheric electric field may be sensed by using a passive antenna, which is charged slowly by exchanging the charges in the atmosphere. The potential of the atmosphere is obtained by the measurement of potential difference between the antenna and earth's surface, which is same as the atmospheric potential. In case of a passive antenna at 1m above the surface, the voltmeter system attached with the antenna system and it is operated over a typical input range of ± 500V. This voltage is generated by a floating voltage generator. The input bias current used in the system is of the order of nearly 10^{-14} A with input resistance of ~10^{15} Ω. This combination must be considered in this circuit is to provide an appreciably higher resistance than atmospheric resistance. In this passive antenna system a high voltage guard is also desirable. The output is given to the ADC and thus the potential can be measured. This system can be operated at a remote place with minimum power consumption. Damages to the electrometer due to severe electrical storms can be cheaply repaired.

The antenna consists of 20m of 1mm diameter tined copper wire, suspended horizontally between short metal masts. At each end there are porcelain egg insulators, and PTFE fixing under steady compression at the masts. Sketch diagram of passive antenna shown in Figure 2. The insulators are regularly cleaned with isopropanol. A guard potential, which is close to the potential on the wire, is applied to the support wires at each end. This is to minimize the leakage through the insulators, which would occur if the support wires were merely grounded. As a precaution against the guard potential influencing the potential sensed by the antenna, the parallel cable that is carrying the guard signal to the far end of the antenna has an earthed screen.

SYSTEM DESCRIPTION

The antenna is connected, with a short wire made of same material as that of the antenna, through a UHF male connector to operational amplifier LMC 6042, which is configured as a unity gain follower. LMC 6042 is a low input bias current operational amplifier, which is the input amplifier, and OP-97 is used as driver stage for the source amplifier. The input potential is connected, via a PTFE standoff, to the input of LMC 6042. A 9V battery powers LMC 6042, with the 0V reference set at 1.2 V above the battery negative supply by TC04. This ensures an adequate performance by LMC 6042 around 0 V. The data sheet of the LMC 6042 shows that for positive input voltages, the ultra low bias current (nearly 1fA) is maintained which can otherwise increase 9by the order of magnitude) for negative input voltage. Thus, by ensuing that the input voltages to LMC 6042 will always be positive at start-up

(for input voltages within the range ± HT), no large current will be drawn from the high-impedance source, which could otherwise lead to oscillation. If the input does fail due to large transients from nearby lightning discharges, for which its voltage slew rate and dynamic range will be inadequate, LMC 6042 may fail and can be cheaply replace. Instead of relying on a push-pull unity-gain output buffer stage, the output stage is taken directly from the internal integrator of the LMC 6042, which provides low output impedance and large gain. It is quite common to use large values of feedback resistance with amplifiers with ultra-low input bias current, like LMC 6042. When high input impedances are damaged, guarding of the IC is suggested. Guarding input lines will not only reduce leakage, but lowers stray input capacitance as well. Simplified block diagram shown in Figure 3.

To provide a low impedance output to a voltmeter or logging system the operation potential of LMC 6042 is reduced by a 100: 1. 100 MΩ potential divider (trimmed by high voltage transformer T1), and presented to the input of MAX 430, also a follower stage. Max 430 is a chopper stabilized amplifier (with a 1pA input bias current) so that any additional dc error is minimized. A low pass filter (C210 and R211) protects Max 430 from external short circuits. The negative supply of the output amplifier (Max 430) is taken from a voltage inverter ICL 7661. This work by first accumulating charge in a bucket capacitor connected between pin 2 and 4 and then transfers it into reservoir capacitor connected between pin 5 and ground. A third power supply bypass capacitor is recommended (0.1 μF to 10 μF). Internally there is a main signal path amplifier and a separate nulling amplifier in MAX 430. The main amplifier is in the primary signal path and is continuously connected to the external inputs. The nulling amplifier alternately corrects its own offset, and then of the main amplifier, as its input switches between the two compensating FETs in the input stage's bias circuitry. The offset values that drive these trim FETs are stored for the duration of the correction cycle on two internal capacitors. It also provides correction for CMRR, PSRR, and A_{vol} at low frequencies. Internal compensation and internal chopper removes all offset voltages and drift.

An isolated, high-tension supply generates approximately ± 500V (designated +-HT), which is supplied to two high-voltage MOSFETS Q1 and Q2 is wired as a source follower, operated at constant current (generated by Q2) to improve the linearity. OP-97 is a unity gain driver stage, which has frequency compensated for phase shifts caused by driving the considerable input capacitances of Q1, and the capacitance of the cable

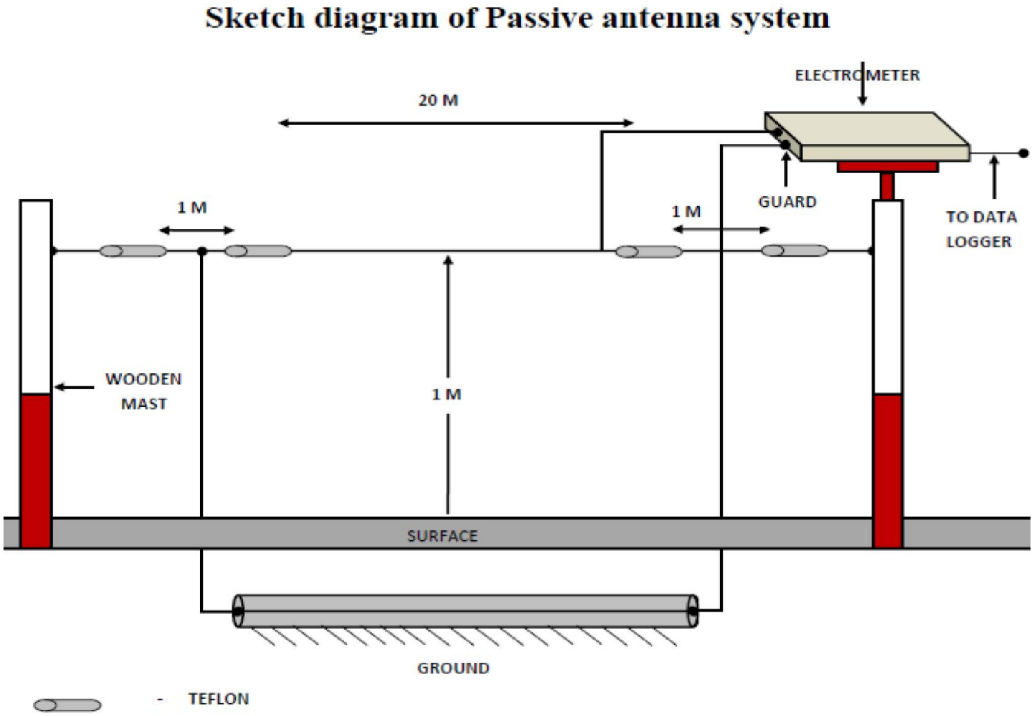

Figure 2 : Sketch diagram of passive antenna

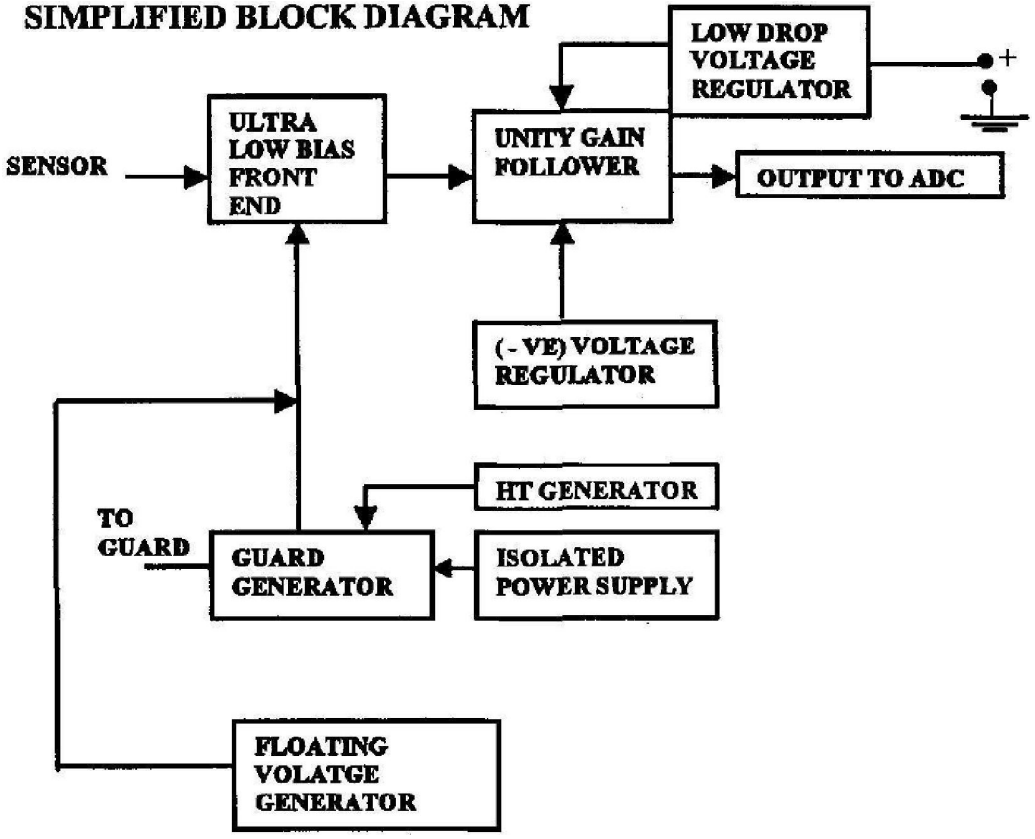

Figure 3 : Simplified block diagram of passive antenna system

to the antenna support wires (auxillary guard). To maintain the extremely high input impedance of OP-97, care must be taken in circuit board layout and manufacturing. Both surfaces must be clean and free of moisture. Even a clean PC board can have 100pA of leakage currents between adjacent traces. So that the guard rings should be used around the inputs, so that the leakage currents become minimal. OP-97 is powered from a transformer derived supply, but shares 0V connection with LMC 6042. This arrangement ensures that LMC 6042 (which has poorer power supply rejection than OP-97 at high frequencies) is powered from ultra-smooth supply, and OP-97 has adequate supply current to drive the capacitance load. OP-97 drives the gate of Q1, which is operated at a fixed drain-source current of 100 micro ampere set by the high-voltage constant current source of Q2 and LM334. (This is also serves to safely limit the current if the guard connections are accidentally grounded).

Constant current is established in LM334 with one external resistor and no other parts are required. The sense voltage used to establish operating current is 64mV at 25^0C and is directly proportional to absolute temperature (K). It generates a current with nearly +0.33 %^{o}C temperature dependence. The follower stage has a high effective gain: Q1 was observed to switch on at Vgs = 3.3V, i.e., an output swing of approximately 1kV for a Vgs variation of 0.2V. This high-voltage gain ensures good dc precision for the unity-gain combination of LMC 6042, OP-97, Q1, but requires a low pass filter for satiability. At start up, the potential on LMC 6042 and the input of the supply can differ by the full bipolar HT voltage (1kV). This can cause damage to LMC 6042. And hence a series resistor of 100 MΩ is connected to LMC 6042 to restrict the input current under voltage overload. A stable voltage offset is generated by the circuitry around TC04-LM7555 (IC 201). By adjusting the potentiometer T2, the output at pin 1 of LMC 6042 can made to precisely track the input 5. This output can also used to provide a local guard (body of the UHF female connector) potential for LMC 6042's input connection. The amplifier section circuit is shown in Figure 4. The main power for the unit is supplied from two 12V (7AH)

rechargeable batteries, from which a 9V (± 4.5) is obtained using a 9V fixed regulator and is given to LM 6042. 10.5V supply is derived from, such as load dump (60V), when the input voltage to the regulator exceed the specified maximum operating voltage (33V type), the regulator will automatically shut down to protect both internal circuits and the load. The LM 2931 cannot be harmed by temperature mirror-image insertion. The power supply circuit is shown in Figure 5. The output of the output amplifier is connected to a PC based data logger with a 12 bit ADC to record the field variations continuously. From the circuit, the tracks are drawn using software called, PROTEL EASTEDIT 2.0. A printout of tracks is taken and from the printout the tracks is taken and from the printout the tracks are transplated into the PCB using screening technique. After this the PCB is etched using ferric chloride e copy of the printer output is shown in Figure 6.

RESULTS AND CONCLUSION

This system was tested by using a variable voltage supply operating over the range ± 500 V, and by high-impedance operation on the antenna. The measurement were compared with Keithley electrometer and is shown in Figure 7, which allows the ± 5 V span compared to ±500 V on the antenna and the frequency response curve shown in Figure 8. The measurements were taken

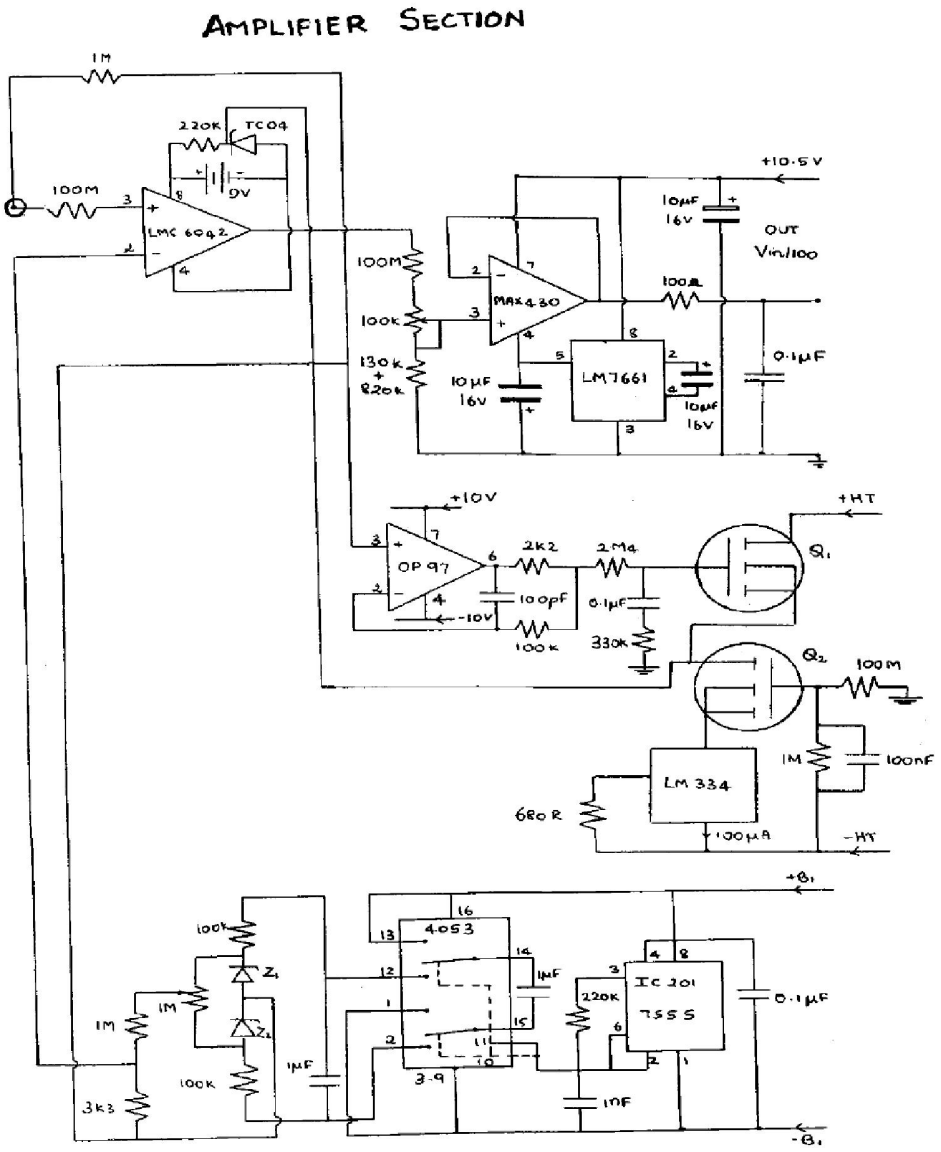

Figure 4 : The amplifier section circuit

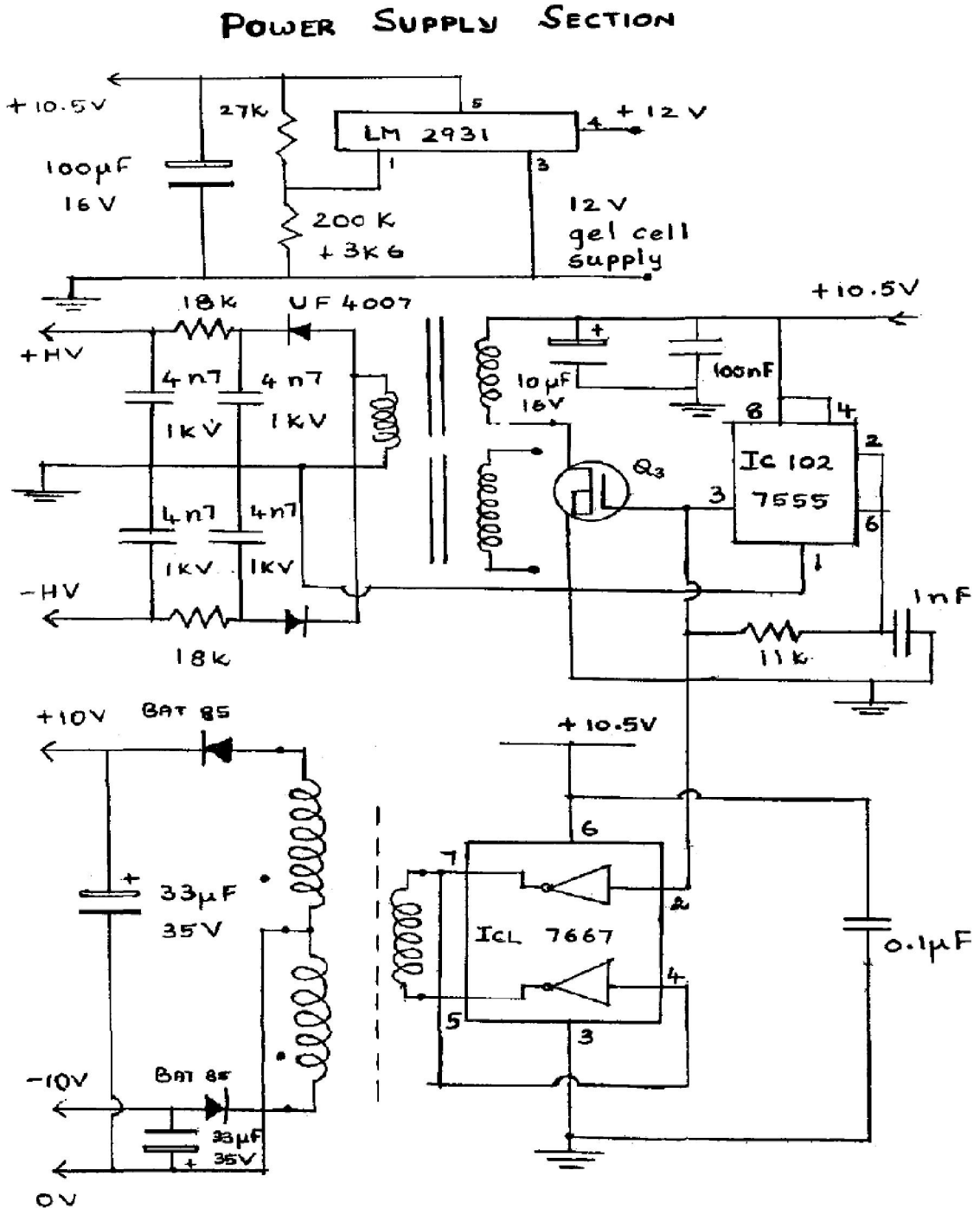

Figure 5 : The power supply section circuit

in the field during the clear sky days and meteorologically disturbed days and the measured atmospheric field compared with the other device which is measuring the same atmospheric electric field and have similar variation. These measured atmospheric electric field compared with the other atmospheric electrical parameters and it shows during the fair-weather days the atmospheric electric field and current shows similar variation that means the atmospheric conductivity during the fair weather days more are less table or constant, but in meteorologically disturbed days the variation of field and current always not similar because of atmospheric conductivity. During blizzard conditions due to high wind speed, falling and drifting snow brings different charges

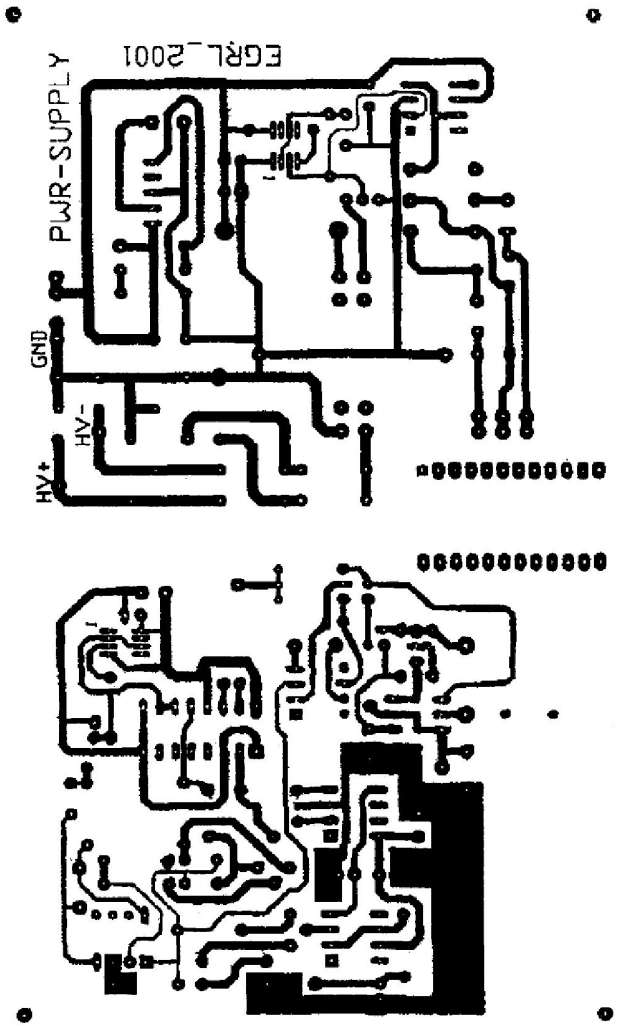

Figure 6 : Printed circuit board

near to the sensor complex. And hence, the conductivity changes according to the polarity of the charged particles. Due to the change of the conductivity the current and field changes occur. Diurnal variation of atmospheric electric field and current during fairweather day as well meteorologically disturbed days shown in Figure 9(a) and 9(b).

The relationship between observed in atmospheric current (I) and electric field (E) and column resistivity (*R*), given by $E = wV/R = w.I$, where w is the resistivity at the observation point, V is the total potential difference between the earth's surface and the atmospheric electric equalization layer, and I is the current. Though the field intensity depend strongly on the meteorological processes through its dependence on the local resistivity w, the current, given by $I = V/R$, is less sensitive to local changes in conductivity. However, changes in

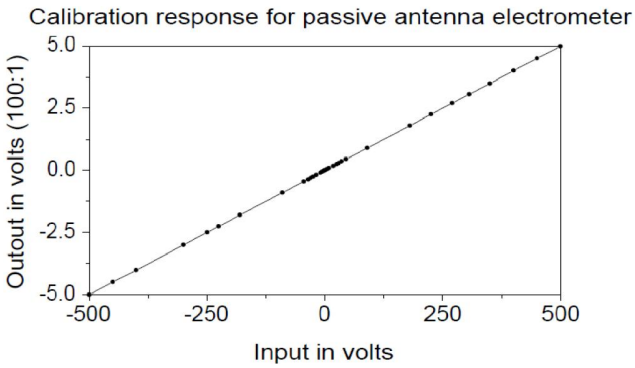

Figure 7 : Voltage response curve

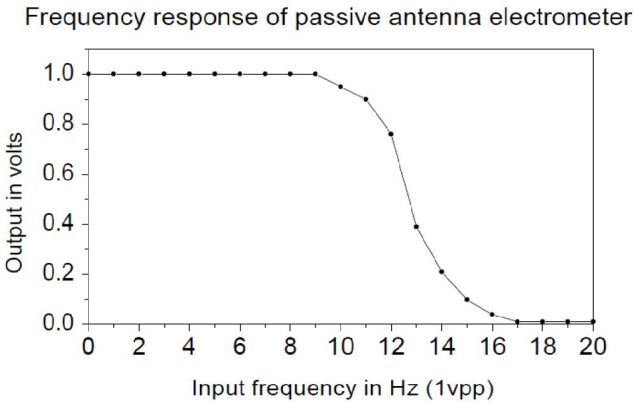

Figure 8 : Frequency response of passive antenna electrometer

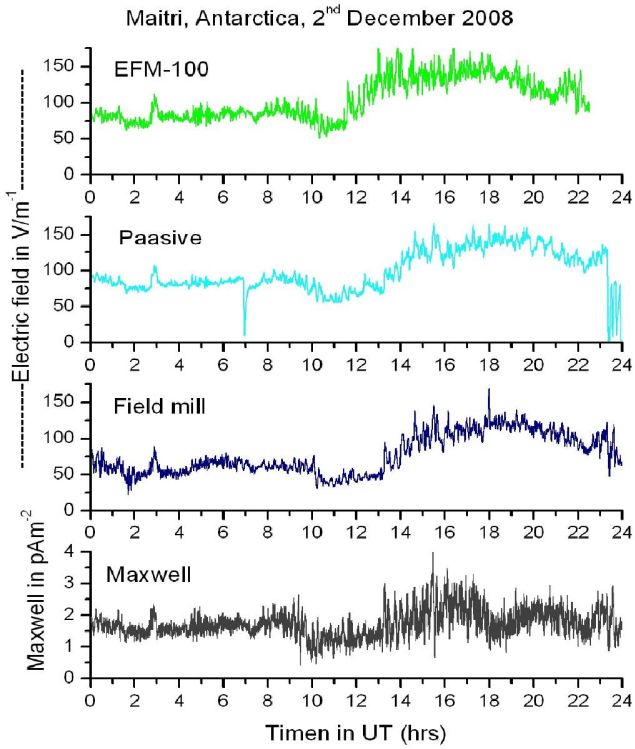

Figure 9(a) : Variation of GEC parameters during fairweather day

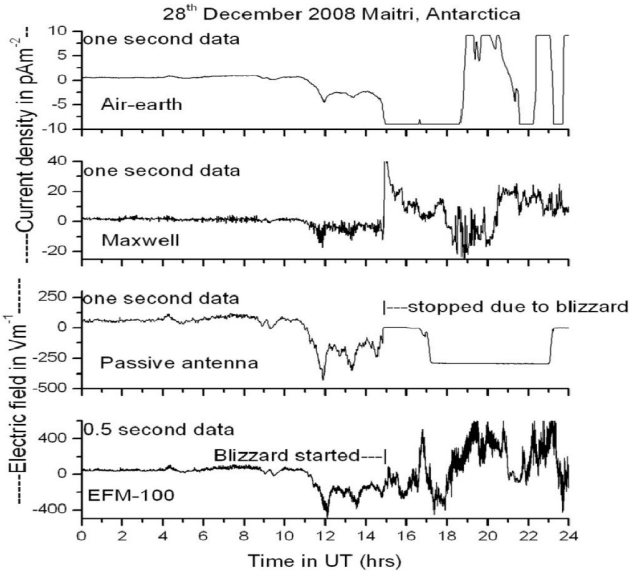

Figure 9(b) : Variation of GEC parameters during blizzard day.

the columnar resistance, induced by the atmospheric suspension content and its vertical transport, may be expected to dominate the vertical current and its variations. Thus the behavior of I depends on whether the percentage changes in *V* or *R* dominate. Over the continental stations one can expect that the changes associated with *R* are larger than those associated with *V*[12]. Gringel *et al.*[7] showed that the first two km of the atmosphere contribute about 50 percent to the total columnar resistance and the first 13 km about 95 percent. With observations conducted at Weissnau, Germany, Gringel *et al.*[7] measured a variation in *R* of about 30 percent, and attributed the variation to a changing ionization near ground and by varying aerosol concentrations in the lower troposphere. Muir[14,15] tried to explain it on the basis of sunrise effect at the height of electrosphere leading to build up of a potential through dynamic motion associated with tides.

Monitoring atmospheric electrical parameters during clear sky days has been achieved by this system Panneerselvam, et al.[16]. This present electrometer design can measure potentials safely at a height of up to 2m only. In future with suitable modifications in the electrometer front end, so as to measure the potential up to 60kms using electrometer as a play load in balloons and rockets. Making suitable modifications in the electrometer can be used to sense lighting clouds well in advance so as to make it as a lighting warning device. The potential of the atmosphere, at the same height as the antenna, is obtained by a measurement of potential difference between the antenna and the surface and thereby to measure the atmospheric electric field. The observations at several heights allow micrometeorological processes to be investigated. This battery-powered electrometer is preferable to a commercial laboratory device both because of cost and ability to cheaply replace the front-end amplifier chip damaged by transients. By setting up systems for the measurements of conductivity and current this system can be used to verify the Ohm's law $J = \sigma E$.

Simpson[18] observed that blizzards are intensely electrified and produce high positive potential gradients on the ground. In our observations we observe that whenever high winds are accompanied with some snowfall, i.e., atmospheric Maxwell current, Air-earth-current, electric field of all the three categories begin to decrease about 3 – 4 hours before the appearance of blizzard. For example, on December 28, 2008, winds begin to strengthen at 1200 UT and blizzard started from 1500 UT shown in Figure 9(b). Devendraa Siingh, Vimlesh Pant and A K Kamra made similar observations at the same place in summer 2005 on atmospheric air-earth current density, temperature are below freezing point, positive ion concentration of all four categories begin to decrease 3-4 hours before the onset of blizzard. The decrease observed in all types atmospheric electrical parameters during snowfall indicates that snow particles effectively scavenge the ions. The fact that the air-earth current density and electric field almost reduces to zero value indicates that scavenging of atmospheric ions is almost total at that time. The observations that the decrease in different ion categories is not always parallel to each other are likely to result from the non-uniform rate of scavenging of the ions of different sizes. This observation can be used as a forecasting for the convoy persons and other activities around Maitri for human safety and preliminary percussions. The detailed mechanisms underlying the formation of severe blizzards are not yet well understood and form one of the interesting topics for future polar research.

Surface atmospheric electrical parameters were found to be sensitive to convective clouds, fog, rain and snow. The variations of electrical parameters will always be in the positive side, and goes to well in negative side at about 3 hours before the onset of a blizzard at the measuring site. Hence at high latitude station

Maitri, it may perhaps be used as a tool for forecasting the onset of blizzards. With the continuous measurements of atmospheric electrical parameters and geomagnetic field variations, there is scope for addressing the problems related to the modulation of GEC by the influence of magnetosphere-ionosphere-lower atmosphere coupling processes on the near-surface electrical parameters in the polar caps. And also help to understand lightning activity in globe and regional, global warming problems and micrometeorological studies.

REFERENCES

[1] E.J.Adlerman, E.R.Williams; Seasonal variation of the global electric circuit, J.Geophys.Res., **101**, 29,679-29,688 **(1996)**.

[2] G.Beccaria; Della elettricite terrestre atmosferica a cielo serno, Turin, **(1775)**.

[3] C.G.Deshpande, A.K.Kamra; Diurnal variations of the atmospheric electric field and conductivity at Maitri, Antarctica, J.Geophys.Res., **106**, 14,207-14,218 **(2001)**.

[4] Devendra Siingh, V.Gopalakrishnan, R.P.Singh, A.K.Kamra, Shubha Singh, Vimlesh Pant, R.Singh, A.K.Singh; The atmospheric global electric circuit: An overview. Atmos.Res., **84**, 91-100 **(2007)**.

[5] H.Gerdien; Messungen der Dichte des vertikalen elektrische in der freien Atmosphäre bei der Ballonfahrt am 11 V 1905 Nachrichten von der Gesellschaft der Wissenschaften zu Göttingen 1905, 258-270 **(1995a)**.

[6] H.Gerdien; Messungen der Dichte des vertikalen elektrische in der freien Atmosphäre bei der Ballonfahrt am 30 VIII 1905 Nachrichten von der Gesellschaft der Wissenschaften zu Göttingen 1905, 447-458 **(1905b)**.

[7] W.Gringel, J.M.Rosen, D.J.Hofmann; The Earth's electrical environment, Ch. 12, Studies in Geophysics. National Academy Press, U.S.A., **(1986)**.

[8] R.G.Harrison; An atmospheric electrical volymeter follower, Rev.Sci.Instrum., **67(7)**, July **(1996)**.

[9] R.G.Harrison, W.J.Ingram; Air-earth current measurements at Kew, London, 1909-1979, Atmos. Research., **76(1-4)**, 49-64 **(2005)**.

[10] J.R.Herman, R.A.Goldberg; Sun, weather and climate, Scientific and Technical Information Branch, National Aeronautics and Space Administration, Washington, D.C, **(1978)**.

[11] V.F.Hess; Über Beobachtungen der durchdringenden Strahlung bei sieben Freiballonfahrten, Phys.Zeitschr., **13**, 1084 **(1912)**.

[12] H.Israel; Atmospheric electricity, Isr.Program for Sci.Transl., Jerusalem, **2**, **(1973)**.

[13] A.K.Kamra; Measurements of the electrical properties of dust storms, J.Geophys Res., 5856-5869 **(1972)**.

[14] M.S.Muir; The ionosphere as the source of the atmospheric electric sunrise effect, J.Atmos.Terr. Phys., **37**, 553-559 **(1975)**.

[15] M.S.Muir; The potential gradient sunrise effect in atmospheric electricity, J.Atmos.Terr.Phys., **39**, 229-233 **(1977)**.

[16] C.Panneerselvam, K.U.Nair, K.Jeeva, C.Selvaraj, S.Gurubaran, R.Rajaram; A comparative study of atmospheric Maxwell current and electric field from a low latitude station Tirunelveli, Earth Planets Space, **55**, 697-703 **(2003)**.

[17] C.Panneerselvam, K.U.Nair, C.Selvaraj, K.Jeeva, C.P.Anil Kumar, S.Gurubaran; Diurnal variation of atmospheric Maxwell current over the low-latitude continental station, Tirunelveli, India (8.7°N, 77.8°E), Earth Planets Space, **59**, 429-435 **(2007)**.

[18] G.C.Simpson; British Antarctic Expedition 1910-1913. Thacker, Spink and Co., 326 **(1919)**.

[19] S.P.Thompson; The Life of William Tomson, MacMillan, **1**, **(1910)**.

[20] W.Thompson; On the necessity for incessant recording, and for simultaneous observations in different localities, to investigate atmospheric electricity, 29th Meeting, British Association for the Advancement of Science (Aberdeen), **(1859)**.

[21] W.M.Watson; Observations upon so much of Monsieur Le Monnier the Younger's Memoir, Lately Presented to the Royal Society, as Relates to the Communicating the Electric Virtue to Non-Electrics, Philosophical Transactions (1683-1775), **44**, 388-395 **(1746)**.

[22] C.T.R.Wilson; On the measurement of the earth-air current and on the origin of atmospheric electricity, Cambridge Proc.Phil.Soc., **13(6)**, 363-382 **(1906)**.

[23] C.T.R.Wilson; On some determinations of the sign and magnitude of electric discharges in lightning flashes. Proc.Roy.Soc.Lond.A, **92**, 555-574 **(1916)**.

[24] C.T.R.Wilson; The electric field of the thundercloud and some of its effects, Proc.Phys.Soc.London, Sect.A 111 32D, **(1925)**.

The following is the copy of the manuscript submitted to Current Science journal and is accepted for publication.

Schumann resonances observed at Maitri, Antarctica: Diurnal variations and their interpretations in terms of global thunderstorm activity

S. Manu[1], R. Rawat[2], A. K. Sinha[2], S. Gurubaran[2] and K. Jeeva[1]

[1]Equatorial Geophysical Research Laboratory, Indian Institute of Geomagnetism, Tirunelveli 627 011, India

[2]Indian Institute of Geomagnetism, New Panvel (W), Navi Mumbai 410 218, India

Corresponding author: S. Gurubaran (gurubara@iigs.iigm.res.in)

Email ids of other authors: S. Manu (manu12384@gmail.com, R. Rawat (rrawat@iigs.iigm.res.in), A. K. Sinha (ashwini@iigs.iigm.res.in), K. Jeeva (123.jeeva@gmail.com)

Abstract

Schumann resonances (SR) are the AC components of the global electric circuit (GEC) and are excited by the lightning activity within the Earth-ionosphere waveguide. An induction magnetometer, which was operated from the Indian Antarctic station, Maitri (70.8^{o}S, 11.7^{o}E), served to examine the SR parameters, namely, the amplitude and frequency, in the north-south (H_{NS}) and east-west (H_{EW}) magnetic components over the icy continent. The analysis for the first resonant mode presented in this work reveals a strong UT variation in its amplitude in seasonal as well as yearly time scales. The NS amplitude reveals a semi-diurnal variation with peaks at ~1000 UT and ~2100 UT, whereas the EW amplitude exhibits a strong diurnal variation with a pronounced peak at 1600 UT. The diurnal curves for the frequency for both components are similar in nature to those for the amplitude but for a time shift. The diurnal trend in the amplitude is retained irrespective of seasons, whereas significant difference is noticed for the frequency between the summer and winter seasons, especially in the EW component. The observed diurnal variation in the SR intensity is explained in terms of the dominant thunderstorm activity centered over the three convectively active regions: Asia/Maritime Continent (Indonesia), South America and Africa. The diurnal variation in frequency depends not only on the location of the thunderstorm region with respect to the observer but also on the ionospheric day/night conditions and the Earth-ionosphere cavity thickness.

Keywords: Schumann Resonances, Global Electric Circuit, Lightning

The region of space between the Earth and the ionosphere forms a cavity which can support electromagnetic standing waves with wavelengths comparable to planetary dimensions. Schumann Resonances (SR) are the principal components of the natural background electromagnetic spectrum of the Earth-atmosphere system over the frequency range 5-50 Hz. They arise because the global thunderstorm activity at any moment excites the aforesaid cavity and the resulting electromagnetic impulses circumnavigate the globe several times without much attenuation to produce the resonance spectrum. Schumann resonances can be used as a proxy to study the global thunderstorm activity due to their global nature[1] and can be monitored from single stations away from lightning sources[2-4]. Recent observations have demonstrated that SR parameters can provide crucial information about the global lightning activity, the global climate and the planetary scale variability of the lower ionosphere[5].

Many researchers have reported that SR intensities undergo diurnal variation at various locations[2,6,7]. Earlier, the diurnal intensity variations have been shown to have a local time dependence with maxima near local noon[2]. It is now recognized that the diurnal and seasonal variations of the SR are due to changes in the propagation conditions and the source characteristics. The variation in the propagation conditions for electromagnetic waves arising from lightning is expected to be due to the day-night differences in ionospheric morphology. Further, the location of the observing site with respect to major lightning centres would also contribute to the diurnal variation in the intensity of the Schumann resonances.

The present article describes the diurnal and seasonal variation of the magnetic components of the first resonant mode of SR observed over a period of one year at Maitri,

one of the two Indian Antarctic stations currently operating from the icy continent. The results are examined in the context of our current understanding of the temporal behaviour of the SR parameters.

Though there were several studies on SR parameters based on measurements made over several mid and high latitude sites, measurements from the Antarctic have been sparse. As Maitri is far away from any lightning activity, useful studies on global lightning activity can be carried out with the measurements of SR parameters from this site. Moreover, as demonstrated in an earlier work[5], long-term records of SR intensities would serve to monitor trends in the global surface temperature. While undertaking an exercise of such a kind, it is important that we understand their diurnal and seasonal variations and are able to relate them to the corresponding variations in the source regions and the geometry between the source and observer as well as to the variations occurring in the ionospheric height and cavity thickness. The present study is an effort in this direction.

Experimental Setup

Measurements made by the three-component induction coil magnetometers (ICM) (Make: LEMI-30i of Lviv Center of Institute for Space Research, Ukraine) deployed at the Indian Antarctic station, Maitri, were utilized for the present study. The magnetometer units comprise of three induction coils and a Communication and Measuring (CAM) unit. Two of the coils were installed along geomagnetic north-south and east-west directions to yield the respective magnetic field components (H_{NS} and H_{EW}, respectively) and the third was aligned in the vertical. The magnetometers were designed to capture the desired

magnetic field signals in the frequency range 0.01 to 30 Hz. Data gathered by the CAM unit are transmitted for storage to an external PC.

For our analysis purpose in the present work, we have considered only the NS and EW magnetic components and for the year 2011. Data were recorded at a sampling rate of 64 Hz. The raw time series data were stored and the SR parameters were obtained during the post processing of the raw data. The raw data were corrected to the geographic coordinates using the transformation equations. We could gather 132 days of useful observations for this year after eliminating days with noisy data or when the experiment was not conducted. For the present study, we have used the frequency range from 5 to 30 Hz which includes the first three SR modes recognized at Maitri, Antarctica station. To calculate the amplitude and peak frequency, the spectra were fitted with Lorentzian curves as has been done in the past[8], yielding the frequency, the resonance quality factor and the peak power spectral density for each mode. Results pertaining to the SR parameters (power/amplitude and frequency) computed for the first resonant mode between 7 and 9 Hz for both NS and EW components are presented and discussed in this work.

The 30-min individual spectra for all days were averaged over the whole year. The results from this exercise are depicted in Figure 1. The amplitudes are expressed in $pT/\sqrt{Hz}$. As expected, the first three modes at 8, 14 and 20 Hz can be prominently seen and the instrument captures well these three modes. A similar instrument has been used by earlier workers from the low latitude station, Agra, in the Indian sector[9].

Diurnal variation of the Mode 1 amplitude and frequency

A prominent feature of the observations reported here is the strong diurnal variation of the intensities of the SR modes. This was anticipated as the rotation of the Earth changes the location of the observer with respect to major afternoon thunderstorm centres and the propagation conditions for the electromagnetic waves would also vary when part of the ionosphere would lie on the dayside and the rest on the nightside. In Figure 2 we depict the temporal variation (in UT hours) of the amplitude and frequency variation of the first mode in the two components in the annually averaged sense. Wherever error bars are shown, they represent the standard deviation for the corresponding data point averaged over the selected period. We immediately notice that the diurnal curves of the amplitudes for the two components reveal a very systematic variation. The amplitude of the NS component displays a semi-diurnal pattern having peaks, one around 1000 UT and the other around 2100 UT. The EW component shows a small peak around 0700 UT and a single larger peak, stronger than the NS component, at around 1600 UT.

From Figure 2 (left panel), we infer that the diurnal variation of the NS magnetic component, which shows two maxima, is possibly associated with the thunderstorm activity over Asia and South America (the times of occurrence in both maxima correspond to late afternoon local times over these continents with respect to the observing station; for example, peaks between 0600 and 0800 UT would correspond to the deep convective activity over the western Pacific region, peaks around 1000 UT would correspond to the activity over the Indian sector and peaks around 2100 UT could be related to the thunderstorm activity over the American region). As the magnetic

perturbation vector is aligned perpendicular to the propagation wave vector, we anticipate the sensors would pick up those waves whose propagation vector is orthogonal to the alignment of the sensor. For the NS component, we expect the waves to arrive at a substantial angle to the observer at Maitri and that implies their sources to be possibly located in the thunderstorm regions far away towards north-east over the Asian sector for the 1000 UT peak and towards north-west over South America for the 2100 UT peak. It may be noted that the continental regions in the tropics over those locations would support deep convection during the corresponding local afternoon hours. In the EW magnetic component (H_{EW}), a strong maximum around 1600 UT suggests an association with the peak thunderstorm activity in Africa (north of Maitri).

On the right panel of Figure 2, we show the diurnal frequency variation in the first mode of SR for the whole year. Two prominent peaks are visible in NS and one in EW components. The reasons for this behavior of the diurnal frequency variation are not known yet but we expect contributions to the diurnal frequency variations to arise not only from the source-observer geometry but also from the ionospheric height movements and conductivity variations.

Seasonal dependence of the diurnal variation of Mode 1 amplitude

Figure 3 (left panel) shows the diurnal variation of the amplitude of the first SR mode in the NS component during the Southern Hemisphere summer (November, December, January, and February (NDJM)), winter (May, June, July, and August (MJJA)) and Equinox (March, April, September, October (MASO)) during 2011. Larger error bars shown for the equinox months are due to the fact that the results for the two

equinox seasons have been combined and also that there were few days available in the month of March. Two peaks are observed in the NS component of SR, one between 0800 UT and 1000 UT and the other at around 2000 UT in all three seasons, which were earlier ascribed to the thunderstorm activity occurring over the Asian/Maritime Continent and the South American continent, respectively. Figure 3 (right panel) shows the diurnal variation of SR in the EW component. Here, we notice a strong peak at 1600 UT in all three seasons with similar amplitudes along with a secondary peak between 0600 UT and 0800 UT. Earlier, the results for the annual average for this component indicated the potential sources to lie in Africa.

The results for the amplitudes and phases of the diurnal and semidiurnal variations of the SR parameters estimated in the least squares sense are provided in Tables 1 and 2. With regard to the intensity of the SR mode (Table 1 and Figure 2), one can notice a stronger and dominant diurnal signature in the EW component and a stronger semi-diurnal signature in the NS component. Moreover, the diurnal amplitudes in the EW component are double the amplitudes in the NS component.

The diurnal variation of SR power or amplitude generally has a tendency to respond to the thunderstorm activity occurring in the three tropical chimneys, namely, Asia, in particular, over the Indo-Tibetan landmasses as well as the Maritime Continent (Indonesia), Africa and America. The influence of thunderstorm activity over the Asian sector has been shown to be important for the behaviour of Schumann resonance intensities over Kolkata, a tropical station in the Indian sector[10]. In experiments carried out over Negev Desert, Israel, three dominant maxima (0800, 1400 and 2000 UT) were observed in the diurnal variation of SR power[11]. These maxima were attributed to the

thunderstorm active regions over Asia (0800 UT), Africa (1400 UT) and South America (2000 UT). It may be noted that this site is away from the three major thunderstorm active regions (Asia, Africa and America), zonally all separated from each other by 90º. Whereas for Maitri, the major thunderstorm regions are quite far away from the source regions and the arrival angle for the ELF waves will be ~45º for the Asian and American thunderstorm regions and 90º for the African thunderstorm region. Therefore, the variation in the amplitude between these stations (Negev Desert and Maitri) will have some similarities for the NS component corresponding to the thunderstorm activity of Asian and American sectors at 0800 and 2000 UT, respectively. We expect similarities in the EW component as well when the respective sensor oriented in that direction responds to the thunderstorm region located in the African sector.

Amplitude monitoring from widely separated stations was also carried out in the past[3,13]. Results from these experiments support the idea that the global thunderstorm activity is concentrated over the continents in the tropical zone and its current peak is located in the zone closest to the dusk terminator (local afternoon hours). Thus, the source-observer distance reaches its minimum near the local time corresponding to the late afternoon hours[12]. From the SR observations made at Barentzburg (78°06′N 14°12′E), Russia, nearly a conjugate station for Maitri, it was noticed that the SR intensity has a double peak in H_{NS}, one at about 0800 UT and the other at about 2000 UT[13]. However, the east-west component, H_{EW}, shows a prominent single peak at ~1400UT and a secondary peak at ~0600 UT. The features observed at Maitri are nearly similar to the observations made from the Northern Hemisphere conjugate station. From the above, one may conclude that the observed diurnal variations in SR amplitude over Maitri are due to

thunderstorm activity occurring on a global scale over the three regions located in the Asian/Maritime Continent and the American and African sectors.

Seasonal dependence of the diurnal variation of Mode 1 frequency

The resonance frequency for Mode 1 undergoes a very systematic and consistent diurnal pattern during different seasons. The diurnal pattern of frequency variation for both magnetic components is shown in Figure 4. In spite of the large scatter, especially for the equinox seasons, we see in all three seasons two peaks near 0600 UT and 2000 UT in the NS component and a single peak near 1300 UT in the EW component, a clear semi-diurnal variation of the frequency in the NS component and a diurnal type variation in the EW component with time similar to the variations observed in the mode amplitude (refer to Figure 3). The maximum occurrence time of one of the components is almost coincident with the minimum occurrence time of the other. For example, the occurrence of the minimum at 1400 UT in the NS component coincides with that of maximum in the EW component. Another feature to be noted is that there are greater seasonal changes of mean frequency in the EW component than those in the NS component. The diurnal mean frequencies for the EW component are larger during winter and comparatively smaller during summer. It may be noted that the results for the mean frequency reported for Negev Desert reveals greater seasonal change in the NS component with the time of occurrence of maximum varying with time and season. Further, a comparison of Figures 3 and 4 and the results presented in Tables 1 and 2 for Maitri reveal that the frequency variation leads the amplitude variation by 2-4 hours.

The diurnal variation of the resonance frequency was earlier hypothesized to be caused by the motion of the thunderstorm active centres around the globe[15,16]. Later, it was speculated that the diurnal variation of SR frequencies was due to the combined effect of day-night asymmetry and the eccentricity of the geomagnetic field, since the ionospheric parameters are different for day and night sides of the globe[17]. The magnetic dipole component is stronger on one side of the globe than on the other side. Further, the dipole is closer to the centre of the night hemisphere during noon (UT), where the effective height of the ionosphere is greater and later as the dipole moves towards the day hemisphere, the ionosphere gets lower. Thus, the periodic modulation of the thickness of the Earth-ionosphere cavity was suggested to drive the frequency variation of the global resonance.

The mode frequency was shown to depend not only on the zenith angle of the Sun along the signal propagation path from a lightning source to an observer point, but also on the planetary magnetic disturbances[17]. The variation of frequency on any day has been attributed to the solar proton events[18,19]. Measurements in the Himalayan region indicate that the resonance frequency is determined by the effective size of the thunderstorms and associated ionospheric conductivity[20]. Results from Agra, in the Indian sector, demonstrated a variation in the mode frequency with solar cycle that is believed to occur essentially through the conductivity and the subsequent ionospheric height changes[9].

It was also suggested that the shifts in the frequency are due to leakage of power in the dissipative medium. The power leakage is primarily dependent on the distance of the excitation source, as late afternoon thunderstorm regions vary with time for an

observer fixed to the Earth. This is an artifact of the source-observer geometry and is not related to the properties of the Earth-ionsophere cavity[21].

All these investigations clearly reveal that the diurnal variation in frequency can significantly be altered by the ionospheric parameters in the propagation path of the signal as well as the distance between the source and the observer. Since the source of the resonance is the thunderstorm activity over the respective three tropical chimneys separated by 90^o longitude, i.e., between Africa and Asia and Africa and America, the peak of the resonance frequency is expected to have a complicated diurnal pattern owing to these conditions.

Returning to the discussion pertaining to the present observations, the steady rise in the diurnal frequency of H_{EW} component in Figure 4 (right panel) suggests that the thunderstorm activity in the tropical Asian and African regionsresonates the cavity with the frequency rise attributed to the increase in the energy of the cavity. At about 1200 UT, it attains its maximum and thereafter a steady fall is seen despite the continuation of energy in the cavity. This is probably due to the rise in the conductivity in the propagation path between the source and the observer. The decreasing trend continues till 1800 UT with the lowest value occurring around this time. Thereafter, it rises as the conductivity decreases. It is to be remembered here that though the H_{EW} component is dominated by the African thunderstorm activity, it is also influenced by the other two tropical chimneys located in Asia and America, as the angle between the source and observer is more than 0^o. An inverse of the above pattern is seen in the H_{NS} component which can be understood based on the reasoning provided above but taking into account the other two thunderstorm generators.

Conclusion

From the SR observations carried out from Maitri, Antarctica, it is evident that it is the lightning flash density along with an alignment of the resonance cavity with respect to the sensor that determines the strength of the detected power or amplitude. In this work, the characteristics of the AC component of the global electric circuit, namely, the amplitude and frequency of the SR parameters were studied. It has been shown that the NS and EW induction coils reveal maximum intensity of signal when the signal propagation path is 90^o to the direction of orientation of the sensor and nearly half the intensity when the signal propagation direction is inclined to about 45^o. The geographical location of Maitri, in Antarctica, is just south of Africa. The signal propagation path from Africa to Maitri is nearly 90^o and the maximum intensity at 1600 UT revealed by the observations made by the EW sensor could very well be in response to a source in the African continent. The H_{NS} sensor reveals two maxima, one at around 1000 UT and the other at 2100 UT. The amplitude of SR (H_{NS}) is nearly half of that of the signal detected by EW sensor as the source of the thunderstorm activity (MC and American sector) is nearly at 45^o bearing. Considering the signal strength and occurrence of these maxima, it is evident that these features are consequences of the thunderstorm activity over the Asian and the American sectors. In accordance with the earlier reports, we conclude that the variation of the resonance frequency in Mode 1 is related to the variation in the intensity of the thunderstorm activity as well as the behaviour of the Earth-ionosphere cavity.

References

1. Heckman, S.J., Williams, E. and Boldi, B., Total lightning inferred from Schumann resonance measurements. *J. Geophys. Res.*, 1998, 103, 31775–31779.

2. Sentman, D.D. and Fraser, B.J., Simultaneous Observations of Schumann Resonances in California and Australia: Evidence for Intensity Modulation by the Local Height of the D Region. *J. Geophys. Res.*, 1991, 96, 15,973-15,984.

3. Fullekrug, M. and Fraser-Smith, A.C., Further evidence for a global correlation of the earth-ionosphere cavity resonances. *Geophys. Res. Lett.*, 1996, 23, 2773–2776.

4. Price, C., Evidence for a link between global lightning activity and upper tropospheric water vapour. *Nature*, 2000, 406,290–293.

5. Williams, E.R., The Schumann Resonance: a global tropical thermometer. *Science*, 1992, 256, 1184–1188.

6. Fullekrug, M., Schumann resonances in magnetic field components, *J. Atmos. Terr. Phys.*,1995, 57, 479– 484.

7. Satori, G. and Zieger, B., Spectral characteristics of Schumann resonances observed in Central Europe. *J. Geophys. Res.*, 1996, 101, 29,663–29,669.

8. Shvets, A. V., Y. Hobara and M. Hayakawa, Variations of the global lightning distribution revealed from three-station Schumann resonance measurements. J. Geophys. Res., 2010, 115, A12316, doi:10.1029/2010JA015851.

9. Singh, B. and D. Pundhir, Shift of effective lightning areas during pre to post period of solar cycle minimum of 2008-2009 as determined from Schumann resonance studies at Agra, India. Annals Geophys. (2014), 57, 6, doi:10.4401/ag-6596.

10. De, S. S., B. K. De, B. K. Sarkar, B. Bandyopadhyay, D. K. Haldar, Suman Paul and S. Barui, Analyses of Schumann resonance spectra from Kolkata and their possible interpretations. Indian J. Radio & Space Phys. (2009), 38, 208-214.

11. Price, C. and Melnikov, A., Diurnal, seasonal and interannual variations in the Schumann resonance parameters. *J. Atmos. Solar-Terr. Phys.*, 2004, 66, 1179-1185.

12. Nickolaenko, A.P. and Hayakawa, M., *Resonances in the Earth-Ionosphere Cavity*, Kluwer Academic Publishers, Dordrecht/Boston/London, 2002, 380pp.

13. Roldugin, V.K. and Vasil'ev, A.N., Variations in the Schumann Resonance Polarization Ellipse in the Horizontal and Vertical Planes according to Observations at the Barentsburg and Lovozero Observatories. *Geomag. Aeron.*, 2012, 52, 68–76.

14. Schlegel, K. and Fullekrug, M., Diurnal harmonics in Schumann resonance parameters observed on both hemispheres. *Geophys. Res. Lett.*, 2000, 27, 2805-2808.

15. Balser, M. and Wagner, C.A., Diurnal power variations of the earth-ionosphere cavity modes and their relationship to worldwide thunderstorm activity. *J. Geophys. Res.*, 1962a,67, 619–625.

16. Balser, M. and Wagner, C.A., On the frequency variations of the earth-ionosphere cavity modes. *J. Geophys. Res.*, 1962b,67, 4081–4083.

17. Bliokh, P.V., Nikolaenko, A.P. and Filippov, Y.F., Diurnal variations of the natural frequencies of the earth-ionosphere resonator in relation to the eccentricity of the geomagnetic field (in Russian). *Geomag. Aeron.*, 1968, 8, 250-260.

18. Roldugin, V.C., Maltsev, Y.P., Vasiljev, A.N. and Vashenyuk, E.V., Changes of the first Schumann resonance frequency during relativistic solar proton precipitation in the 6 November 1997 event. *Ann. Geophys.*, 1999, 17, 1293– 1297.

19. Roldugin, V. C., Y. P. Maltsev, A. N. Vasiljev, A. Y. Schokotov and G. G. Belyajev, Schumann resonance frequency increase during solar X-ray bursts, *J. Geophys. Res.*, 2004, 109, A01216.

20. Chand, R., Israil, M.and Rai, J., Schumann resonance frequency variations observed in magnetotelluric data recorded from Garhwal Himalayan region India.*Ann. Geophys.*, 2009, 27, 3497-3507.

21. Sentman, D., Schumann resonances, *Handbook of AtmosphericElectrodynamics*, vol. 1, edited by H. Volland, 1995, pp. 267– 295, CRC Press,Boca Raton, Fla.

Table 1. Diurnal and semi-diurnal amplitudes and phases of the SR parameters of the first mode (phases given in brackets)

SR parameter	Season	NS diurnal	EW diurnal	NS semi-diurnal	EW semi-diurnal
Amplitude ($\times 10^{-3}$ pT/Hz$^{1/2}$)	Summer	3.85 (10.3)	17.8 (13.7)	7.74 (9.7)	14.5 (5.1)
	Equinox	1.97 (2.3)	16.2 (16.6)	9.34 (10.6)	9.0 (4.8)
	Winter	2.66 (8.2)	15.1 (15.4)	8.41 (11.4)	4.16 (4.1)

Table 2. Same as in Table 1 but for frequency of the first mode

SR parameter	Season	NS diurnal	EW diurnal	NS semi-diurnal	EW semi-diurnal
Frequency ($\times 10^{-2}$ Hz)	Summer	4.07 (5.0)	1.89 (14.1)	4.27 (7.4)	3.74 (2.1)
	Equinox	3.34 (3.5)	4.92 (13.7)	3.28 (6.9)	3.0 (1.5)
	Winter	5.28 (3.8)	4.95 (11.7)	3.44 (7.9)	3.3 (0.7)

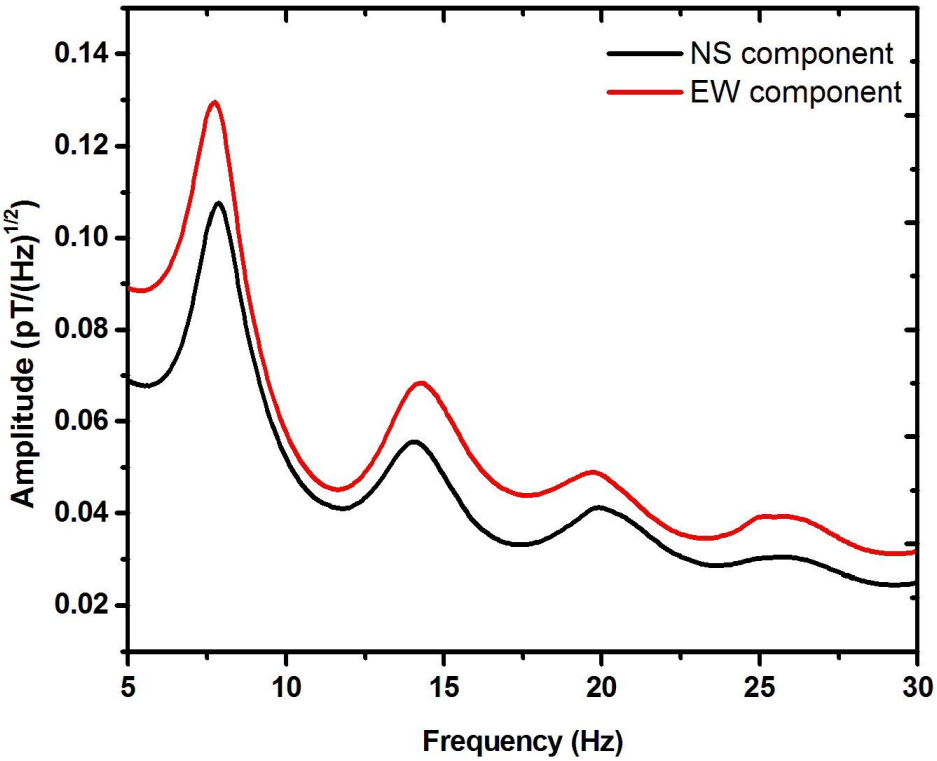

Figure 1. Annually averaged amplitude spectra of Schumann resonance over Maitri, Antarctica.

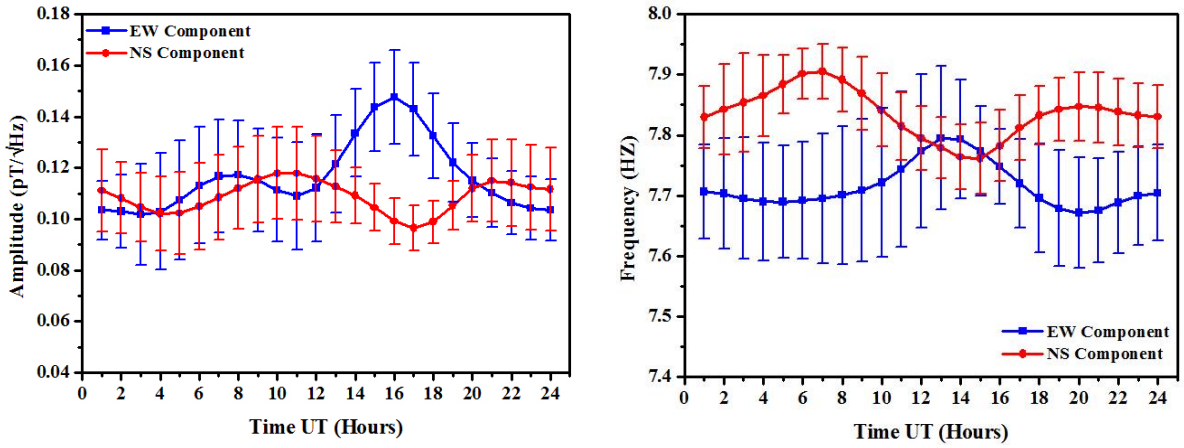

Figure 2. Annually averaged amplitude (left panel) and frequency (right panel) variation of the first SR mode at Maitri, Antarctica.

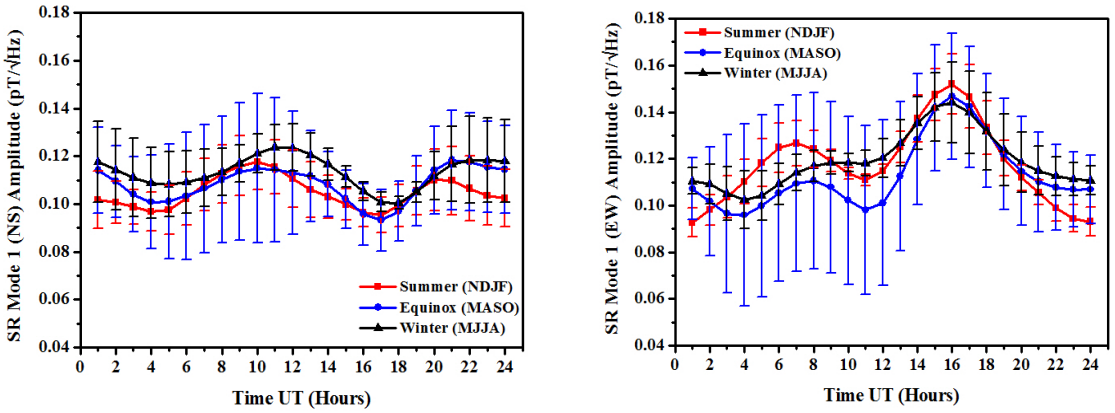

Figure 3. Mean diurnal-seasonal amplitude variation of the first SR mode in NS (left panel) and EW (right panel) magnetic components at Maitri, Antarctica.

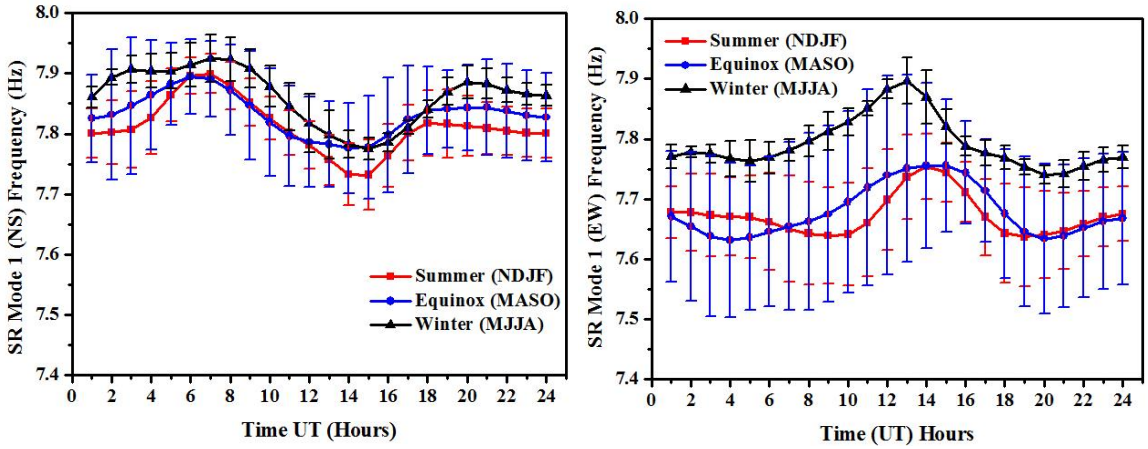

Figure 4. Mean diurnal-seasonal frequency variation of the first SR mode in NS (left panel) and EW (right panel) magnetic components at Maitri, Antarctica.

Manu S <manu12384@gmail.com>

[cs] Editor Decision

Prof. S.K. SATHEESH <profsks@gmail.com> Wed, May 6, 2015 at 9:22 AM
To: Subramanian Gurubaran <gurubara@iigs.iigm.res.in>
Cc: Shanmugam Manu <manu12384@gmail.com>, Rahul Rawat <rrawat@iigs.iigm.res.in>, Ashwini K Sinha <ashwini@iigs.iigm.res.in>, Krishnamoorthy Jeeva <123.jeeva@gmail.com>

Dear Dr. Subramanian Gurubaran:

We have reached a decision regarding your submission to Current Science, "Schumann resonances observed at Maitri: Diurnal and seasonal variations".

Our decision is to: Accept

Note: In the case of multi-author papers belonging to the category of Scientific Correspondence, Research Communication, Research Article and Research Account, when the proof comes to you, you may, if you wish, indicate the contribution by each author. This is not mandatory.

Prof. S.K. SATHEESH
Centre for Atmospheric and Oceanic Sciences
Indian Institute of Science
Bangalore, India
Phone 22933070
profsks@gmail.com
SKS
Chandrika Ramesh
for Editor
Current Science